

CANADIAN THESES ON MICROFICHE

I.S.B.N.

THESES CANADIENNES SUR MICROFICHE



National Library of Canada
Collections Development Branch

Canadian Theses on
Microfiche Service

Ottawa, Canada
K1A 0N4

Bibliothèque nationale du Canada
Direction du développement des collections

Service des thèses canadiennes
sur microfiche

NOTICE

The quality of this microfiche is heavily dependent upon the quality of the original thesis submitted for microfilming. Every effort has been made to ensure the highest quality of reproduction possible.

If pages are missing, contact the university which granted the degree.

Some pages may have indistinct print especially if the original pages were typed with a poor typewriter ribbon or if the university sent us a poor photocopy.

Previously copyrighted materials (journal articles, published tests, etc.) are not filmed.

Reproduction in full or in part of this film is governed by the Canadian Copyright Act, R.S.C. 1970, c. C-30. Please read the authorization forms which accompany this thesis.

THIS DISSERTATION
HAS BEEN MICROFILMED
EXACTLY AS RECEIVED

AVIS

La qualité de cette microfiche dépend grandement de la qualité de la thèse soumise au microfilmage. Nous avons tout fait pour assurer une qualité supérieure de reproduction.

S'il manque des pages, veuillez communiquer avec l'université qui a conféré le grade.

La qualité d'impression de certaines pages peut laisser à désirer, surtout si les pages originales ont été dactylographiées à l'aide d'un ruban usé ou si l'université nous a fait parvenir une photocopie de mauvaise qualité.

Les documents qui font déjà l'objet d'un droit d'auteur (articles de revue, examens publiés, etc.) ne sont pas microfilmés.

La reproduction, même partielle, de ce microfilm est soumise à la Loi canadienne sur le droit d'auteur, SRC 1970, c. C-30. Veuillez prendre connaissance des formules d'autorisation qui accompagnent cette thèse.

LA THÈSE A ÉTÉ
MICROFILMÉE TELLE QUE
NOUS L'AVONS REÇUE



National Library of Canada

Bibliothèque nationale du Canada

Canadian Theses Division / Division des thèses canadiennes

Ottawa, Canada K1A 0N4

54033

0-315-06113-8

PERMISSION TO MICROFILM — AUTORISATION DE MICROFILMER

Please print or type — Écrire en lettres moulées ou dactylographier

Full Name of Author — Nom complet de l'auteur

BIRBAL SINGH

Date of Birth — Date de naissance

JULY 10, 1943

Country of Birth — Lieu de naissance

INDIA

Permanent Address — Résidence fixe

5720-40 AVENUE
EDMONTON, ALBERTA, CANADA T6L 1B2

Title of Thesis — Titre de la thèse

APPLICATION OF THE FINITE ELEMENT METHOD
TO STUDY DENDRITIC GROWTH

University — Université

UNIVERSITY OF ALBERTA

Degree for which thesis was presented — Grade pour lequel cette thèse fut présentée

Ph. D.

Year this degree conferred — Année d'obtention de ce grade

1981

Name of Supervisor — Nom du directeur de thèse

Prof. ROBERT R. GILPIN

Permission is hereby granted to the NATIONAL LIBRARY OF CANADA to microfilm this thesis and to lend or sell copies of the film.

The author reserves other publication rights, and neither the thesis nor extensive extracts from it may be printed or otherwise reproduced without the author's written permission.

L'autorisation est, par la présente, accordée à la BIBLIOTHÈQUE NATIONALE DU CANADA de microfilmer cette thèse et de prêter ou de vendre des exemplaires du film.

L'auteur se réserve les autres droits de publication; ni la thèse ni de longs extraits de celle-ci ne doivent être imprimés ou autrement reproduits sans l'autorisation écrite de l'auteur.

Date

July 24, 1981

Signature

Birbal Singh

THE UNIVERSITY OF ALBERTA

APPLICATION OF THE FINITE ELEMENT METHOD
TO STUDY DENDRITIC GROWTH

by



BIRBAL SINGH

A THESIS

SUBMITTED TO THE FACULTY OF GRADUATE STUDIES AND RESEARCH
IN PARTIAL FULFILLMENT OF THE REQUIREMENTS FOR THE DEGREE
OF DOCTOR OF PHILOSOPHY

DEPARTMENT OF MECHANICAL ENGINEERING

EDMONTON, ALBERTA

FALL, 1981

THE UNIVERSITY OF ALBERTA

RELEASE FORM

NAME OF AUTHOR BIRBAL SINGH

TITLE OF THESIS APPLICATION OF THE FINITE ELEMENT
METHOD TO STUDY DENDRITIC GROWTH

DEGREE FOR WHICH THESIS WAS PRESENTED . Ph.D

YEAR THIS DEGREE WAS GRANTED . Fall 1981

Permission is hereby granted to THE UNIVERSITY OF ALBERTA LIBRARY to reproduce single copies of this thesis and to lend or sell such copies for private, scholarly or scientific research purposes only.

The author reserves other publication rights, and neither the thesis nor extensive extracts from it may be printed or otherwise reproduced without the author's written permission.

(Signed) *B. S. Singh*

PERMANENT ADDRESS:

. . . 5720 - 40 AVENUE .
. . . EDMONTON ALBERTA
. . . T6L 1B2

DATED July 24, 1981

THE UNIVERSITY OF ALBERTA
FACULTY OF GRADUATE STUDIES AND RESEARCH

The undersigned certify that they have read, and recommend to the Faculty of Graduate Studies and Research, for acceptance, a thesis entitled "Application of the Finite Element Method to Study Dendritic Growth," submitted by Birbal Singh in partial fulfillment of the requirements for the degree of Doctor of Philosophy.

Robert G. ...
Supervisor

Tom Krest

T. Hendry

...

Frank ...

William A. Wilcox

External Examiner

Date . June . 19, 1981

ABSTRACT

This work has been an investigation of the applicability of the finite element method to the study of crystal growth processes. The finite element method was chosen because a review of past analytical research in the area of crystal growth theory indicated that analytical techniques may have reached the limit of their usefulness and further progress in the area may require the exploitation of numerical methods.

To demonstrate its applicability, the method has been used to analyze the problems such as, the stability of cylindrical and spherical particles growing in supercooled liquid, dendritic growth, and the evolution of dendritic shape with time. Quantitative comparisons between this approach, other theories and experimental data are made for all examples to assess the value of the method.

The method has also been used to obtain a time invariant shape of a dendrite growing in a supercooled liquid. The results indicate that the velocity of growth of a dendrite with time invariant shape is closer to that predicted by the Langer-Krumbhaar stability criterion than to that predicted by the maximum velocity principle used by many researchers.

These results on the applicability of the finite element method to crystal growth problems are encouraging.

However, certain concerns still remain regarding accuracy in calculations of surface curvatures and separation of numerical instabilities from physical instabilities. If these concerns and problems can be overcome, a number of interesting applications of the finite element method to the study of crystal growth phenomena are possible.

ACKNOWLEDGEMENTS

I am deeply indebted to Professor Robert R. Gilpin for his consistent support, his guidance, and his stimulating approach to numerical modelling which has made my study richly profitable. I also wish to express my thanks and appreciation for the cooperation I received from the faculty and graduate students of the Mechanical Engineering Department at the University of Alberta.

I wish to thank my wife and children for their faith and support during the difficult years. I also wish to express my thanks to Mrs. Marilyn Wahl for the excellent typing of this thesis.

I also wish to acknowledge with thanks the financial support I received from the Department of Mechanical Engineering, the Province of Alberta Graduate Scholarship Programme and the National Research Council grants during the course of this study.

TABLE OF CONTENTS

CHAPTER		PAGE
1	INTRODUCTION	1
2	LITERATURE SURVEY	7
	2.1 Introduction	7
	2.2 Experimental Investigations	7
	2.2.1 Dendritic Growth Rate	8
	2.2.2 Morphological Stability	14
	2.3 Theoretical Investigations	17
	2.3.1 Dendritic Growth Rate	17
	2.3.2 Morphological Stability	27
3	FUNDAMENTAL THEORY	30
	3.1 The Physics of Freezing	30
	3.2 Physical Model and Assumptions	38
	3.2.1 Discussion of Assumptions	42
	3.3 Mathematical Formulation and Governing Equations	44
	3.3.1 Non-Dimensionalization	45
	3.4 Variational Formulation	50
	3.5 The Finite Element Method	54
	3.5.1 The Finite Element Method Applied to the Dendritic Growth Problem	56
4	STABILITY OF PARTICLES GROWING IN A SUPERCOOLED MELT	65

CHAPTER	PAGE
4.1 Introduction	65
4.2 The Unperturbed Growth of a Sphere From a Slightly Supercooled Melt	65
4.3 The Stability of a Sphere Grouping in a Slightly Supercooled Liquid	77
4.3.1 Theoretical Solutions	77
4.4 The Stability of a Solid Cylinder Growing in a Supercooled Liquid	85
4.4.1 The Unperturbed Growth of a Cylinder	85
4.4.2 The Stability of a Perturbed Cylinder	89
5 DENDRITIC GROWTH	101
5.1 Introduction	101
5.2 Selection of Domain to be Studied	101
5.3 Dendritic Growth Velocity	108
5.3.1 Isothermal Dendrite	108
5.3.2 Non-Isothermal Dendrite	111
6 SIMULATION OF DENDRITIC GROWTH	124
7 SUMMARY AND CONCLUSIONS	136
REFERENCES	141
APPENDICES	
1: THERMODYNAMIC EQUILIBRIUM ACROSS A CURVED INTERFACE	148
2: DERIVATION OF ELEMENT MATRICES	152
3: AUTOMATIC MESH GENERATION	166

CHAPTER	PAGE
APPENDICES: 4: PHYSICAL CONSTANTS FOR WATER TIN AND SUCCINONITRILE USED IN THIS WORK . .	169

LIST OF TABLES

TABLE		PAGE
4.1	A COMPARISON OF THE EXACT SOLUTION AND THE FINITE ELEMENT SOLUTION FOR THE GROWTH RATE OF VARIOUS POINTS ALONG THE INTERFACE OF A SPHERE GROWING IN SUPERCOOLED LIQUID ($R = 50^*$, $k_s = 0$)	74
4.2	A COMPARISON OF THE EXACT SOLUTION AND THE FINITE ELEMENT SOLUTION FOR THE GROWTH RATE OF VARIOUS POINTS ALONG THE INTERFACE OF A SPHERE GROWING IN SUPERCOOLED LIQUID ($R = 100 R^*$, $k_s = 0$)	75
4.3	A COMPARISON OF THE EXACT SOLUTION AND THE FINITE ELEMENT SOLUTION FOR THE GROWTH RATE OF VARIOUS POINTS ALONG THE INTERFACE OF A SPHERE GROWING IN SUPERCOOLED LIQUID ($R = 250^*$, $\frac{k_s}{k_l} = 4$)	76
4.4	SOME SPHERICAL HARMONICS, $Y_{\ell m}$	78
4.5	A COMPARISON OF THE ANALYTICAL METHOD AND THE FINITE ELEMENT METHOD TO STUDY THE STABILITY OF A SLIGHTLY PERTURBED SPHERE GROWING IN A SUPERCOOLED LIQUID (THE SPHERE PERTURBED BY THE HARMONIC Y_{20})	86
4.6	A COMPARISON OF THE ANALYTICAL METHOD AND THE FINITE ELEMENT METHOD TO STUDY THE STABILITY OF A SLIGHTLY PERTURBED SPHERE GROWING IN A SUPERCOOLED LIQUID (THE SPHERE PERTURBED BY THE HARMONIC Y_{30})	87
4.7	A COMPARISON OF THE EXACT SOLUTION AND THE FINITE ELEMENT SOLUTION FOR THE GROWTH RATE OF VARIOUS POINTS ALONG THE INTERFACE OF A CYLINDER GROWING IN A SUPERCOOLED LIQUID ($R = 1024 R^*$, $R_\lambda/R = 60$, $k_s/k_l = 4$)	93

TABLE	PAGE	
4.8	A COMPARISON OF THE EXACT SOLUTION AND THE FINITE ELEMENT SOLUTION FOR THE GROWTH RATE OF VARIOUS POINTS ALONG THE INTERFACE OF A CYLINDER GROWING IN A SUPERCOOLED LIQUID ($R = 512 R^*$, $R_\lambda/R = 60$, $k_s/k_l = 4$)	94
4.9	A COMPARISON OF THE ANALYTICAL METHOD AND THE FINITE ELEMENT METHOD TO STUDY THE STABILITY OF A SLIGHTLY PERTURBED CYLINDER GROWING IN A SUPERCOOLED LIQUID (THE CYLINDER PERTURBED BY THE HARMONIC $k = 6$)	99
4.10	A COMPARISON OF THE ANALYTICAL METHOD AND THE FINITE ELEMENT METHOD TO STUDY THE STABILITY OF A SLIGHTLY PERTURBED CYLINDER GROWING IN A SUPERCOOLED LIQUID (THE CYLINDER PERTURBED BY A HARMONIC $k = 2$)	100
5.1	A COMPARISON OF THE IVANTSOV'S METHOD AND THE FINITE ELEMENT METHOD FOR THE AXIAL GROWTH VELOCITIES OF VARIOUS POINTS ON THE INTERFACE OF AN ISOTHERMAL DENDRITE (NON-DIMENSIONAL TIP CURVATURE = -0.022)	109

LIST OF FIGURES

FIGURE		PAGE
3.1	IDEAL COOLING CURVE FOR WATER (FROM KNIGHT [58])	32
3.2	A LESS IDEAL COOLING CURVE FOR WATER SHOWING SUPERCOOLING (FROM KNIGHT [58])	34
3.3	FREE ENERGY - TEMPERATURE DIAGRAM WITH A P-T DIAGRAM, SHOWING HOW THE LATTER IS RELATED TO THE FORMER	35
3.4	(a) HEAT EXTRACTION THROUGH THE SOLID; (b) HEAT REMOVAL THROUGH THE LIQUID	37
3.5	WHEN A GROWING INTERFACE IS CONVEX TOWARDS THE LIQUID (b) IT DISSIPATES THE LIBERATED HEAT OF FUSION FASTER THAN WHEN IT IS PLANAR (a)	39
3.6	THERMAL PROFILE IN FRONT OF A DENDRITE TIP GROWING IN A MELT UNDER COOLED AN AMOUNT $\Delta T = T_f - T_\alpha$	41
3.7	DOMAIN UNDER CONSIDERATION FOR THE STUDY OF DENDRITIC GROWTH	48
3.8	THE SIX-NODE TRIANGULAR ELEMENT WITE AREA CO-ORDINATES OF THE NODES	58
3.9	A NODE PATTERN FOR AUTOMATIC NODE NUMBERING	59
4.1	THE GEOMETRY OF A SPHERE GROWING IN A SUPERCOOLED LIQUID	66
4.2	THE DOMAIN TO BE CONSIDERED FOR THE STUDY OF THE GROWTH OF A SPHERE IN SUPERCOOLED LIQUID	70
4.3	A COMPARISON OF THE EXACT SOLUTION AND THE FINITE ELEMENT SOLUTION FOR THE TEMPERATURE DISTRIBUTION AROUND A SPHERE GROWING IN A SUPERCOOLED LIQUID ($R = 100 R^*$; $\theta = \frac{T - T_f}{T_f - T_\alpha}$)	71

4.4	A COMPARISON OF THE EXACT SOLUTION AND THE FINITE ELEMENT SOLUTION FOR THE TEMPERATURE GRADIENT AROUND A SPHERE GROWING IN SUPER-COOLED LIQUID ($R = 100 R^*$)	72
4.5	A COMPARISON OF THE EXACT SOLUTION AND THE FINITE ELEMENT SOLUTION FOR THE TEMPERATURE GRADIENT AROUND A SPHERE GROWING IN A SUPER-COOLED LIQUID ($R = 100 R^*$)	73
4.6	A SPHERE PERTURBED BY THE HARMONIC Y_{30} . THE FIGURE IS CYLINDRICALLY SYMMETRIC ABOUT THE VERTICAL AXIS	79
4.7	A COMPARISON OF THE ANALYTICAL SOLUTION AND THE FINITE ELEMENT SOLUTION FOR THE GROWTH RATE OF A SPHERE PERTURBED BY THE HARMONIC Y_{30} ($R = 100 R^*$; $\frac{k_s}{k_l} = 1$)	82
4.8	A COMPARISON OF THE ANALYTICAL SOLUTION WITH THE FINITE ELEMENT SOLUTION FOR THE GROWTH RATE OF A SPHERE PERTURBED BY THE HARMONIC Y_{30} ($R = 100 R^*$; $\frac{k_s}{k_l} = 0$)	83
4.9	A COMPARISON OF THE ANALYTICAL SOLUTION AND THE FINITE ELEMENT SOLUTION FOR THE GROWTH RATE OF A SPHERE PERTURBED BY THE HARMONIC Y_{30} ($R = 100 R^*$; $\frac{k_s}{k_l} = 4$)	84
4.10	A COMPARISON OF THE ANALYTICAL SOLUTION AND THE FINITE ELEMENT SOLUTION FOR THE TEMPERATURE DISTRIBUTION AROUND A CYLINDER GROWING IN A SUPERCOOLED LIQUID ($R = 50 R^*$; $R_\lambda/R = 60$)	90
4.11	A COMPARISON OF THE ANALYTICAL SOLUTION AND THE FINITE ELEMENT SOLUTION FOR THE TEMPERATURE GRADIENT AROUND A CYLINDER GROWING IN A SUPER-COOLED LIQUID ($R = 50 R^*$; $R_\lambda/R = 60$)	91
4.12	A COMPARISON OF THE ANALYTICAL SOLUTION AND THE FINITE ELEMENT SOLUTION FOR THE TEMPERATURE GRADIENT AROUND A CYLINDER GROWING IN A SUPER-COOLED LIQUID ($R = 50 R^*$; $R_\lambda/R = 60$)	92

FIGURE	PAGE
4.13 A COMPARISON OF THE ANALYTICAL SOLUTION WITH THE FINITE ELEMENT SOLUTION FOR THE GROWTH RATE OF A PERTURBED CYLINDER ($R = 1024 R^*$; $\frac{k_s}{k_l} = 0$; $K = 6$)	96
4.14 A COMPARISON OF THE ANALYTICAL SOLUTION WITH THE FINITE ELEMENT SOLUTION FOR THE GROWTH RATE OF A PERTURBED CYLINDER ($R = 1024 R^*$; $\frac{k_s}{k_l} = 1$, $K = 6$)	97
4.15 A COMPARISON OF THE ANALYTICAL SOLUTION WITH THE FINITE ELEMENT SOLUTION FOR THE GROWTH OF A PERTURBED CYLINDER ($R = 512 R^*$; $\frac{k_s}{k_l} = 1$, $K = 6$)	98
5.1 THE DOMAIN TO BE CONSIDERED FOR THE FINITE ELEMENT STUDY OF DENDRITIC GROWTH	102
5.2 PLOT TO DETERMINE THE EFFECT OF THE FINITE ELEMENT DOMAIN SIZE ON THE GROWTH RATE OF DENDRITES ($\frac{k_s}{k_l} = 4$, $Ste = 0.05$ $R_1 = 900$, $R_3 = 2R_2$, $\bar{K} = -0.022$)	105
5.3 PLOT OF THE TEMPERATURE DISTRIBUTION AROUND A DENDRITE GROWING IN A SUPERCOOLED LIQUID ($\frac{k_s}{k_l} = 4$, $Ste = 0.05$, $\bar{K} = -0.022$)	106
5.4 PLOT OF THE TEMPERATURE DISTRIBUTION AROUND A DENDRITE GROWING IN A SUPERCOOLED LIQUID ($\frac{k_s}{k_l} = 4$, $Ste = 0.05$, $\bar{K} = -0.022$)	107
5.5 A COMPARISON OF THE FINITE ELEMENT SOLUTION AND THE IVANTSOV SOLUTION FOR THE GROWTH RATE OF A DENDRITE AS A FUNCTION OF THE TIP RADIUS OF CURVATURE	110

FIGURE		PAGE
5.6	PLOT OF THE GROWTH VELOCITY OF A DENDRITE GROWING IN A SUPERCOOLED WATER AS A FUNCTION OF THE TIP CURVATURE FOR VARIOUS STEFAN NUMBERS $\left(\frac{k_s}{k_l} = 4\right)$	112
5.7	PLOT OF TIP GROWTH VELOCITY OF A DENDRITE AS A FUNCTION OF THE TIP CURVATURE $\left(\frac{k_s}{k_l} = 4, Ste = 0.05\right)$	113
5.8	PLOT OF THE GROWTH VELOCITY OF ICE DENDRITES AS A FUNCTION OF SUPERCOOLING	114
5.9	PLOT OF THE TIP RADIUS OF CURVATURE AS A FUNCTION OF SUPERCOOLING FOR ICE DENDRITES	116
5.10	PLOT OF THE GROWTH VELOCITY OF TIN DENDRITES AS A FUNCTION OF SUPERCOOLING	117
5.11	PLOT OF THE GROWTH VELOCITY OF SUCCINONITRILE DENDRITES AS A FUNCTION OF SUPERCOOLING	118
5.12	PLOT OF THE GROWTH VELOCITY OF ICE DENDRITES AS A FUNCTION OF SUPERCOOLING FOR VARIOUS DENDRITE TIP SHAPES	120
5.13	PLOT OF THE GROWTH VELOCITY OF VARIOUS POINTS ALONG THE INTERFACE OF A PARABOLOIDAL DENDRITE $\left(\frac{k_s}{k_l} = 4, Ste = 0.05\right)$	121
5.14	PLOT OF THE GROWTH VELOCITY OF VARIOUS POINTS ALONG THE INTERFACE OF A PARABOLIC DENDRITE $\left(\frac{k_s}{k_l} = 4, Ste = 0.05\right)$	122
6.1	COMPUTER PLOT OF THE LONG TERM GROWTH OF A DENDRITE INTERFACE ($k_s = 0$; INITIAL SHAPE - PERFECT PARABOLOID)	128
6.2	PLOT OF GROWTH RATE AND TIP CURVATURE VERSUS TIME TO DETERMINE THE TIME INVARIANT SHAPE OF A DENDRITE ($k_s = 0$)	129

FIGURE		PAGE
6.3	PLOT OF GROWTH RATE AND TIP CURVATURE VERSUS TIME TO DETERMINE THE TIME INVARIANT SHAPE OF A DENDRITE ($k_s = 0$)	130
6.4	THE FINAL SHAPE OF A TIME INVARIANT DENDRITE INTERFACE AND A PARABOLOID WITH SAME TIP CURVATURE	131
6.5	PLOT OF GROWTH RATE AND TIP CURVATURE VERSUS TIME TO DETERMINE THE TIME INVARIANT SHAPE OF A DENDRITE STARTING FROM TWO DIFFERENT PARABOLIC TIP CURVATURE $\left(\frac{k_s}{k_l} = 4\right)$	133
6.6	PLOT OF DENDRITE GROWTH RATE AS A FUNCTION OF SUPERCOOLING ΔT FOR ICE	134

NOMENCLATURE

Notation

A	constant defined after equation (2-8)
A_i	area of subtriangle in six node element
A^m	area of m^{th} element
a	thermal diffusivity
a_k	defined after equation (3-50)
b_k	defined after equation (3-49)
c	specific heat
D	domain under consideration
d_c	characteristic length
E_i	exponential error integral
\bar{G}	vector defined after equation (3-56)
g_l	defined after equation (3-37)
g_s	defined after equation (3-38)
$I(\theta)$	variational integral
K	index in a description of the ϕ perturbation of the form $\cos(K\phi)$
\bar{K}	curvature
k	thermal conductivity
L	latent heat of fusion
L_1	defined after equation (2-12)
L_2	defined after equation (2-13)
n	constant defined after equation (2-8)
\bar{n}	unit normal vector
P_i	defined after equation (3-48)

QA_{ij}^m	matrix defined after equation (3-55)
R, r	radius of curvature
r, ϕ, z	cylindrical coordinates
r^*, R_c	critical radius after equation (3-1)
Ste	Stefan number
ΔT	supercooling
T_f	equilibrium fusion temperature
t	time
U_n	velocity defined after equation (3-4)
v	interface velocity, equation (3-14)
v_c	characteristic velocity
v'	non-dimensional velocity
V	velocity of growth
x, y, z	cartesian coordinates
Y_{lm}	spherical harmonics
$\alpha, \beta, \hat{\theta}$	defined after equation (3-28)
γ	specific surface energy
Γ	γ/L
$\Gamma, \Gamma_1, \Gamma_2$	contours under consideration
δ	amplitude of perturbation
$\delta I(\theta)$	first variation of the integral $I(\theta)$
ϵ	defined after equation (3-4)
η	non-dimensional coordinate in r direction
θ	non-dimensional temperature
θ_{if}	non-dimensional interface temperature
μ	chemical potential

ξ	non-dimensional coordinate in z direction
α	stability criterion
σ	density
ψ_i	area coordinates
χ_i	defined after equation (3-42)
∇^2	Laplacian operator

Subscripts

l	liquid
s	solid
if	interface conditions

CHAPTER 1

INTRODUCTION

The problems related to the crystallization mechanism of supercooled liquids have been studied theoretically and experimentally for some time by physical chemists and materials scientists. In recent years, however, the subject of crystal nucleation and growth has received a large amount of attention from scientists and engineers working in such diverse areas as solid state physics, medicine, biological sciences, atmospheric sciences, solar energy utilization (thermal energy storage), and desalination of ocean water. The overall crystallization process is determined by transport effects (heat and mass transfer) as well as interface effects (surface tension and growth kinetics). Discussions of mechanism of crystal growth must consider both, as well as the nucleation process itself. As Mott [1] pointed out, the transport process may usually be treated as macroscopic, involving the processes of diffusion of heat or matter. On the other hand, the interface process involves the detailed atomic structure of the surface.

Depending on the system studied, either the transport or the interface effects may be the slower and hence will be the rate controlling process. Alternatively, both processes may control

the rate together and indeed, interact with each other [2]. In many situations, however, the rate of removal of latent heat controls the rate at which crystallization can proceed. If this is the case the problem of determining the rate at which the interface boundary advances through the medium reduces to one of calculating the temperature distribution in the solid and liquid phases.

An important factor controlling the micro- and macro-structure of the crystal grown from the melt is the direction of the heat flux at the interface boundary. For solidification of a melt which is above its equilibrium fusion temperature, heat flows from the melt to the interface and solidification must be maintained by conduction of heat from the interface into the crystal. For a one component system in which heat transfer is the limiting process the resulting interface tends to be smooth and isothermal. However, for a crystal growing into a supercooled melt (temperature less than the equilibrium fusion temperature) heat flows from the interface to the melt. In this case the growing interface will tend to be unstable and dendritic growth will result. It is to problems of instability and dendritic growth that this thesis will be addressed.

The term 'dendritic growth' when used in reference to solidification suggests a tree-shaped crystal structure, that is a crystal with an intricate network of branches. Dendritic solidification is characterized by a morphology resulting

from the growth of long, thin spikes in specific crystallographic directions, with regular branches in other equivalent directions. The branching habit extends to secondary, tertiary, and sometimes higher orders. The main qualitative experimental observations are: (a) that for a pure melt, dendritic growth takes place only when the melt is supercooled, (b) that the directions of growth are always strictly crystallographic, (c) branching occurs at roughly regular spacing, smaller for each successive order of branching, and (d) that only a small portion of liquid solidifies in this way [3]. Crystal growth from all three states of matter—vapour, liquid and solid—is known to produce this type of morphology.

The subject of dendritic growth has a whole series of important consequences for the growth of crystals of many commonly used materials. Some idea of the scale of this can be judged from the fact that hundreds of million tons of steel are produced annually, all of which has undergone dendritic growth. There is a wide range of data available in the literature on the growth of dendrites in different systems (metals, ice, phosphorus, solid state precipitates, and ionic crystals from aqueous solutions). These data give an understanding, in a qualitative sense, of the basic phenomena associated with dendritic growth. However, to examine this understanding from a quantitative viewpoint, the complex heat flow problem with moving boundary has to be solved. In

a general theoretical examination of the problem the essential difficulty resides in the fact that the position of the boundary on which one wishes to apply boundary conditions is not known; finding its position is part of the problem. This makes the problem non-linear so that solutions may not be built up by superposition. Consequently, analytical solutions must be sought through application of approximate methods.

A review of past analytical research in the area of dendritic growth theory suggests that these techniques may have reached the limit of their usefulness and further progress in the area may require the exploitation of numerical methods. It is believed that the Finite Element Method is well suited to solve such problems, since the basic concepts of this method have already been found to possess general applicability to a wide range of field problems. Indeed, in addition to the usual applications in structural and continuum mechanics [4], use can also be found in many other fields. Problems in such diverse fields as water seepage [5], irrotational flow of ideal fluids [6], electrical fields [7], and heat conduction [8] have already been studied by the finite element approach.

It is the purpose of the present work to examine the applicability of the finite element method to the study of crystal growth transport processes. Specifically, the method will be tested on two types of problems. The first is an

investigation of the morphological stability of cylindrical and spherical particles undergoing radial growth controlled by diffusion. The second is the prediction of the growth velocity of a fully developed dendrite as a function of supercooling. The primary motivation is to see if the finite element method can improve our understanding of the crystallization process.

To this end, a brief literature survey is made in Chapter 2 in order to establish a relation between the present work and what has been reported previously. Chapter 3 is devoted to fundamental theory, which includes definitions and basic equations relevant to this study, the variational principle, and fundamental concepts of finite element analysis and the Ritz technique. Chapter 4 presents the analysis of morphological stability of spherical and cylindrical particles growing in supercooled liquids. Chapter 5 contains the analysis of dendrites with the shapes of parabolic cylinders and paraboloids of revolution. In Chapter 6, an attempt has been made to demonstrate that the finite element method can be used to study the time dependent growth of dendrites.

The results obtained by the present approach are compared with those previously obtained by other methods, either theoretical or experimental. It is found that good agreement exists among the results predicted by these different methods.

Based on the fact that the results compare well for the problems that were treated, it is suggested that the finite element method may be developed into a useful tool in the analysis of other crystal growth problems.

CHAPTER 2

LITERATURE SURVEY

2.1 Introduction

A review of the most significant contributions to the area of morphological stability in crystal growth and in particular to that of dendritic growth will be presented here. Due to the vast literature associated with crystal growth problems, only those papers which are pertinent to the present investigation will be cited. An excellent survey of literature on crystal growth mechanisms is given in the works of Parker [2] and Jackson [9]. For a historical review of the general problem of dendritic growth, the reader is referred to the study by Smith [10].

2.2 Experimental Investigations

The term dendrite was apparently first introduced to the world of crystal growth by Tschernoff in 1879 [10]. He used it to describe the highly branched structure he found in the centre of metal ingots. With the recognition of crystal structure of metals it was assumed, and later demonstrated, that the directions of the various dendrite arms coincided with crystallographically significant directions of the structure.

The modern impetus to this area of crystal growth science may be traced to the experimental studies of Chalmers and his collaborators [11-16], who demonstrated that the dendrites represent the most advanced stage of interfacial instabilities in a wide class of materials. With the help of experiments, Wineburg and Chalmers [11,12] also showed that dendritic growth is observed only if the liquid is at a lower temperature than the interface.

2.2.1 Dendritic Growth Rate

The growth rate of dendrites for various amounts of supercoolings has been measured in pure water [17], tin [14,18], nickel [19], lead [14], and plastic crystals [20]. However, some of these investigations dealt with the growth rate of crystals in contact with a solid substrate, which bear little relationship to the results obtained in free growth from the melt.

Wineburg and Chalmers [12] measured the free growth of lead dendrites, and showed that the dendrites grew much faster than the smooth interface. Rosenberg and Winegard [18] measured the growth rate of dendrites in a supercooled bath of tin with a range of supercooling from 0.4°C to 11°C. They found that there was a substantial scatter in the results, and a factor of three existed between the highest and lowest values for a given temperature.

Lindenmeyer and Chalmers [13] measured the free growth of ice in pure water along the basal plane at bath supercoolings between 2° and 6.5°C. They reported the free growth rate v in distilled water to be

$$v = 0.028 (\Delta T)^{2.39} \quad \text{cm/sec,} \quad (2-1)$$

where ΔT is in °C. In distilled water having similar supercooling, they observed that the growth rate upon a substrate was as much as an order of magnitude faster. It was surmized that this difference was due to the proximity of a heat sink which allowed a more efficient removal of latent heat. They concluded from this result that the rate of growth of ice crystals in water is limited by the conduction of latent heat into the water for free growth, and into the water, the solid wall, and across the solid wall into the bath for growth on a substrate.

Walker [19] made extensive measurements on the growth of dendrites in nickel and cobalt, and plotted the growth velocity against the square of the supercooling. He found that up to a supercooling of almost 175°C, the results fell on the $v \propto (\Delta T)^2$ line.

Ryan [21] investigated the free growth of single ice crystals in supercooled water, and measured growth rates for supercoolings ranging from 0.1 to 2.5°C. His data do not conform to the $v \propto (\Delta T)^n$ law for the entire range of supercooling. In the range of 0.1°C to 1.3°C, the growth rate obeys

approximately a power law of supercooling. Ryan also reported that in the range of subcoolings from 0.2 to 1.5°C the shape of the dendrite tip may be approximated by a parabolic platelet. His results also showed that the tip radius decreases as the supercooling increases.

Mason [22] has reported that ice crystals grow as needles (paraboloids of revolution) when grown in water in the supercooling range from 3 to 5°C. Hallet [23] measured the growth rates of ice dendrites growing parallel to the basal plane in supercooled water, and his data followed the relation

$$v = 0.08 (\Delta T)^{1.9} \text{ cm/sec,} \quad (2-2)$$

for supercooling between 0.1°C and 2.0°C. He also found that the dendrite arm width and spacing decreased with increased supercoolings.

Macklin and Ryan [24] made a detailed study of the growth of ice in pure water at supercoolings up to 7.5°C. They reported growth velocities which approximately fit the relationship

$$v = 0.0227 (\Delta T)^{2.29} \text{ cm/sec,} \quad (2-3)$$

where ΔT is in 0.°C.

Pruppacher [25] determined the rate at which ice crystals grow freely in supercooled water and in dilute aqueous solutions of various salts. He reported that at

supercoolings between 0.5°C and 9°C, the growth rate of ice dendrites can be represented by the relation

$$v = 0.035 (\Delta T)^{2.22} \text{ cm/sec,} \quad (2-4)$$

He also concluded that dissolved salts affected the growth rate of ice crystals in a systematic manner. At concentrations larger than 10^{-2} moles/liter all salts reduced the growth rate below the one in pure water by an amount which depended on type of salt in solution. At concentrations smaller than 10^{-2} moles/liter some salts did not affect the growth rate whereas others increased it over and above in the pure water. He concluded that at low solute concentrations the growth rate of ice in aqueous solutions is limited by the rate of dissipation of latent heat. As the solute concentration increased, the rate of diffusion of solute atoms away from the interfacial became increasingly important.

Glicksman and Schaefer [26] have reported some results on the in situ observations of dendritic solidification in pure tin. They used cinematographic techniques to obtain quantitative data on the variation of tip profile as a function of the growth speed, and on the transition of periodic edge-profile perturbations into true dendritic side branches. They observed that the approximation of a parabolic dendrite tip appeared satisfactory over a distance of about 9 tip-radii back from the nose of each dendrite. Further back than about 9 tip-radii the dendrite's shape became increasingly distorted

from a parabola by the combined influences of side-branching and interferring neighboring thermal diffusion fields.

Kallungal [27] and Kallungal and Barduhn [28] conducted extensive experiments to measure the growth rate of ice crystals in slightly supercooled water. They observed that the shape of ice dendrites was neither 2-D parabolic cylinder nor axisymmetric paraboloid of revolution, but it was similar to an elliptic paraboloid. They also reported that the ice crystal growth in slightly subcooled quiescent water could be represented by the relation

$$v = 0.0118 (\Delta T)^{2.17} \text{ cm/sec,} \quad (2-5)$$

where ΔT is in $^{\circ}\text{C}$.

Kallungal and Barduhn [28] also measured the tip radius of curvature of ice crystals and observed that the tip radii could be expressed by the relation

$$R = 0.61/\Delta T \text{ microns} \quad (2-6)$$

where ΔT is in $^{\circ}\text{C}$ and is in the range of 0.1° to 1°C .

Glicksman, Schaefer, and Ayers [20] designed an experimental set up to study the dendritic growth in supercooled succinonitrile, a low entropy-of-fusion plastic crystal. They measured the growth rate of dendrites for free growth conditions as well as confined growth conditions. They reported that for free growth, the growth rate data fitted a relation

$$v = (\Delta T)^{2.6} \text{ cm/sec,} \quad (2-7)$$

for supercoolings ranging from 0.1°C to 7°C. They also measured the tip radii of curvature, and reported that the tip radius of curvature was inversely proportional to the amount of supercooling. Furthermore, they found that near the tip, the dendrites were almost paraboloids of revolution. They compared their experimental results with three different steady-state theories and found that full agreement between steady-state theory and experiment was clearly lacking. They reported that the velocities obtained by theoretical methods were considerably higher than the experimental values. However, they found that all the non-isothermal steady-state theories considered, predicted the correct Peclet number-supercooling relationship over a limited range of supercooling. They also reported that the interfacial molecular attachment kinetics are sufficiently rapid not to influence significantly the axial growth rate of freely growing dendrites of succinonitrile over a limited range of supercooling.

Summarizing the experimental work on the dendritic growth rate it can be concluded that although no two investigators agree on the reported value of the growth rates, the experimental data usually conform to a curve of the form

$$v = A \Delta T^n \quad (2-8)$$

where v is the growth velocity, ΔT is the supercooling and

A and n are constants for a given material. For all the measurements, n lies between 1.5 and 3.0. Also, the shape of the dendrite tip is somewhere between a paraboloid of revolution and a 2-D parabolic cylinder depending on the material. Finally, the radius of curvature at the tip of dendrites is reported to be proportional to $1/\Delta T$ by all the investigators.

2.2.2 Morphological Stability

Morphological stability in crystal growth is concerned with the stability of a particular shape of solid, growing from melt, solution, or vapour by diffusional process, that is, whether it is stable against small perturbations in shape.

Arakawa [29], and Arakawa and Higuchi [30] studied the growth of ice crystals in water and observed that when the supercooled water (temperature about -0.5°C) was nucleated by placing small hoar frost crystals on the surface, needle and circular disc crystals grew outwards from the nucleating crystals. The circular disc crystals developed notches around their edges as they grew, and later they became six-sided dendrites.

Williamson and Chalmers [31] photographed growing ice discs in slightly subcooled water and observed that at subcoolings greater than 0.4°C , the disc morphology became unstable and small protuberances appeared on the edge of the disc. At subcoolings greater than 0.6°C , ice assumed the characteristic dendritic appearance shown by snow flakes.

They reported that as the supercooling was made greater than 1°C, dendrites with side-branches appeared in specifically preferred growth directions. Also, as the subcooling was increased the spacing between dendrite arms decreased and they found that the dendrite arm width and spacing obeyed the following relation approximately:

$$\begin{array}{llll} \text{arm width} & 10^{-2}/\Delta T & \text{cm} \\ \text{arm spacing} & 10^{-2}/\Delta T & \text{cm} \end{array}$$

Lindenmeyer and Chalmers [32] showed that a circular crystal became hexagonal in shape and finally developed into a dendrite crystal with six arms.

Morris and Winegard [33] photographed the growing dendrites and observed that the dendrites tip grew with a variable shape, and fluctuated in a periodic manner as it propagated into the melt. From their photographs it is evident that the tip continuously grew larger in radius and subsequently small irregularities occurred which eventually grew into primary branches.

Hardy and Coriell [34,35] have made measurements of the growth (and decay) of perturbations on single crystal cylinders of ice growing from slightly supercooled distilled water. Ice crystals were grown with the basal plane normal to the axis of the cylinder. Hence, growth was occurring parallel to this plane; the kinetic coefficient for such

growth is known to be sufficiently large so that the kinetic (interface attachment) contribution to the undercooling was negligible in those experiments. Due to the low undercoolings and small growth velocities, the conditions were close to steady-state. The ice crystal was first allowed to come into equilibrium with a large bath of water at a temperature slightly above 0°C. The temperature of the bath was decreased by about 0.1°C and the ice crystal started to grow from radius of about 0.05 cm. The crystal could be rotated about its axis, and photographed from the side so the radius and size of the perturbations could be measured. They reported that at first the ice crystal grew as a regular cylinder and the solid-liquid interface could be characterized by an equation (in cylindrical coordinates r, ϕ, z) of the form $r = R$ where R depends on time but not on z and ϕ . As the cylinder grew, instabilities developed and the topography of the unstable interface could be approximately characterized by the equation

$$r = R + \delta \cos(K\phi) \quad (2-9)$$

where $K=6$ or 12 , and δ is a small amplitude factor. At a later stage, perturbations also developed along the z direction.

In concluding the experimental literature survey, it should be pointed out that though a wide range of experimental data exist on the problems of morphological stability and dendritic growth, care must be exercised when comparing them with theory because the precise conditions under which the

experiments were conducted are often not known.

2.3 Theoretical Investigations

While the bulk of experimental investigations of dendritic growth have been about equally divided between free growth and confined growth, this certainly is not true of theoretical investigations reported in literature since the overwhelming majority of these works have dealt with free growth conditions. As mentioned earlier, either diffusion process or interface kinetics limit the growth rate under free growth conditions. For this paper we will review only those theories which consider the diffusion process as the rate controlling process as the crystallization proceeds, although we will mention the use of interface kinetic laws as boundary conditions for the transport process.

2.3.1 Dendritic Growth Rate

Papapetrou [36], in a classical study of dendritic growth, suggested that the tip of a dendrite has the form of a paraboloid of revolution. But it was G.P. Ivantsov [37] of the Soviet Union who made the first serious attempt to make a mathematical analysis of dendritic growth rates into its supercooled melt. He showed that some aspects of dendritic growth could be described quantitatively with heat flow theory applied at a suitable microscopic level. Using the suggestion of Papapetrou [36], he assumed that the tip region of a

dendritic trunk may be adequately represented by a paraboloid of revolution. He further assumed that the crystal was isothermal and advancing at a constant velocity v , into an isothermal, undercooled bath at temperature T_α . He obtained the solution to the moving boundary problem diffusion equation and showed that the dendrite obeys the equation

$$-vR/2a_l \exp(vR/2a_l) \text{Ei}(-vR/2a_l) = \Delta T c_l/L \quad (2-10)$$

where v is the growth rate, R is the dendrite tip radius, a_l and c_l are the thermal diffusivity and the specific heat of the melt, L is the latent heat of fusion, ΔT is the amount of bath supercooling, and E_i is the integral error function. However, the above solution does not completely specify the conditions of growth. A diffusion solution can be obtained for a given undercooling provided the product vR is constant, as is evident from above equation (2-10). Thus, for a given bath supercooling, thin dendrites growing rapidly or thick dendrites growing slowly can both satisfy the diffusion conditions. Commonly, a value of R which maximizes v would be sought but this is impossible since $vR = \text{constant}$.

In 1960, D. E. Temkin [38], also of Soviet Union, recognized the limitations of the Ivantsov analysis and argued that the assumption of an isothermal interface was fundamentally incorrect. He noted that the very existence of the variation in curvature along the surface of the dendrite implies that the equilibrium fusion temperature must vary with position in

accordance with the Gibbs-Thompson relationship. Temkin also introduced linear interface kinetics into the problem. For mathematical simplicity, Temkin assumed that the shape is still a paraboloid of revolution. He also assumed that Laplace equation could be used for the problem with small bath undercoolings, that is when $vR/a_l \ll 1$. He obtained the solution to the diffusion problem with above mentioned condition to be

$$vR/2a_l \exp(vR/2a_l) E_i(-vR/2a_l) = \frac{\Delta T}{L} \frac{c_l \rho_l}{\rho_s} \left[\frac{1}{1 + L_1/\mu R + L_2\gamma/vR^2} \right] \quad (2-11)$$

where μ is the interface kinetic coefficient, γ is the specific surface free energy and ρ_l and ρ_s are the density of the liquid and the solid phase respectively. The coefficients L_1 and L_2 are defined by

$$L_1 = (1.33 + 0.60 \frac{k_l}{k_s}) \frac{a_l c_l}{L}, \quad (2-12)$$

and

$$L_2 = (3.86 + 2.08 \frac{k_l}{k_s}) \frac{a_l c_l T_f}{\rho_l L^2}, \quad (2-13)$$

where T_f is the fusion temperature of the pure bulk material and k_l and k_s are the thermal conductivities of the liquid and solid.

The major difference between the Temkin and Ivantsov results is that the former exhibits a maximum in the function v versus R . Temkin chose the value of R to be the actual tip radius which corresponded to the maximum velocity of growth. For $vR/2a_l \ll 1$, Temkin showed that the equation (2-11) may be written in the following approximate form,

$$\frac{vR}{2a_l} = L_3 \left[\frac{\rho_l \Delta T c_l / L}{\rho_s (1 + L_1/\mu R + L_2 \gamma/vR^2)} \right]^n \quad (2-14)$$

where $L_3 = 0.457$, and $n = 1.21$. Temkin applied the maximum growth rate principle to equation (2-14) to get,

$$v = \frac{(2n-1) L_2 \gamma}{R [R - (n-1) L_1/\mu]} \quad (2-15)$$

and R is obtained from the relation

$$\left(2 + \frac{L_1}{\mu R}\right)^n = \frac{2 \rho_l L_3 a_l}{\rho_s (2n-1) L_2 \gamma} \left[\frac{(2n-1) c_l \Delta T}{nL} \right]^n \left[R - (n-1) \frac{L_1}{\mu} \right] \quad (2-16)$$

Thus, according to Temkin, the simultaneous solution of equations (2-15) and (2-16) uniquely predicts both the velocity and tip radius of a freely growing dendrite for a given bath undercooling.

For the special case where the kinetic coefficient, μ , is very large we may neglect the term L_1/μ in equations

(2-15) and (2-16) to obtain

$$R^2 = (2n-1) L_2 \gamma / v, \quad (2-17)$$

and

$$v = \frac{4L_3^2 a_l^2}{(2n-1) \gamma L_2} \left[\frac{(2n-1) \rho_l c_l}{2n \rho_i L} \right]^{2n} \Delta T^{2n} \quad (2-18)$$

At approximately the same time as the Temkin paper, Bolling and Tiller [16] presented an excellent physical picture of the effects of non-isothermality on the growth of a dendrite. Independent of Temkin they also recognized the non-isothermality of a dendrite due to the variation of curvature and kinetics over the surface. They showed that the variation of temperature in the solid gives rise to a heat flux in addition to the latent heat term at the tip of the dendrite. Thus, the velocity of a non-isothermal dendrite will be reduced compared to an isothermal dendrite under similar conditions. Bolling and Tiller also attempted to derive expressions which would determine both the maximum velocity and the corresponding tip radius. In spite of the fact that in a later analysis Kotler and Tarshis [39] have shown that their calculations had some mathematical inconsistencies, the Bolling and Tiller [16] work contains numerous useful contributions to the understanding of dendritic growth. Bolling and Tiller gave a detailed review and discussion of the following general assumptions made in the analysis of

dendritic growth by theoretical investigators in this field.

These assumptions are:

- (a) growth occurs at a constant speed (quasi-stationary process),
- (b) the dendrite shape is either a parabolic cylinder or paraboloid of revolution,
- (c) the liquid domain is infinite,
- (d) the maximum velocity condition is used to specify the velocity,
- (e) natural convection due to density differences in solid and liquid phase is neglected.

Horvay and Cahn [40] analyzed the dendrite growth problem using four different geometries for the crystal shape; namely (a) parabolic cylinder, (b) elliptic paraboloid, (c) paraboloid of revolution, (d) spheroidal. However, they considered the dendritic interface to be isothermal.

Treating the problem in parabolic coordinates in a moving frame of reference; they used the conventional technique of separation of variables. For each geometry, they were able to express the growth rate as

$$v = a_0 (\Delta T)^n / R \text{ cm/sec.} \quad (2-19)$$

where ΔT is in $^{\circ}\text{C}$. The factor a_0 varied by almost two orders of magnitude between the parabolic cylinder and the paraboloid of revolution.

Hillig [41] solved the steady-state growth of a dendrite platelet into its pure supercooled melt by using what he called a "self-consistent" method. This method requires solution for the shape of the crystal that simultaneously satisfies the required heat flow and temperature variation over the dendrite surface. In his method, the temperature at infinity was not assumed but calculated using a Taylor expansion. He concluded that the assumption of steady state is probably invalid. He suggested that possibly the shape is oscillatory in time and the dendrite moves with a constant average velocity.

Trivedi [42] presented an exact solution to the heat flow equation for the growth of dendritic needles (paraboloids of revolution) in a supercooled melt. His final result is similar to the equation [2-11], but his values for L_1 and L_2 are not constants but functions of the thermal Peclet number. He also compared his theoretical results with experimental results on phosphorus and obtained good agreement.

Trivedi [43] also analyzed the growth of non-isothermal dendritic plates (parabolic cylinders) growing in a supercooled melt. He expressed the solution for this problem as

$$\left(\frac{\pi v R}{2a_l}\right)^{1/2} \exp\left(\frac{vR}{2a_l}\right) \operatorname{erfc}\left(\frac{vR}{2a_l}\right)^{1/2} = \frac{c_l \Delta T}{L} \frac{1}{[1 + L_1/\mu R + \gamma L_2/vR^2]}$$

where L_1 and L_2 are of the form defined by equation (2-12) and equation (2-13), but have different values from the case of the paraboloid of revolution. For the case where kinetic effects may be neglected and the Peclet number $\frac{vR}{2a_l}$ is small, the above result can be simplified to give

$$\frac{vR}{2a_l} = \frac{1}{\pi} \left[\frac{c_l T/L}{1 + \gamma L_2/vR^2} \right]^2 \quad (2-21)$$

Differentiating equation (2-21) with respect to R and setting $\frac{dv}{dR} = 0$ gives

$$R^2 = 3\gamma L_2/v. \quad (2-22)$$

Substituting equation (2-22) into equation (2-21) results in the growth model for a parabolic cylinder as

$$v = \frac{27}{64} \frac{a_l^2}{\pi^2 \gamma L_2} \left(\frac{c_l \Delta T}{L} \right)^4 \quad (2-23)$$

Holzman [44,45,46] has made analysis similar to but independent of Trivedi for both parabolic platelet and paraboloid of revolution. He questioned the traditional time invariant shape of the dendrites. To maintain a time invariant shape, the heat balance at the solid-liquid interface requires that the sum of heat fluxes in the solid and liquid at each point of the advancing interface must be equal to the local rate of release of heat of fusion. Holzman found that this

is not true, and he calculated a quantity he called "excess velocity", which is the difference between the true local growth velocity required to satisfy heat balance, and the growth velocity predicted for the hypothetical steady state (shape preserving) model. His results show that the hypothetical parabolic or paraboloidal interface tends to bulge with a pronounced peak at about one radius back from the tip of the dendrite.

The analyses of dendritic growth which we have just reviewed have all been mathematical and based on idealized, though more and more realistic formulations of the problem. With the advent of high speed computers the numerical analysis of more realistic models became possible. Geering, Oldfield and Tiller [47] were the first to analyze the dendritic growth problem using a computer model. They simplified the problem considerably by considering only one-dimensional heat transfer. This was done by choosing the subdivisions (or boxes) of the domain so that two sides were always isotherms and the other four were orthogonal surfaces. The computer algorithm for choosing the boxes in this way was analogous to seeking an orthogonal set in a mathematical solution. They checked the results obtained from the computer model against Ivantsov's solution and found to be in excellent agreement. They also used the model with heat flow and interface curvature effect taken into account and found in agreement with Temkin's analysis for pure tin.

Oldfield [48] extended the above mentioned computer model to simulate the long term growth of tin dendrites. He obtained the smoothed velocity of the dendrite tip and found that the growth of the dendrite was accompanied by changes in shape and a fall in the growth velocity. Oldfield surmized that the dendrite grows with a cyclic fluctuation in velocity, forming a new branch in each phase of slow growth. However, the above mentioned computer models were quite simplified in form and the heat flux in the solid was neglected.

Recently, Langer and Muller-Krumbhaar [49-51] have suggested replacing the widely used maximum velocity principle by a stability criterion of the form $vR^2 = \text{constant}$, where v is the growth velocity and R is the corresponding tip radius of the dendrite. They claim that this type of stability criterion is valid for small Peclet numbers. They found that a direct evaluation of the relevant constant of proportionality yields values of v and R , as function of undercooling which are in substantial agreement with the measurements of Glicksman et al. [20] on dendritic growth of succinonitrile crystals. Using the Langer-Muller-Krumbhaar stability theory Langer, Sekerka and Fujioka [52] have presented a universal law for dendritic growth rates. They checked their universal law with measured values on ice and succinonitrile dendrites and obtained good agreement.

Summarizing, we find that both isothermal and non-isothermal theories predict that the growth rate decreases as

we change the shape from a paraboloid of revolution to that of a parabolic cylinder. The exponents on subcoolings, ΔT varies from 2 to 4 and the growth rates predicted at a given ΔT vary by about 5 orders of magnitude.

2.3.2 Morphological Stability

The stability is tested in theoretical development, by assuming an arbitrarily small perturbation in shape to be present, and then seeing whether this perturbation will grow or decay. This is different from the question of whether the shape and equations are shape preserving (dendritic growth problem).

Mullins and Sekerka [53] in a classical paper, introduced into crystal growth studies the concept of quantitative testing for shape stability. Prior to this paper, the shape preserving ellipsoids of Ham [54] were generally believed to imply that such shapes were stable whereas in fact they had not been tested for stability.

Mullins and Sekerka [53] studied the stability of the shape of a spherical particle undergoing diffusion controlled growth into an initially uniformly supersaturated matrix. This was done by supposing an expansion, into spherical harmonics, of an infinitesimal deviation of the particle from sphericity and then calculating the time dependence of the coefficient of the expansion. It was assumed that the pertinent diffusion field obeyed the Laplace's equation, an assumption

whose conditions of validity were discussed in detail. It was shown that the sphere is stable below and unstable above a certain radius R_c , which is just seven times the critical radius of nucleation theory. They were able to look at any arbitrarily shaped perturbation by examining each of its harmonics. If any of these harmonics evolve with a faster growth rate than the smooth interface, then this interface will become unstable. The perturbation method of Mullins and Sekerka has proven to be a most valuable tool in the development of the theory of interface stability.

Coriell and Parker [55] extended the results of Mullins and Sekerka for the sphere to the case of cylinder. Both perturbations in circular cross-section shape were considered as well as perturbations along the length of the cylinder. For a perturbation of the form $r = R + \delta \cos(K\phi)$, where k is a positive integer, the cylinder was found to be stable when its radius was less than a critical radius R_c , and unstable when greater than R_c , analogous to the case of a sphere.

Tarshis [56] followed the perturbation procedure originally proposed by Mullins and Sekerka [53], but modified it slightly to incorporate a coupling equation which provided a means of systematic inclusion of other physical factors. The results of his study indicated that interface attachment kinetics can markedly affect the stability criterion. Tarshish considered the stability of a single protuberance and not of the individual harmonics making up some arbitrary

distortion, as in the perturbation method.

Kotler [57] analyzed the stability of the dendrite step, employing a right circular cylinder as its physical representation. He also treated the stability of the paraboloid of revolution with the major emphasis on the region near the tip. In each of these cases he took into account the interface curvature effects as well as attachment kinetics. He concluded that the region of greatest instability, for most metals and ice, appeared to be less than one tip radius behind the dendrite tip.

To summarize, it would seem that at present the theoretical methods have arrived at a point at which improvements are very difficult to achieve. It may however be that progress can be made using some form of approximate numerical method. Since the interface shape is always curved, and boundary conditions are complex, the finite element method seems to be an appropriate choice. The finite element method has been successfully used to solve various partial differential equations of fluid-mechanics and heat transfer, and fundamentally the dendrite problem seems to be similar in form. The next chapter describes the proposed method in detail.

CHAPTER 3

FUNDAMENTAL THEORY

In this chapter the fundamental theory on which this research is based will be presented. The first portion deals with the aspects of thermodynamics that have special relevance to the crystallization process, while the later portions deal with the mathematical formulation of the problem. A brief description of the finite element method is also presented for the benefit of those unfamiliar with the method.

3.1 The Physics of Freezing

In most engineering literature the process by which a liquid solidifies is described as occurring in three heat loss stages. First the liquid which was initially at some temperature above freezing cools to its equilibrium freezing temperature. Then with further heat loss, solidification begins and continues for some time (depending on the latent heat of fusion and the rate of heat loss) at constant temperature. Finally, when all the liquid has turned to solid, the solid begins to cool. For example, suppose 1 gm of water, initially at 40°C and atmospheric pressure is to be cooled at a rate of heat loss, say 1 cal/min. The cooling process can be depicted ideally by Figure 3.1. The cooling

continues at a constant rate for 40 minutes, at the end of which the temperature is 0°C . With further heat loss, ice begins to form and continues forming for 80 minutes (the heat of fusion of ice is, 80 cal/gm), during which time the temperature remains at 0°C . At the end of the 80 minutes, cooling proceeds once more, but now at a rate of approximately 2°C/min because the specific heat of ice is approximately $0.5 \text{ cal/gm}^{\circ}\text{C}$.

In reality, when a quantity of liquid is cooled, freezing does not occur in the ideal way shown in Figure 3.1. Actually, if there is no solid phase present a liquid can be cooled substantially below its equilibrium fusion temperature before freezing occurs. Such a liquid is in a metastable supercooled state. It is found experimentally that the maximum supercooling attainable increases with increasing purity of the liquid, particularly as far as foreign particles in suspensions are concerned, and that it is easier to supercool small droplets than larger volumes of liquid. Both these effects are easily accounted for by the assumption that foreign solid particles assist the freezing transition, division of a sample of liquid into many small droplets effectively isolating the most active foreign particles into a small fraction of the total number of droplets. For example, we may easily cool tap water to -4 to -7°C , while water droplets can exist down to -40°C [58]. Except in the case of materials which form glasses, it is not possible to maintain

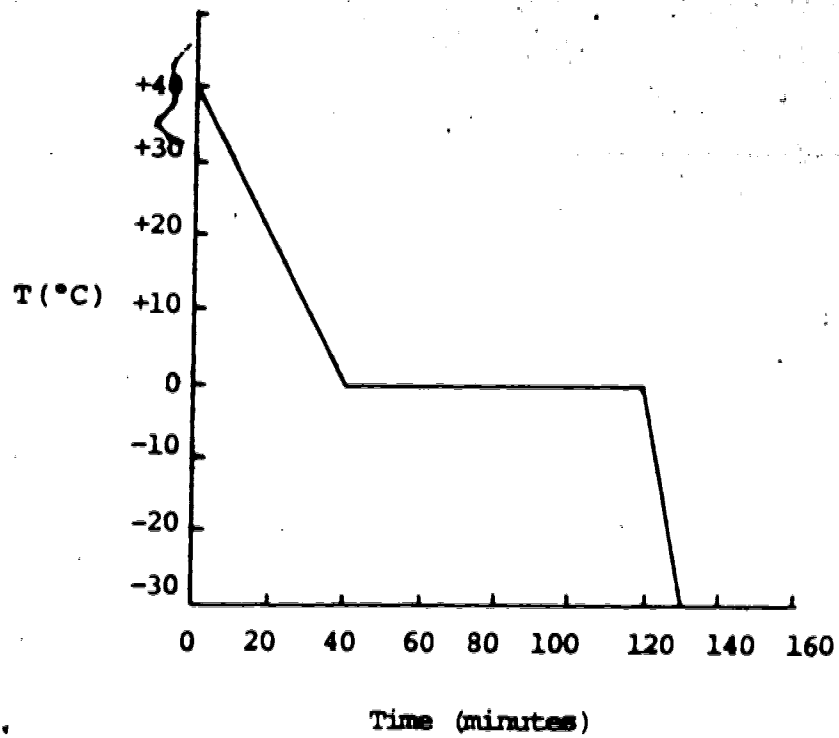


Figure 3.1 Ideal Cooling Curve for Water
(From Knight [58])

the supercooled state indefinitely or to achieve more than a limited degree of supercooling before spontaneous freezing occurs. Figure 3.2 shows a more realistic graph of cooling process of 1 gm of water at 1 atmospheric pressure when cooled at a rate of 1 cal/minute.

This behaviour can be very simply understood from consideration of the process of freezing. From Figure 3.3, which shows the free energy-temperature diagram with a P-T diagram, it is clear that at any temperature below that of equilibrium, the free energy of the solid is less than that of the liquid, thus it is energetically favourable for the liquid to change to the crystalline state. This can not be accomplished discontinuously; first a very small volume of liquid must crystallize and this crystal must then grow until all the liquid has frozen. A small crystal embryo is, however, in an energetically unfavourable state because of its very large surface-to-volume ratio and the positive free energy associated with its interface with the liquid. There is thus a free energy barrier to be overcome before freezing can commence and this barrier can only be surmounted by a nucleation process depending upon thermal fluctuations. The stability of a small crystal embryo may be enhanced if it grows closely upon an insoluble foreign particle and in this case the nucleation process is termed heterogeneous. If there are no foreign particles or surfaces present, then freezing must commence by a process of homogeneous nucleation within the pure liquid

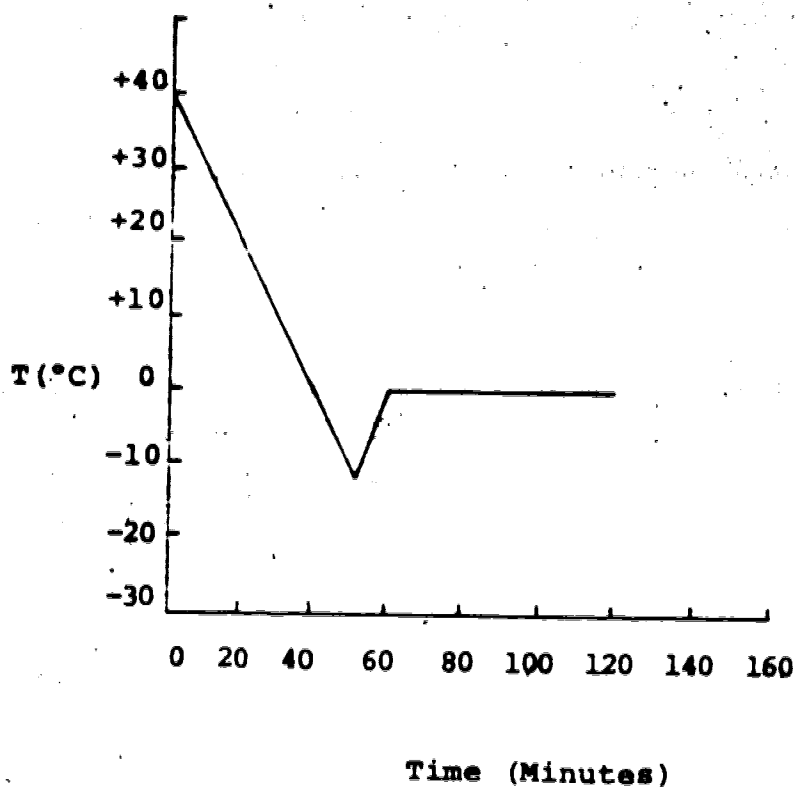


Figure 3.2 A Less Ideal Cooling Curve for Water Showing Supercooling (From Knight [58])

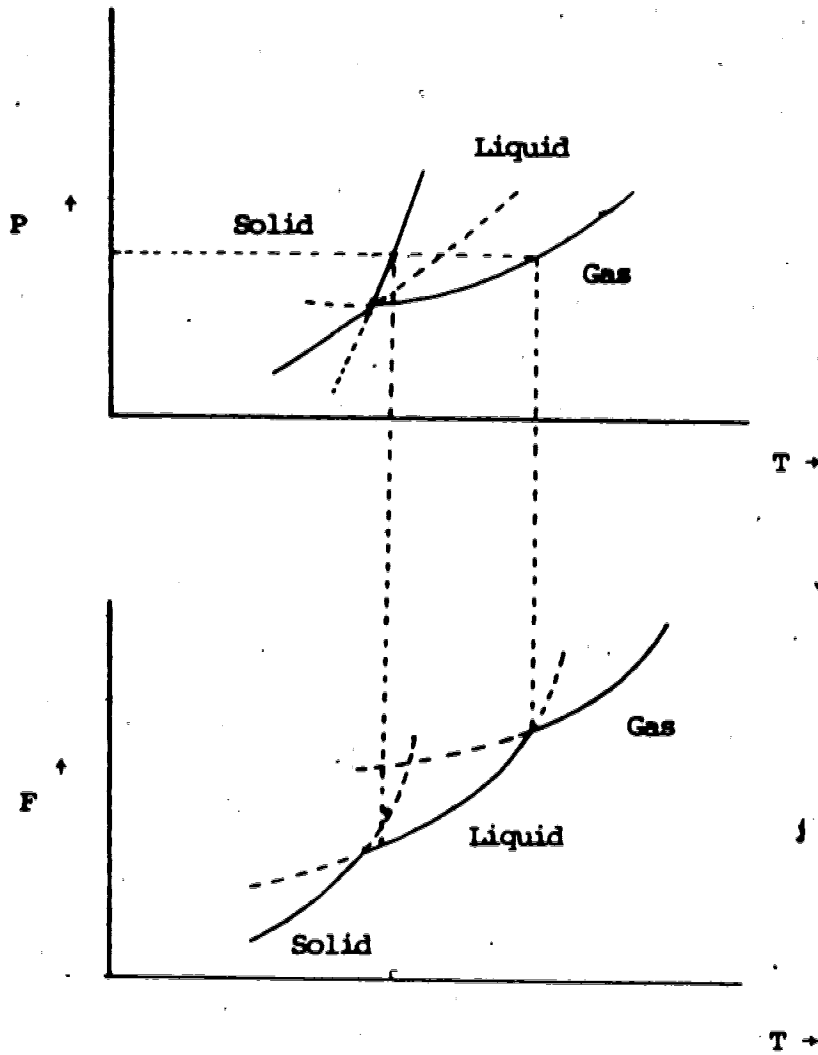


Figure 3.3 Free Energy - Temperature Diagram with a P-T Diagram, Showing How the Latter is Related to Former

itself. This study deals only with the pure liquids, thus only the homogeneous nucleation is of concern here.

From thermodynamic treatment of equilibrium across a curved interface, it can be shown that in a pure supercooled melt a small crystal will melt while a large crystal can continue to exist and grow. The proper criterion for "smallness", in this sense, is the radius of curvature. If this is less than some value, the critical radius, that depends on the temperature, melting occurs; if larger, it does not. The critical radius can be expressed as: [3]

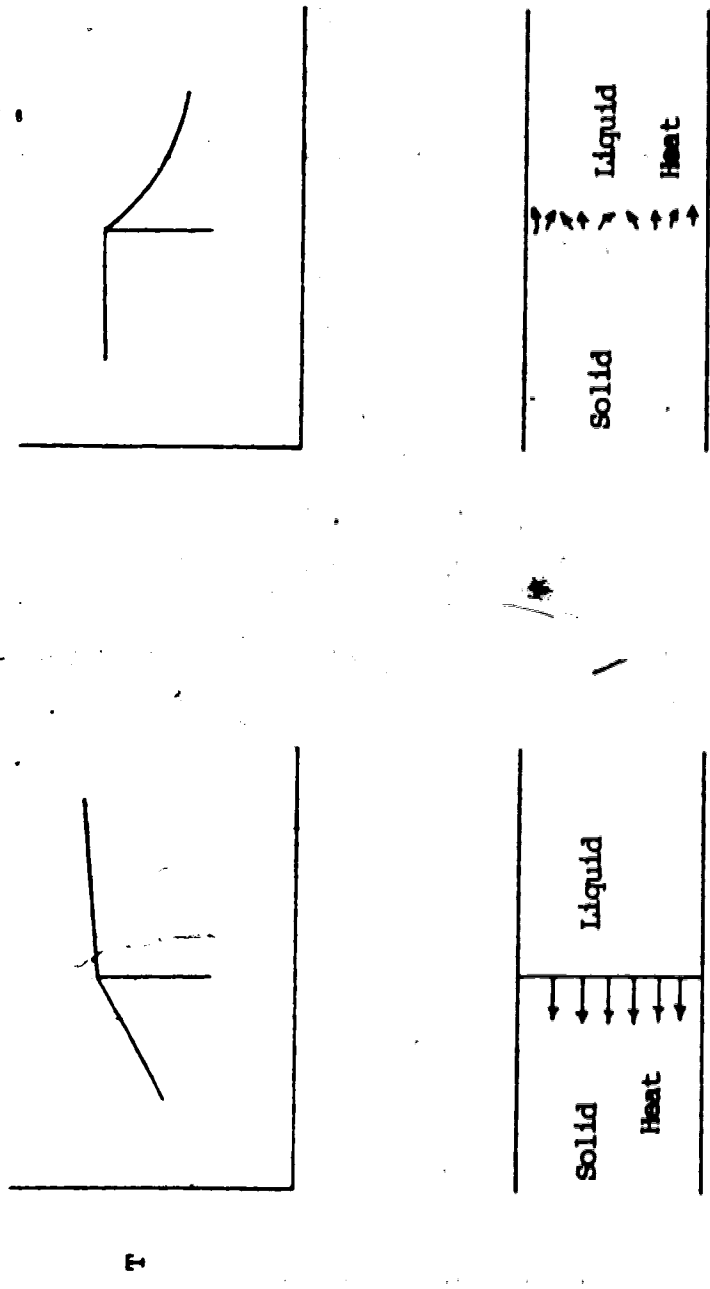
$$r^* = \frac{2\gamma T_f}{L\Delta T} \quad (3-1)$$

where T_f is the equilibrium temperature, γ is the surface free energy per unit area, L is the latent heat of fusion and ΔT is the amount of supercooling.

The basic process to be considered after nucleation is the process of growth. The rate at which freezing proceeds is controlled by the rate of removal of the latent heat. If it is not removed, the temperature rises to the point at which no more freezing can occur--that is, the freezing point.

The latent heat is removed by conduction; this may be through the crystal (as in Figure 3.4(a)) or into the liquid, if this is supercooled and therefore at a lower temperature than the interface where freezing occurs (Figure 3.4(b)).

This study is concerned only with the latter case.



(a)

(b)

Figure 3.4 (a) Heat Extraction Through the Solid;
(b) Heat Removal Through the Liquid

When the liquid is supercooled and freezing proceeds by rejecting latent heat into the liquid, the shape of interface is not smooth. This can be explained as follows. Figure 3.5 shows the schematic of removal of latent heat through the liquid when freezing proceeds in a supercooled melt. On a flat interface $r = \infty$, the latent heat dissipates into a prism of liquid [Figure 3.5(a)], while the heat from a curved interface dissipates into a certain solid angle [Figure 3.5(b)] and hence dissipates at a faster rate. Thus, any part of the crystal interface which gets ahead of neighbouring regions is in a more favourable position to dissipate latent heat of crystallization and so its growth rate is enhanced. This situation leads to instability and dendritic crystal growth with dendrite arms branching out into the liquid.

3.2 Physical Model and Assumptions

To begin simply, this study is concerned with the initial growth development of a solid phase in a pure supercooled melt. The geometries of interest are the following:

- (a) Circular cylinder
- (b) Parabolic cylinder
- (c) Paraboloid of revolution
- (d) Spheroidal

Particular interest in the shapes indicated arises because considerable experimental data and analytical results are available on growth rates and stability of these shapes

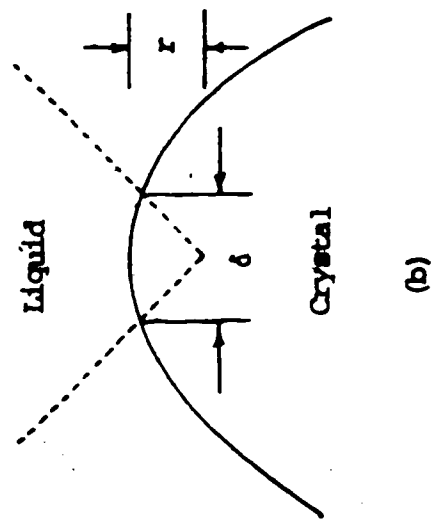
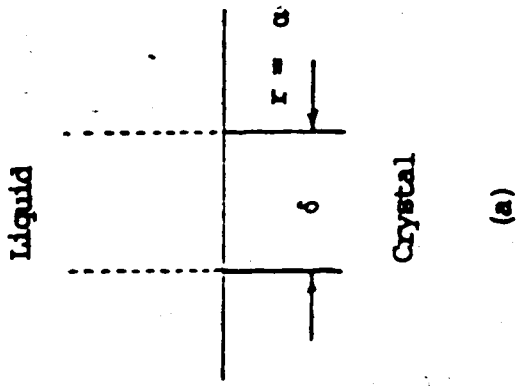


Figure 3.5 When a Growing Interface is Convex Towards the Liquid (b) it Dissipates the Liberated Heat of Fusion Faster than when it is Planar (a)

for growth in supercooled liquids.

It is assumed that the rate controlling process is thermal diffusion, and that interface kinetics may be ignored. The thermal profile in front of the solid is illustrated in Figure 3.6. The equilibrium melting point of the tip (interface) is depressed an amount ΔT_r owing to the radius of curvature of the non-flat interface. The amount of freezing point depression due to curvature effect (Gibbs-Thompson effect) is given by

$$\Delta T_r = \frac{\gamma K}{L} T_f \quad (3-2)$$

in which γ is the surface free energy, K is the mean curvature, L is the latent heat generated per unit volume of solid produced and T_f is the equilibrium fusion temperature. As the solid grows, heat is released, which is dissipated into the supercooled melt. This heat diffuses down a temperature gradient into the melt, resulting from the temperature difference ΔT_α ; thus

$$\Delta T = \Delta T_r + \Delta T_\alpha \quad (3-3)$$

The other basic assumptions to be made are the following:

1. Densities of solid phase (crystal) and the supercooled liquid phase are equal, thus, the moving boundary does

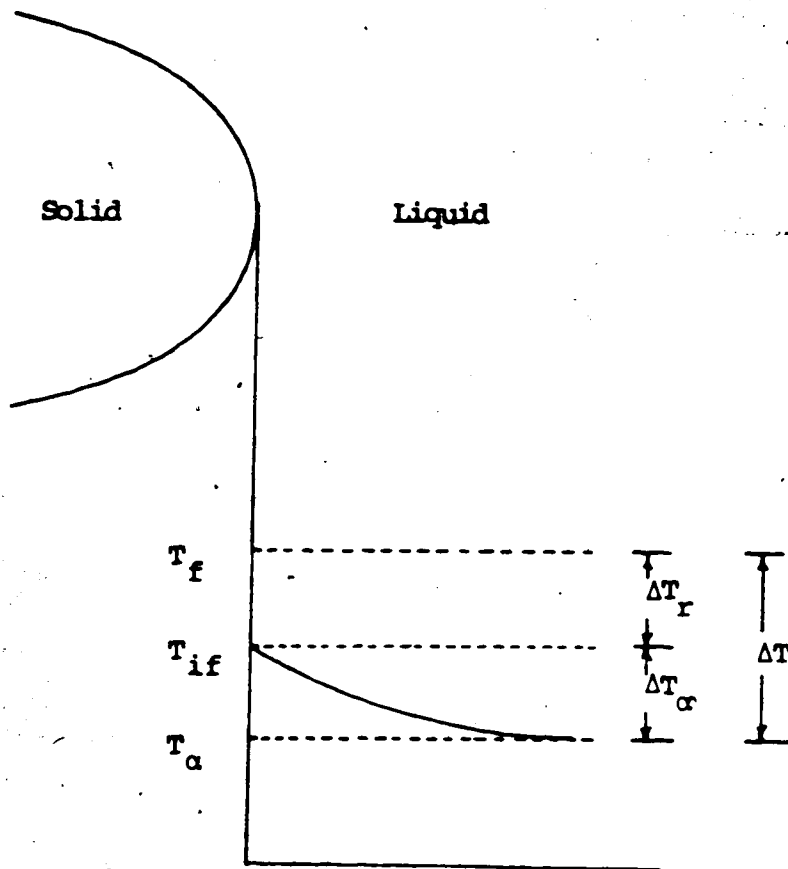


Figure 3.6 Thermal Profile in Front of a Dendrite Tip Growing in a Melt Under Cooled an Amount $\Delta T = T_f - T_\alpha$

not create any convection in the liquid as the growth proceeds.

2. Physical properties are constant throughout each phase.
3. The temperature far from the interface is uniform (T_∞).
4. The solid front moves with an average, constant growth velocity v . This implies a quasi-steady state process. The quasi-steady state implies that the quantities of interest, for example temperatures in this case, do not change with time with respect to a coordinate system moving with velocity v .

3.2.1 Discussion of Assumptions

The assumption that conduction is the main mechanism of heat dissipation is most important. In the fusion problem convection can arise from one of two sources. Firstly, a convection due to displacement of the liquid occurs because of the different densities of the liquid and solid, ρ_l and ρ_s respectively. As the freezing proceeds, it can be shown using the conservation of mass that the liquid is displaced ahead of the crystal with a velocity given by

$$U_n = -\epsilon v_n \quad (3-4)$$

where v_n is the normal velocity of the interface and $\epsilon = (\rho_s - \rho_l) / \rho_l$. Chambre [53] has shown that unless ϵ is

appreciable, with respect to unity, the temperature distribution in the liquid and solid is essentially unchanged from the $\epsilon = 0$ case. Since $\epsilon < 0.1$ for any material we may wish to consider, the effect of this 'displacement' convection upon the temperature distribution during dendritic growth can be justifiably neglected.

The other type of convection, natural convection, occurs due to density differences in the melt. It is not so clear that this type of convection can be neglected in all cases. Gilpin [60] has shown natural convection has a significant effect on the experimental growth of dendritic ice for supercoolings less than about 2°C . These experiments were done in large vessels. Whether or not the same conclusion would apply for dendrites growing in more confined spaces is uncertain. The assumption of constant material properties is justifiable since the temperature range of interest is not very large.

The assumption of uniform temperature far away from the interface boundary was also made. Bolling and Tiller [16] have stated that in practice, if the far field boundary is more than $10 a_l/v$ away from the solid interface, where a_l is the thermal diffusivity of the liquid and v is the dendrite velocity of growth, the temperature remains fairly constant. In this study, the far field boundary is obtained by considering various sizes of domains and choosing the one which justifies the assumption of nearly uniform temperature far away from the interface.

3.3 Mathematical Formulation and Governing Equations

The core problem is to solve the quasi-steady state heat equation for the temperature fields inside and around a crystal, of some predefined initial shape, growing into a pure supercooled melt.

The differential equation for heat transport to be solved for quasi-steady state conditions in the moving coordinate system fixed to the dendrite tip is

$$\nabla^2 T + \frac{v}{a} \frac{\partial T}{\partial z} = \frac{1}{a} \frac{\partial T}{\partial t} \approx 0 \quad (3-5)$$

where a is the thermal diffusivity, and v is the growth velocity of the dendrite. The velocity v , is of course, a quantity that is ultimately to be determined. Setting the right hand side of the equation (3-5) to zero gives the quasi-steady state approximation which will be used throughout this analysis. That is, it is assumed that the diffusion field responds very quickly to changes in the shape of the moving interface. Also, since equation (3-5) is to be solved both inside and around the growing dendrite, subscripts s and l will be used to denote solid and liquid respectively.

Equation (3-5) is to be solved subject to two boundary conditions at the solid-liquid interface. First, there is a thermodynamic boundary condition due to the Gibbs-Thompson effect that is written in the form

$$T_{if} = T_f - \frac{T_f \gamma K}{L}, \quad (3-6)$$

in which T_{if} is the interface temperature; T_f is the fusion temperature of the pure substance, K is the curvature of the surface; γ is the surface free energy; and L is the latent heat per unit volume the solid formed.

The second boundary condition at the interface is the heat balance condition:

$$L v_n = (-k_l \nabla T_l + k_s \nabla T_s) \cdot n \quad (3-7)$$

where n is the outward directed unit normal at a point on the surface; and v_n is the normal velocity of the surface at that point. k_l and k_s are the thermal conductivities of the liquid and solid phases respectively.

In addition to the interface conditions, T_l equals T_α (a constant) at a distance far away from the tip of the dendrite.

3.3.1 Non-Dimensionalization

Equations (3-5) through (3-7) can be non-dimensionalized with help of the following substitutions:

$$\text{Let } \theta = \frac{T - T_f}{T_f - T_\alpha} \quad (3-8a)$$

$$r = \frac{r}{d_c} \quad (3-8b)$$

$$\xi = \frac{z}{d_c} \quad (3-8c)$$

$$v_c = \frac{d_c}{\tau_c} \quad (3-8d)$$

$$v = v' v_c \quad (3-8e)$$

and

$$K = K' / d_c \quad (3-8f)$$

where d_c , v_c and τ_c are characteristic length, velocity and time respectively. The non-dimensional variables, η , ξ , v' , θ and K' are respectively length in r direction, length in z direction, velocity, temperature and curvature.

The differential equation (3-5) now becomes

$$\nabla^2 \theta + \frac{v' v_c d_c}{a} \frac{\partial \theta}{\partial \xi} = 0, \quad (3-9)$$

and the interface conditions become

$$\theta_{if} = - \frac{T_f \gamma K'}{d_c L (T_f - T_\alpha)}, \quad (3-10)$$

and

$$L v_{n'} = [(-k_l \nabla \theta_l + k_s \nabla \theta_s) \cdot n'] \left(\frac{T_f - T_\alpha}{v_c d_c} \right). \quad (3-11)$$

By choosing the characteristic length to be

$$d_c = \frac{\gamma T_f}{L(T_f - T_\alpha)}, \quad (3-12)$$

equation (3-10) reduces to $\theta_{if} = -K'$. Further, equation (3-11) can be simplified by letting

$$\frac{k_l (T_f - T_\alpha)}{L d_c v_c} = 1. \quad (3-13)$$

This determines the characteristic time and velocity;

$$v_c = \frac{d_c}{t_c} = \frac{k_l (T_f - T_\alpha)^2}{\gamma T_f} \quad (3-14)$$

and

$$t_c = \frac{\gamma^2 T_f^2}{k_l L (T_f - T_\alpha)} \quad (3-15)$$

Also, define Stefan number in the liquid

$$\text{Ste}_l = \frac{c_l (T_f - T_\alpha) \rho_l}{L}, \quad (3-16)$$

and the Stefan number in the solid as

$$\text{Ste}_s = \frac{c_s (T_f - T_\alpha) \rho_s}{L}. \quad (3-17)$$

Then to get a complete temperature distribution we need to solve the following differential equations for the domains given in Figure (3-7):

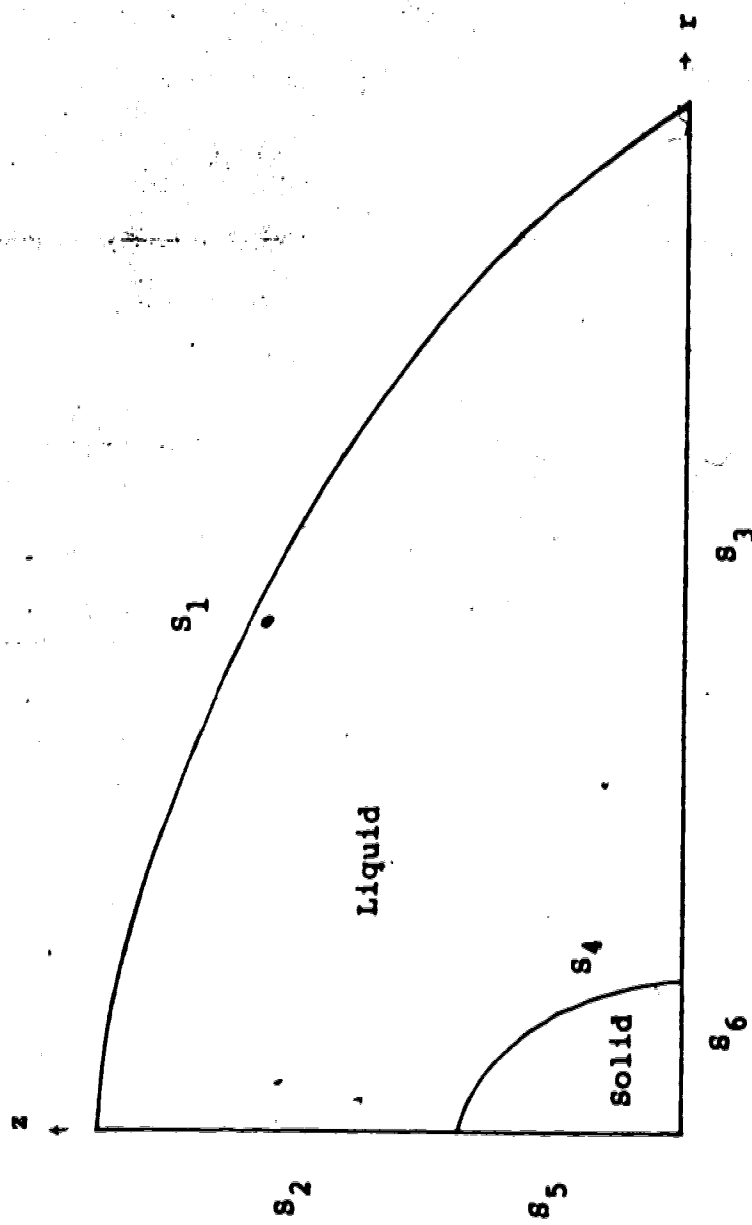


Figure 3.7 The Domain Under Consideration for the Study of Dendritic Growth

(i) Liquid region

$$\nabla^2 \theta_l + v' \cdot \text{Ste}_l \frac{\partial \theta_l}{\partial \xi} = 0, \quad (3-18)$$

with boundary conditions

$$\theta_l = -1 \quad \text{on } S_1 \quad (3-19)$$

$$\frac{\partial \theta_l}{\partial n} = 0 \quad \text{on } S_2, S_3 \quad (3-20)$$

$$\theta_l = \theta_{if} = -R' (n, \xi) \quad \text{on } S_4 \quad (3-21)$$

(ii) Solid region

$$\nabla^2 \theta_s + v' \frac{k_l}{k_s} \text{Ste}_s \frac{\partial \theta_s}{\partial \xi} = 0, \quad (3-22)$$

with boundary conditions

$$\theta_s = \theta_{if} \quad \text{on } S_4 \quad (3-23)$$

$$\frac{\partial \theta_s}{\partial n} = 0 \quad \text{on } S_5, S_6 \quad (3-24)$$

and the interface heat balance condition given by

$$\theta_{if} = \theta_l = \theta_s \quad (3-25)$$

and

$$v_n = \left(\frac{k_s}{k_l} \nabla \theta_s - \nabla \theta_l \right) \cdot n' \quad (3-26)$$

3.4 Variational Formulation

Often boundary value problems have different but equivalent formulations--a differential formulation and a variational formulation. In the first, a partial differential equation is written, and its direct solution is attempted subject to given boundary conditions. In the second, the aim is to find the unknown function or functions which

make stationary a functional or system of functionals subject to the same boundary conditions. The two problem formulations are mathematically equivalent because the functions that satisfy the differential equations and their boundary conditions also extremize or make stationary the functionals. Detailed procedures for formulating many problems of engineering and applied physics by variational approach can be found in texts by Mikhlin [61], Schecter [62], and Kantorovich and Krylov [63].

To formulate a two-dimensional boundary value problem of the type given in the last section by a variational approach, consider the following integral

$$I(\theta) = \iint_D \left[\left(\frac{\partial \theta}{\partial \eta} \right)^2 + \left(\frac{\partial \theta}{\partial \xi} \right)^2 - 2 g \theta \right] d\eta \, d\xi \quad (3-27)$$

where D is the entire domain under consideration. The boundary

conditions are exactly the same as those used in the boundary value problem. The object is to find a function $\theta(\eta, \xi)$, continuous in the region D together with its partial derivatives of the first and second orders, satisfying the specified boundary conditions and giving the integral $I(\theta)$, Eq. (3-27) a minimum value.

Let $\theta(\eta, \xi)$ be a function which minimizes the integral $I(\theta)$; let us consider the value of the integral* for the function

$$\hat{\theta}(\eta, \xi) = \theta(\eta, \xi) + \alpha \beta(\eta, \xi) \quad (3-28)$$

where $\hat{\theta}(\eta, \xi)$ also satisfies the boundary conditions and α a parameter. Since both θ and $\hat{\theta}$ satisfy the boundary conditions, $\beta(\eta, \xi)$ must vanish on the portion of the boundary on which θ is specified.

To minimize $I(\theta)$, a necessary condition is the vanishing of the first variation of $I(\theta)$, which is $\delta I(\theta)$. The requirement is therefore

$$\delta I(\theta) = \left[\frac{d}{d\alpha} I(\theta + \alpha\beta) \right]_{\alpha=0} = 0 \quad (3-29)$$

where $I(\theta + \alpha\beta)$ is given by

$$I(\theta + \alpha\beta) = \iint_D \left[\left(\frac{\partial \theta}{\partial \eta} + \alpha \frac{\partial \beta}{\partial \eta} \right)^2 + \left(\frac{\partial \theta}{\partial \xi} + \alpha \frac{\partial \beta}{\partial \xi} \right)^2 - 2g(\theta + \alpha\beta) \right] d\eta d\xi \quad (3-30)$$

Differentiating (3-30) with respect to α and setting $\alpha = 0$ gives

$$\delta I(\theta) = \iint_D \left[2 \frac{\partial \theta}{\partial \eta} \frac{\partial \beta}{\partial \eta} + 2 \frac{\partial \theta}{\partial \xi} \frac{\partial \beta}{\partial \xi} - 2g\beta \right] d\eta d\xi \quad (3-31)$$

In the above expression for $\delta I(\theta)$, the first two terms can be transformed by means of Green's formula, and equation (3-31) can be written as

$$\delta I(\theta) = -2 \left\{ \iint_D (\nabla^2 \theta + g)\beta d\eta d\xi + \int_{\Gamma} \left[-\frac{\partial \theta}{\partial \eta} d\xi - \frac{\partial \theta}{\partial \xi} d\eta \right] \beta \right\} = 0 \quad (3-32)$$

where Γ is the contour of the domain. As the area integrals and the line integrals are independent and that $\beta(\eta, \xi)$ is arbitrary, the result is,

$$\nabla^2 \theta + g = 0 \quad \text{on } D \quad (3-33)$$

and

$$\int_{\Gamma} \left[\frac{\partial \theta}{\partial \eta} d\xi - \frac{\partial \theta}{\partial \xi} d\eta \right] \beta = 0 \quad (3-34)$$

However, on the portion of Γ (say Γ_1), on which θ is specified, $\beta(\eta, \xi) = 0$, and on the remaining portion (say Γ_2), equation (3-34) gives

$$\frac{\partial \theta}{\partial \eta} d\xi - \frac{\partial \theta}{\partial \xi} d\eta = 0 \quad \text{on } \Gamma_2 \quad (3-35)$$

Equation (3-35) can be reduced to the form

$$\frac{\partial \theta}{\partial n} = 0 \quad \text{on } \Gamma_2 \quad (3-36)$$

when n is the unit normal.

Thus, we can see that the minimization of the integral represented by equation (3-27) results in recovering the boundary value problems arrived at in section 3.3 provided an approximation is made such that

$$g_l = v' Ste_l \frac{\partial \theta_l}{\partial \xi} \quad (3-37)$$

for the liquid region and

$$g_s = \frac{k_l}{k_s} v' Ste_s \frac{\partial \theta_s}{\partial \xi} \quad (3-38)$$

for the solid region. It is seen that the functional does not lead to the partial differential equation if g is taken as a function of θ . However, the approximation considering g as only a function of position is justified because the terms described by Eq. (3-37) and (3-38) are introduced iteratively in the computer program.

A similar analysis can be made for the case where the growing dendrite has an axis of symmetry. The integral to be minimized for arriving at the boundary value problems represented by equations (3-18) and (3-22) for the axisymmetric case is

$$I(\theta) = \iint_D \left[\left(\frac{\partial \theta}{\partial n} \right)^2 + \left(\frac{\partial \theta}{\partial \xi} \right)^2 - 2 g \theta \right] n \, dnd\xi \quad (3-39)$$

where the growing dendrite is symmetric about the ξ axis.

3.5 The Finite Element Method

The finite element method is one of the newest and most popular numerical techniques for solving the differential equations of engineering and applied physics. This method has been used extensively in recent years because it has, in general, several outstanding advantages. Some of the main ones include:

1. Irregularly shaped boundaries can be approximated using elements with straight sides or matched exactly using elements with curved boundaries. The method, therefore, is not limited to "nice" shapes with easily defined boundaries.

2. The size of the elements can be varied. This property allows the element grid to be expanded or refined as the need arises.

3. The material properties in adjacent elements do not have to be the same. This allows the method to be applied to non-homogeneous and anisotropic configurations with relative ease.

4. Once a computer program has been developed, all problems for which the equations are the same can be solved

simply by supplying the computer with appropriate boundary coordinates and material properties.

The finite element method, when applied to heat transfer problems, generally consists of the following steps:

1. Discretization of the domain under study; defining the nodal points and elements.
2. Defining the element function for a single element and evaluation of the matrices of the elements.
3. Assembling the complete matrix of the continuum and application of the boundary conditions.
4. Solution of the resulting system of equations to obtain nodal temperatures.
5. Calculation of any other functions (temperature gradients) based on the nodal temperatures.

The first step of discretizing the domain involves the decision as to the number, size, and shape of the elements used to model the domain. This decision has to be based on physical reasoning and experience. For example, the element size can be decreased in the areas where the desired result may vary quite rapidly (high gradient values), and can be increased in regions where the desired result is relatively constant.

Each element is then analyzed separately and its properties are generally derived from the minimization of the functional or Galerkin type expression governing the problem, after choosing a set of functions to define uniquely the

temperature within each "finite element". These approximate functions have to satisfy the admissibility and completeness conditions for the problem. Admissibility implies continuity of essential variables between elements, and that the order of the expansion is such that the terms are well defined in the variational statements; for completeness, when the elements tend to be infinitely small and hence derivatives inside the variational statement tend to be constant, the approximate function must represent this constant derivative condition. If these conditions are satisfied the solution will converge to its correct value as the total number of elements is increased.

3.5.1 The Finite Element Method Applied to the Dendritic Growth Problem

In variational form the temperature distribution problem to be solved is that of minimizing the functional given by equation (3-27) for the two-dimensional problem and for the axisymmetric case the functional given by equation (3-39) is to be minimized. Since the procedures to be followed in the finite element formulation are the same for two-dimensional and axisymmetric problems, only the axisymmetric case is described here in detail. The main difference comes in evaluating the element matrices, which are given in Appendix 2.

Consider the case of an axisymmetric dendrite growing in a supercooled liquid. The ultimate objective is to determine the temperature distribution inside and around the

dendrite, and the temperature gradients at the interface to calculate the growth velocity of the dendrite under given conditions.

First the region under consideration is divided into a number of elements. The type of the element chosen for this study is a triangular element with six nodes, as shown in Figure (3.8). In order that the element mesh may be generated automatically by the computer on supplying a minimum amount of input data, the elements are chosen in a block pattern as shown in Figure (3.9). The node numbering system also follows a distinct pattern. The numbering system of nodes and the pattern for elements allowed for easy changes in total number of nodes and the size of individual elements. Details of the automatic mesh generation procedure are given in Appendix 3.

The six node triangular element enables a quadratic variation of the temperature within the element. The quadratic element is known to give good results with very little extra computational work compared to the linear element, and without the programming complications present in other higher order elements or the isoparametric elements.

The generation of the interpolation function for a triangular element is simplified considerably if one works with the area coordinates. The area coordinates are defined by

$$\psi_i = \frac{A_i}{A^m} \quad i = 1, 2, 3 \quad (3-40)$$

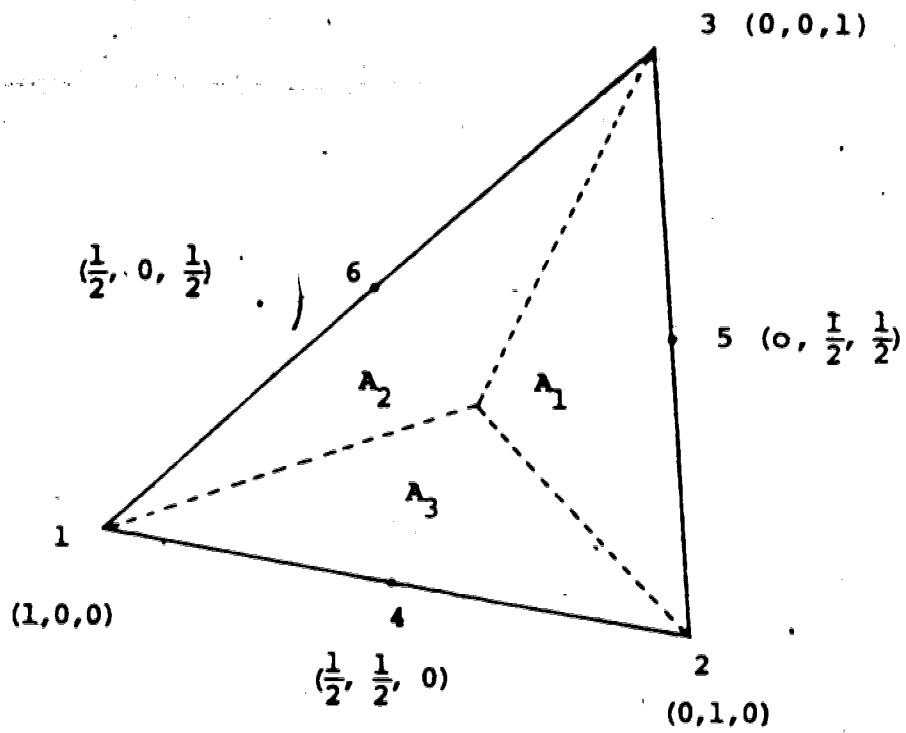


Figure 3.8 The Six-node triangular Element with area co-ordinates of the Nodes

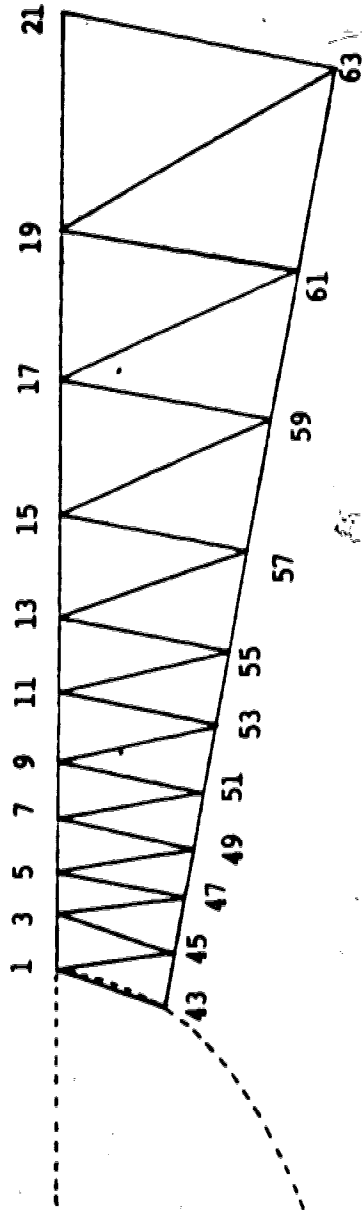


Figure 3.9 A Node Pattern for Automatic Node Numbering

where A^m is the area of the triangular element and A_i are the areas of the subtriangles as shown in Figure (3-8). Thus, the side connecting nodes 1 and 2 is described by $\psi_3 = 0$ etc. We have then three area coordinates (ψ_1, ψ_2, ψ_3) but only two are independent since

$$\psi_1 + \psi_2 + \psi_3 = 1 \quad (3-41)$$

The quadratic variation of the temperature, θ^m , in the m th element, expressed in terms of the six nodal values θ_i^m ($i = 1$ to 6) is

$$\theta^m = \sum_{i=1}^6 \theta_i^m \chi_i \quad (3-42)$$

where

$$\chi_i = \langle \psi_1(2\psi_1 - 1), \psi_2(2\psi_2 - 1), \psi_3(2\psi_3 - 1), 4\psi_1\psi_2, 4\psi_2\psi_3, 4\psi_3\psi_1 \rangle \quad (3-43)$$

Since η is a linear function in the η - ξ plane, it is given exactly by

$$\eta = \sum_{i=1}^3 \eta_i \psi_i \quad (3-44)$$

on any triangle in the η - ξ plane, provided η_i are the vertex radial coordinates. Hence, the functional (3-39) may be expressed as the weighted sum of three portions

$$I(\theta)^m = \sum_{i=1}^3 \eta_i^m \iint_D \psi_i \left[\left(\frac{\partial \theta^m}{\partial \eta} \right)^2 + \left(\frac{\partial \theta^m}{\partial \xi} \right)^2 - 2g \theta^m \right] d\eta d\xi \quad (3-45)$$

Next, the derivatives with respect to η and ξ may be written as

$$\frac{\partial \theta^m}{\partial \xi} = \sum_{i=1}^6 \theta_i^m P_i \quad (i=1 \text{ to } 6) \quad (3-46)$$

and

$$\frac{\partial \theta^m}{\partial \eta} = \sum_{i=1}^6 \theta_i^m \hat{P}_i \quad (i=1 \text{ to } 6) \quad (3-47)$$

where

$$P_i = \frac{1}{2A^m} \{ (4\psi_i - 1)b_1; (4\psi_2 - 1)b_2; (4\psi_3 - 1)b_3;$$

$$4(\psi_2 b_1 + \psi_1 b_2); 4(\psi_3 b_2 + \psi_2 b_3); 4(\psi_1 b_3 + \psi_3 b_1) \}$$

(3-48)

$$b_k = \eta_i - \eta_j \quad (3-49)$$

and

$$a_k = \xi_j - \xi_i \quad (3-50)$$

and \hat{p}_i^m is obtained by replacing the b's with a's in the expression for p_i^m .

Let the term g be approximated by an interpolation expression

$$g = \sum_{i=1}^6 g_i \chi_i, \quad (3-51)$$

then the equation (3-45) can be written as

$$I(\theta^m) = \sum_{i=1}^3 \eta_i^m \iint_D \psi_i \left[\left(\sum_{k=1}^6 \theta_k^m p_k \right)^2 + \left(\sum_{j=1}^6 \theta_j^m \hat{p}_j \right)^2 - 2 \sum_{n=1}^6 g_n \chi_n \right] dnd\xi \quad (3-52)$$

To minimize (3-52), we set

$$\frac{\partial I(\theta^m)}{\partial \theta_k^m} = \sum_{i=1}^3 \eta_i^m \iint_D \psi_i \left[\sum_j \theta_j^m (p_k p_j + \hat{p}_k \hat{p}_j) - 2 \sum_{n=1}^6 g_n \chi_n \chi_k \right] dnd\xi = 0 \quad (3-53)$$

Equation (3-53) can be simplified considerably if all quantities independent of the triangle size and shape are evaluated once for all. To assist in doing so, define

$$SA_{iJ}^m = \sum_{k=1}^3 \eta_k^m \iint_D \psi_k (p_i p_J + \hat{p}_i \hat{p}_J) dnd\xi \quad (3-54)$$

and

$$QA_{iJ}^m = 2 \iint_D \psi_i \chi_i \chi_J dnd\xi \quad (3-55)$$

With this notation, the minimization equation (3-53) becomes

$$SA \theta + QA G = 0 \quad (3-56)$$

where SA and QA are 6x6 matrices and θ and G are 6x1 vectors.

The functional minimization problem has thereby been reduced to a simple matrix equation, in which the coefficient matrices SA and QA are easily assembled. The element matrices SA and QA for axisymmetric elements and S and Q for two-dimensional elements are listed in Appendix 2. Also given is a sample integration.

For a dendrite growing at constant speed, the second part of the above matrix equation contains terms involving v' and $\frac{d\theta}{d\xi}$ (see equations 3-37 and 3-38). Since v' and $\frac{d\theta}{d\xi}$ can only be obtained after the temperature field has been determined, an iterative process is used. That is, the first computation is done with $Ste = 0$ so the $v' \frac{d\theta}{d\xi}$ term drops out. The resulting temperature field is used to calculate v' and $\frac{d\theta}{d\xi}$ and the term $g = v' Ste \frac{d\theta}{d\xi}$ is introduced as an effective distributed heat generation in the second iteration. Typically 5 or 6 iterations were required to converge to a self-reproducing result. It should be noted that for growth of a sphere or a cylinder, this problem does not arise because Ste is assumed to be zero.

Once the individual matrices for all the elements are obtained, essentially a bookkeeping operation is required to assemble the element matrices and apply the boundary conditions. The method for assembling the element matrices and application of the boundary conditions can be found in standard texts [64-66].

The global matrix arrived at by the above mentioned assembly process is always symmetric and banded. The band width is proportional to the largest difference between nodes in the same element. Thus, considerable saving in storage requirements is realized if only the diagonal and upper (or lower) diagonal elements are stored. As shown in Figure (3-9) the numbering of the nodes is such that the minimum bandwidth is realized.

CHAPTER 4

STABILITY OF PARTICLES GROWING IN A SUPERCOOLED MELT

4.1 Introduction

The purpose of this chapter is to examine the applicability of the finite element method to study the stability of a phase boundary. As mentioned previously, the stability is tested by introducing a perturbation in the original interface shape and determining whether this perturbation will grow or decay.

Because some of the heat flow problems arising out of stability studies can be solved exactly by analytical methods, an opportunity exists for checking computer modelling methods. The computer models and their results can be compared at each stage with analytical results.

4.2 The Unperturbed Growth of a Sphere From a Slightly Supercooled Melt

Consider the case of a solid sphere (Figure 4.1) growing in an originally uniformly supercooled melt. If the growth is assumed to be diffusion (heat transfer) controlled, we need to solve the time dependent diffusion equation.

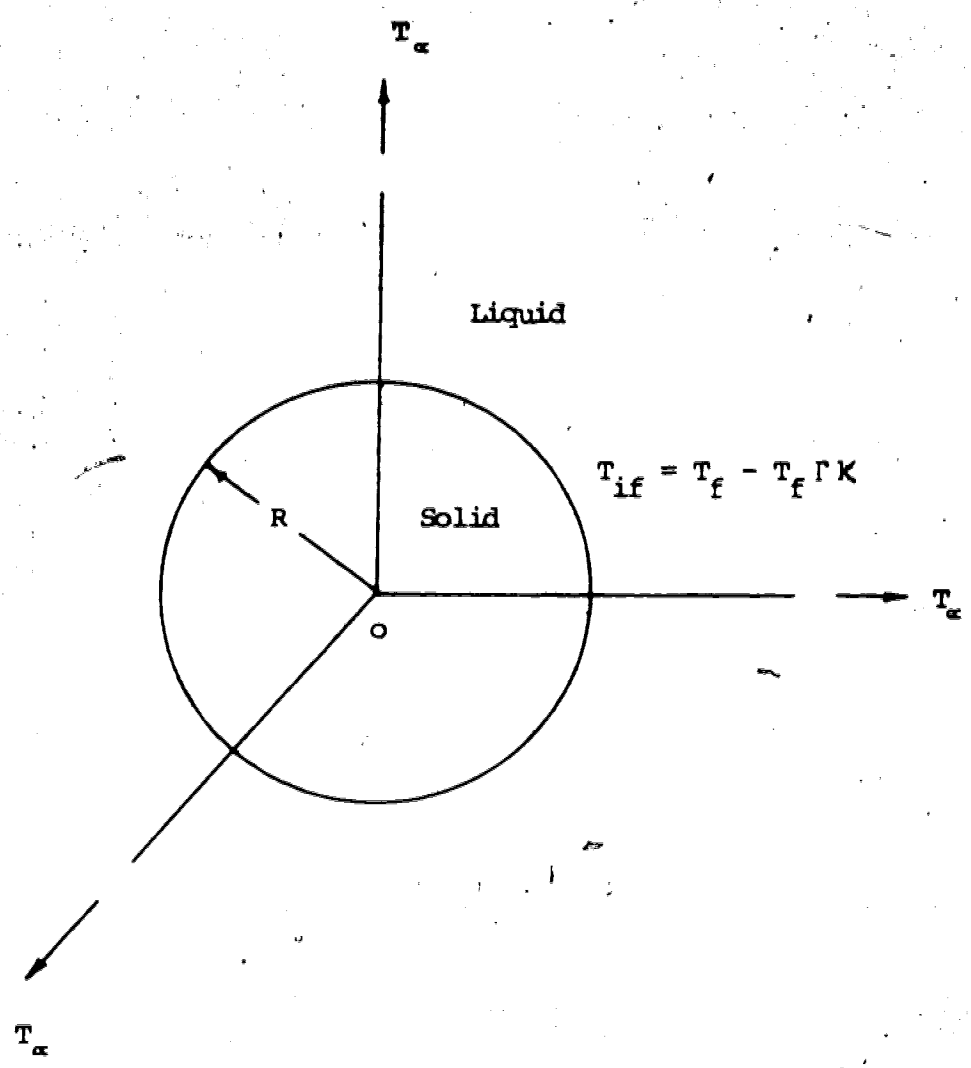


Figure 4.1 The Geometry of a Sphere Growing in a Supercooled Liquid

$$a \nabla^2 T = \frac{\partial T}{\partial t} \quad (4.1)$$

subject to the boundary conditions

$$T_l (r \rightarrow \infty, t) = T_\infty \quad (4.2a)$$

$$T_s (r \rightarrow 0, t) = \text{finite} \quad (4.2b)$$

$$T_l (r=R, t) = T_s (r=R, t) = T_{if} = T_f - T_f \Gamma k \quad (4.2c)$$

and the heat balance condition

$$-k_l \left[\frac{\partial T_l}{\partial r} \right]_{r=R} + k_s \left[\frac{\partial T_s}{\partial r} \right]_{r=R} = L \frac{dR}{dt}, \quad (4.3)$$

to arrive at a formal solution for the growth of a sphere. An exact solution to the above mentioned time dependent diffusion (heat flow) equation is possible only if the effect of capillarity (interface curvature effect) is neglected. But it is not justifiable in real situations to neglect capillarity.

It is reasonable to assume that if the supercooling is small then the temperature at any point near the growing particle changes slowly with time and the term $\frac{\partial T}{\partial t}$ in equation (4.1) is negligible. Mathematically speaking, if

$$\text{Ste} = \frac{c (T_f - T_\alpha)}{L} \ll 1, \quad (4.4)$$

then we are justified in approximating equation (4.1) by the Laplace equation as was shown for the case of a growing dendrite in Section 3.3.

$$\nabla^2 T_\ell \approx 0. \quad (4.5)$$

The solution of the Laplace equation (4.5) subject to the boundary conditions (4.2) gives

$$T_\ell = T_\alpha + \frac{(T_{if} - T_\alpha)}{R} R. \quad (4.6)$$

we find from equation (4.6)

$$\left[\frac{\partial T_\ell}{\partial r} \right]_{r=R} = - \frac{T_{if} - T_\alpha}{R}, \quad (4.7)$$

and the growth rate of the sphere can be obtained from equation (4.3) to be

$$\dot{R} = \frac{dR}{dt} = \frac{k_\ell}{LR} [T_{if} - T], \quad (4.8)$$

assuming $T_s = T_{if}$ for all $r < R$.

The results based on the equations (4.6-4.8) provide an excellent starting ground for testing the accuracy of the finite element method for solving crystal growth problems. The finite element programme was run for a sphere having an

initial radius ranging from $50 R^*$ to $250 R^*$, where $R^* = 2\Gamma T_f / (T_f - T_\alpha)$ is the classical nucleation radius of a sphere. Since it is not possible to have the outer boundary of the supercooled melt at infinity while using the finite element method, an approximation has to be made that at some sufficiently large finite distance away from the interface of the growing sphere the melt is at a uniform temperature, T_α . In the present analysis the radius of the outer boundary was taken to be 60 times the radius of the ice sphere.

The domain to be considered for the finite element solution of the sphere growth problem is shown in Figure (4.2). For this it is enough to consider just the one quadrant as shown in Figure (4.2).

Figures (4.3-4.5) and Tables (4.1-4.3) present the comparison of the results obtained by the finite element method with the analytical solutions. It is evident that the finite element method approximates the distribution of temperature and temperature gradient around a growing sphere very accurately, and the same is true for predicting the growth rate for spheres of different initial radii. Further, it is seen that the finite element method predicts the temperature distribution extremely accurately near the interface, while the accuracy is not so great far away from the interface. But, in stability problems and the problems of dendritic growth we only need the temperature distribution near the interface, thus further justifying the assumption of considering an

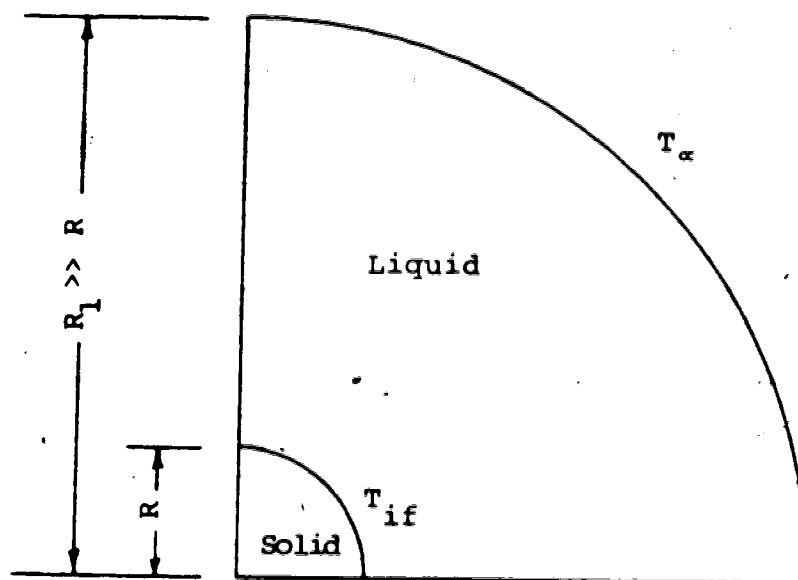


Figure 4.2 The Domain to be Considered for the Study of the Growth of a Sphere in Supercooled Liquid

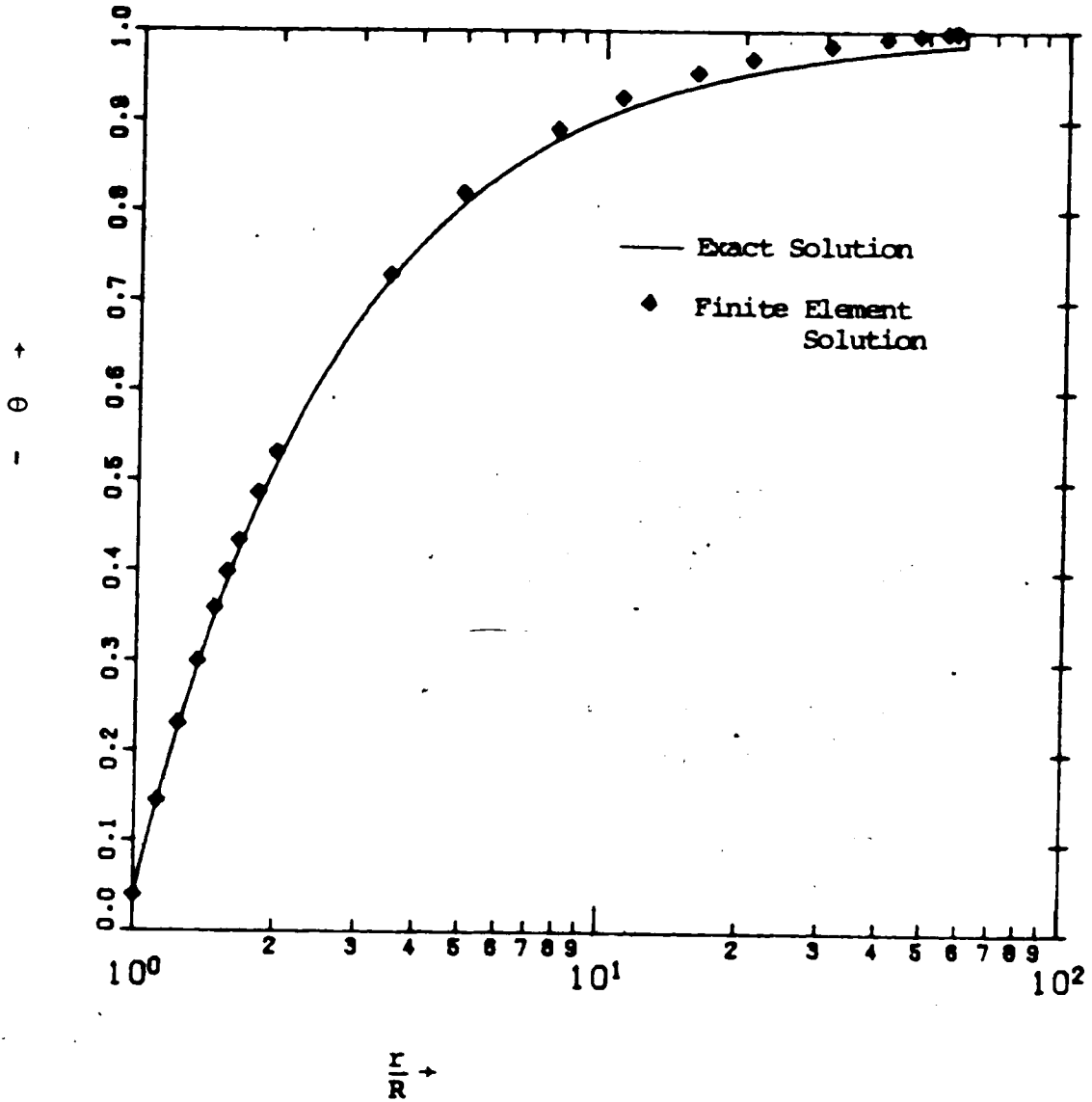


Figure 4.3

A Comparison of the Exact Solution and the Finite Element Solution for the Temperature Distribution Around a Sphere Growing in a Supercooled Liquid

$$(R = 100 R^* ; \theta = \frac{T - T_f}{T_f - T_\alpha})$$

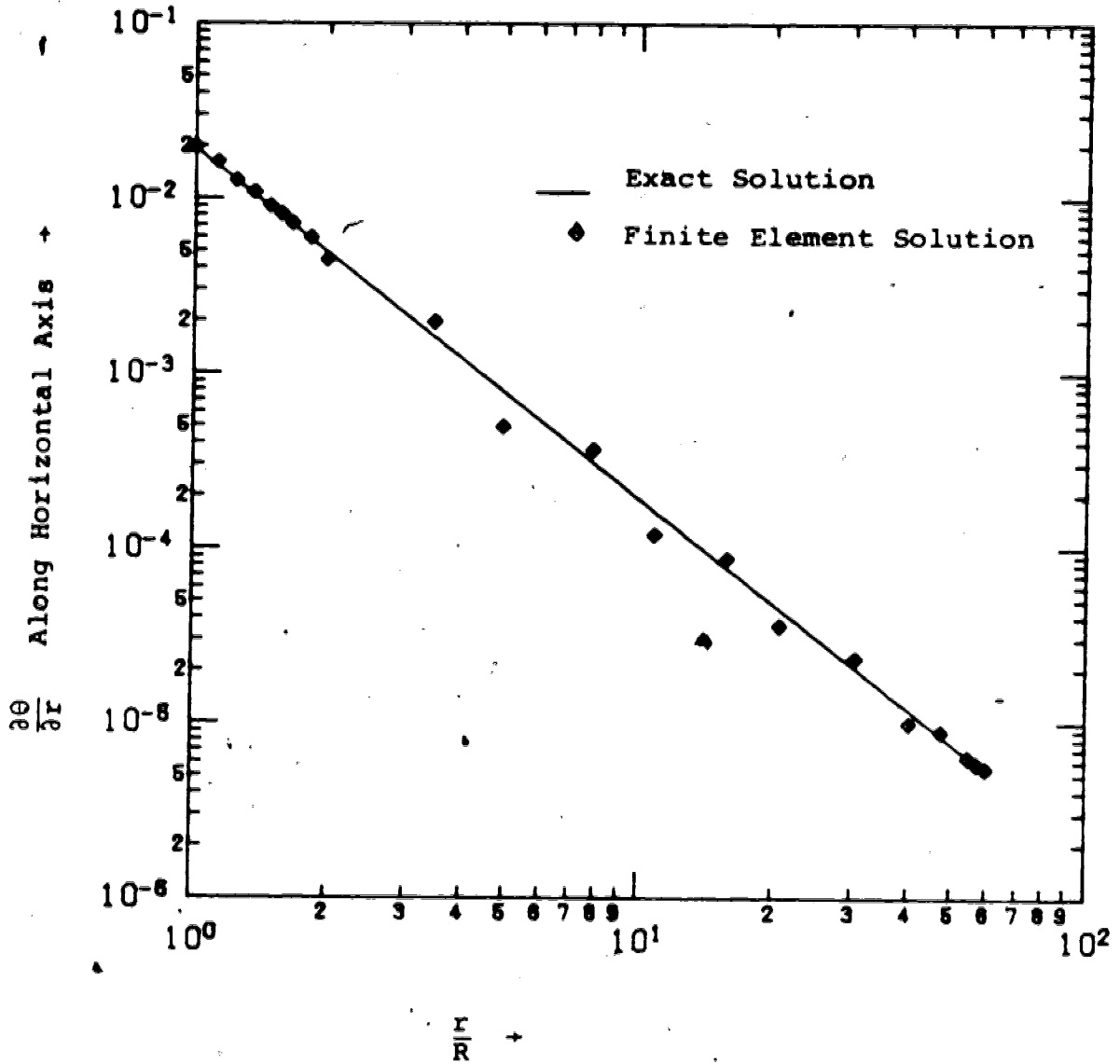


Figure 4.4 A Comparison of the Exact Solution and the Finite Element Solution for the Temperature Gradient Around a Sphere Growing in Supercooled Liquid

$$(R = 100 R^*)$$

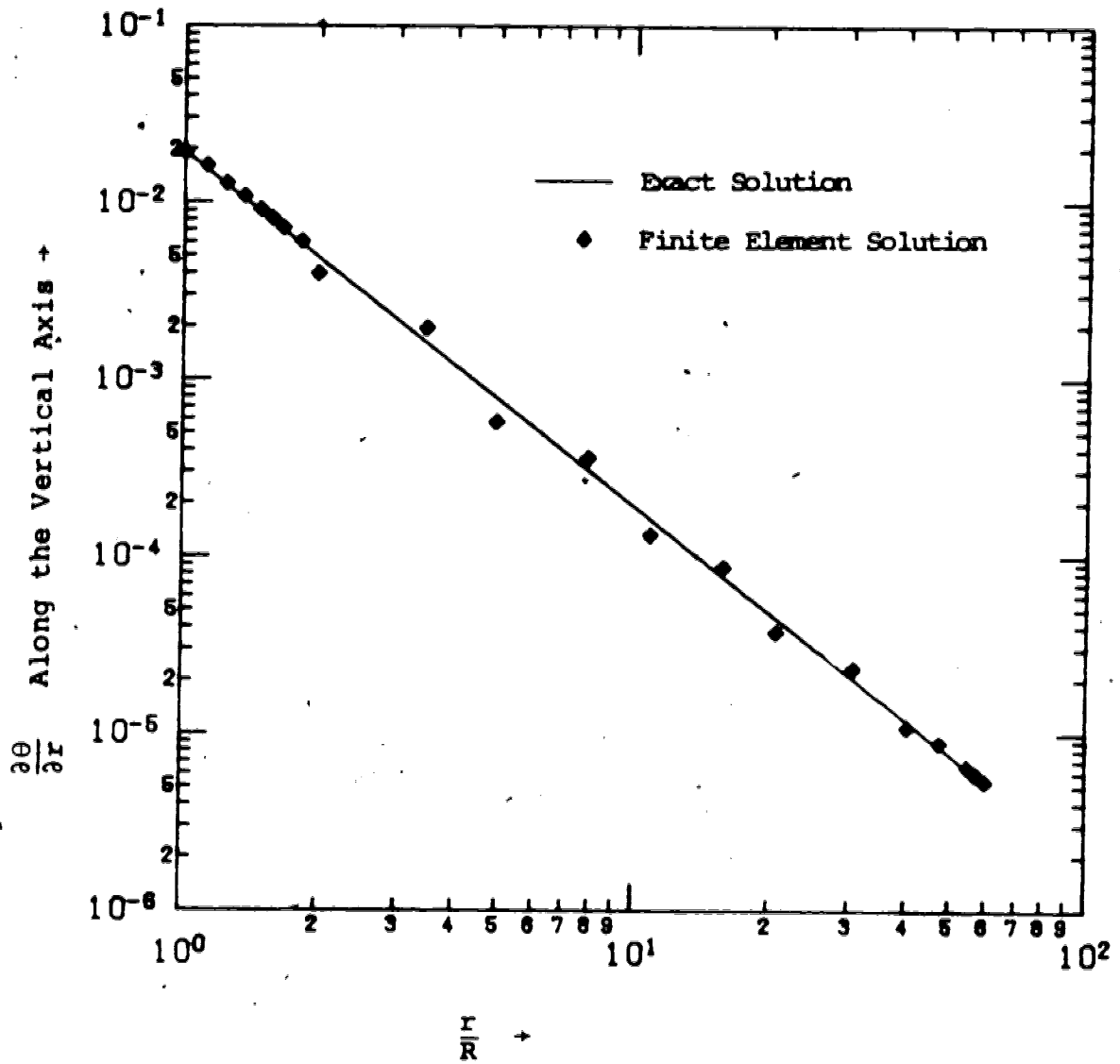


Figure 4.5

A Comparison of the Exact Solution and the Finite Element Solution for the Temperature Gradient Around a Sphere Growing in a Supercooled Liquid

($R = 100 R^*$)

TABLE 4.1

A COMPARISON OF THE EXACT SOLUTION AND THE FINITE ELEMENT
 SOLUTION FOR THE GROWTH RATE OF VARIOUS POINTS
 ALONG THE INTERFACE OF A SPHERE GROWING IN
 SUPERCOOLED LIQUID ($R = 50 R^*$, $k_s = 0$)

Position Along the Interface (Angle in Degrees from the Z Axis)	Finite Element Solution for the Growth Rate (Non- Dimensionalized)	Exact Solution for the Growth Rate (Non-Dimen- sionalized)
0	0.002460	0.002506
9	0.002506	0.002506
18	0.002502	0.002506
27	0.002503	0.002506
36	0.002504	0.002506
45	0.002506	0.002506
54	0.002507	0.002506
63	0.002508	0.002506
72	0.002506	0.002506
81	0.002507	0.002506
90	0.002506	0.002506

TABLE 4.2

A COMPARISON OF THE EXACT SOLUTION AND THE FINITE ELEMENT SOLUTION FOR THE GROWTH RATE OF VARIOUS POINTS ALONG THE INTERFACE OF A SPHERE GROWING IN A SUPERCOOLED LIQUID ($R = 100 R^*$, $k_s = 0$)

Position Along the Interface (Angle in Degrees from the Z Axis)	Finite Element Solution for the Growth Rate (Non-Dimensionalized)	Exact Solution for the Growth Rate (Non-Dimensionalized)
0	0.001245	0.001253
9	0.001261	0.001253
18	0.001262	0.001253
27	0.001264	0.001253
36	0.001264	0.001253
45	0.001264	0.001253
54	0.001265	0.001253
63	0.001264	0.001253
72	0.001263	0.001253
81	0.001263	0.001253
90	0.001263	0.001253

TABLE 4.3
 A COMPARISON OF THE EXACT SOLUTION AND THE FINITE ELEMENT
 SOLUTION FOR THE GROWTH RATE OF VARIOUS POINTS
 ALONG THE INTERFACE OF A SPHERE GROWING IN A
 SUPERCOOLED LIQUID ($R = 250^*$, $\frac{k_s}{k_l} = 4$)

Position Along the Interface (Angle in Degrees from the Z Axis)	Finite Element Solution for the Growth Rate (Non-Dimensionalized)	Exact Solution for the Growth Rate (Non-Dimensionalized)
0	0.000495	0.000499
9	0.000502	0.000499
18	0.000502	0.000499
27	0.000503	0.000499
36	0.000503	0.000499
45	0.000503	0.000499
63	0.000503	0.000499
72	0.000502	0.000499
81	0.000502	0.000499
90	0.000502	0.000499

arbitrary distance far away from the interface to be infinitely away from the origin. A node that caused consistent problems is the one on the ice surface at zero degrees. The growth rate calculated for this node is consistently lower than that for other nodes around the sphere. This anomaly is an artifact produced by the fact that this node is at a corner of the solution domain where a constant temperature surface meets an insulated surface (i.e. a singularity exists). Methods to reduce the error resulting from such singularities are available in the finite element literature (67, 68, 69).

4.3 The Stability of a Sphere Growing in a Slightly Supercooled Liquid

4.3.1 Theoretical Solutions

We consider a sphere of radius R slightly perturbed by a spherical harmonic $Y_{\ell m}(\theta, \phi)$. The position of the perturbed surface is given by

$$r = R + \delta Y_{\ell m}(\theta, \phi), \quad (4.9)$$

where δ is a small first order quantity ($\frac{\delta}{R} \ll 1$); and $Y_{\ell m}(\theta, \phi)$ is a spherical harmonic which determines the shape contours position along the surface of the sphere as shown in Table 4.4 and Figure 4.6. For a small perturbation, the curvature of a slightly perturbed sphere may be approximated by

$$K = \frac{2}{R} - \frac{2 Y_{\ell m} \delta}{R^2} + \frac{Y_{\ell m} (\ell^2 + \ell) \delta}{R^2} \quad (4.10)$$

TABLE 4.4

SOME SPHERICAL HARMONICS, $Y_{\ell m}$

$$Y_{10} = \cos \theta$$

$$Y_{11} = \sin \phi \sin \theta \quad \text{or} \quad \sin \theta \cos \phi$$

$$Y_{20} = 0.5 (3 \cos^2 \theta - 1)$$

$$Y_{21} = 3 \cos \theta \sin \theta \cos \phi \quad \text{or} \quad 3 \cos \theta \sin \theta \sin \phi$$

$$Y_{22} = 3 \sin^2 \theta \cos (2\phi) \quad \text{or} \quad 3 \sin^2 \theta \sin (2\phi)$$

$$Y_{30} = 0.5 (5 \cos^3 \theta - 3 \cos \theta)$$

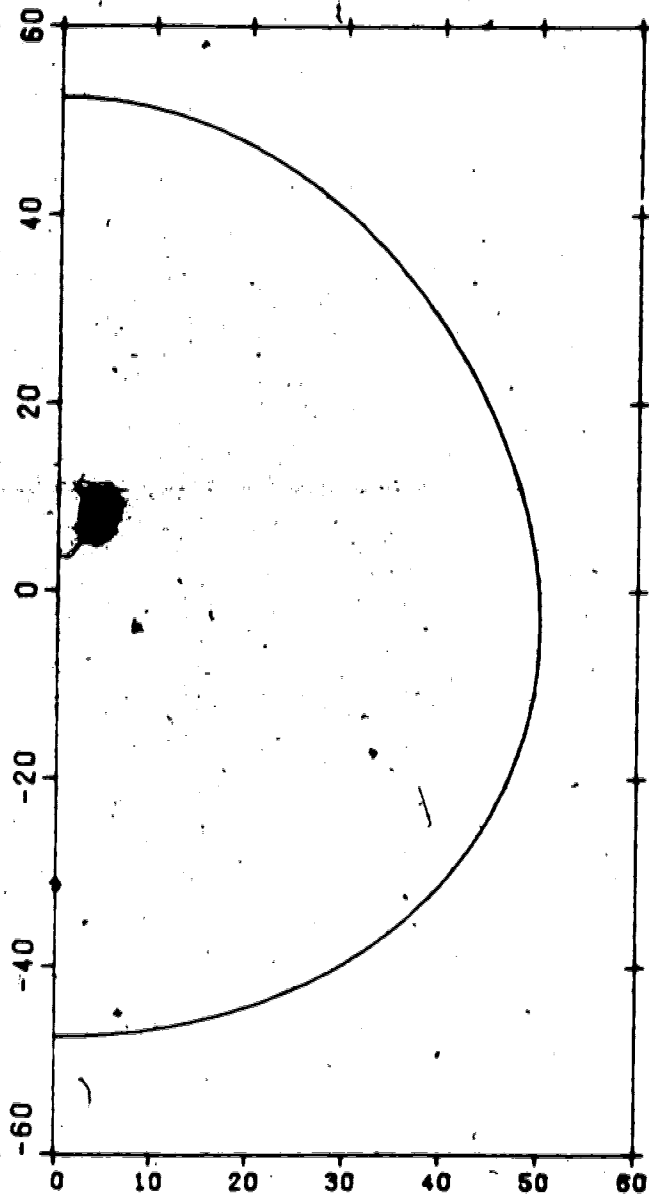


Figure 4.6 A Sphere Perturbed by the Harmonic Y_{30} . The Figure is Cylindrically Symmetric About the Vertical Axis

Further, since δ is small compared to R and in linear stability theory each harmonic develops independently of the others, the velocity of the growth of the perturbed sphere is also given by

$$v = \dot{R} + \dot{\delta} Y_{\ell m} \quad (4.11)$$

It can be shown that the temperature distribution in the liquid and solid around a perturbed sphere discussed above is given by [53]

$$T_{\ell}(r, \theta, \phi) = \frac{(T_f - T_{\alpha})R - 2T_f\Gamma}{r} + \frac{\{(T_f - T_{\alpha})R^{\ell} - T_f\Gamma R^{\ell-1}\ell(\ell+1)\} \delta Y_{\ell m}}{r^{\ell+1}} + T_{\alpha} \quad (4.12)$$

and

$$T_s(r, \theta, \phi) = T_f \left(1 - \frac{2\Gamma}{R}\right) - \frac{T_f (\ell+2) (\ell-1)\Gamma r^{\ell} \delta Y_{\ell m}}{R^{\ell+2}} \quad (4.13)$$

Knowing the temperature distribution from equations (4.12) and (4.13), the velocity v of each element of the interface may be calculated from

$$v = \frac{k_s}{L} \left(\frac{\partial T_s}{\partial r}\right)_{i.f.} - \frac{k_l}{L} \left(\frac{\partial T_l}{\partial r}\right)_{i.f.} \quad (4.14)$$

where the subscript i.f. indicates that the quantity is to be evaluated at the interface. It is assumed in the equation

(4.14) that the normal gradients on the interface are the same as the radial gradients.

The quantity $\dot{\delta}/\delta$ can now be evaluated using the equation (4.11) and it can be shown to be

$$\frac{\dot{\delta}}{\delta} = \frac{(\ell-1) T_f K_\ell}{R^2 L} \left\{ \frac{T_f - T_\alpha}{T_f} - \frac{\Gamma}{R} \left[(\ell+2)(\ell+1) + 2 + \ell(\ell+2) \frac{k_s}{k_\ell} \right] \right\} \quad (4.15)$$

The two criteria for stability are defined as

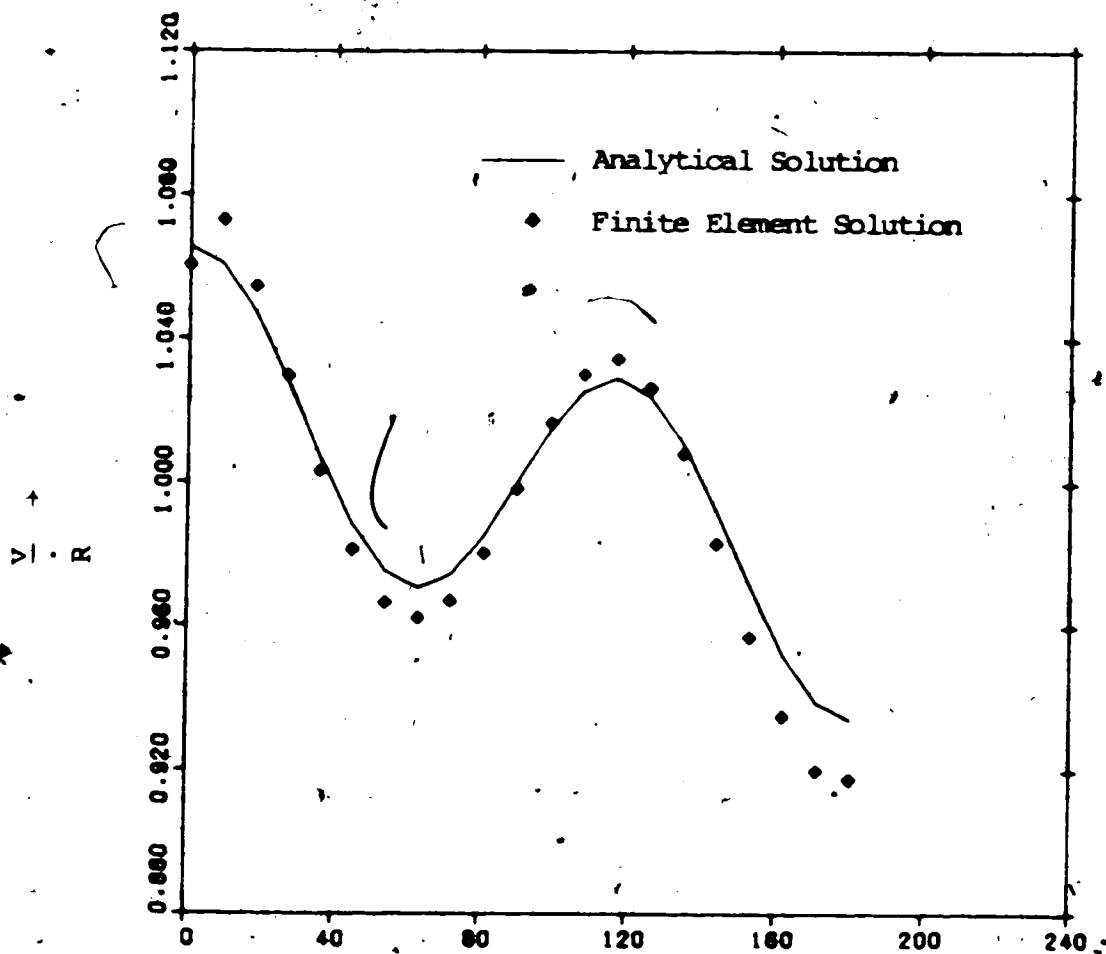
$$(\dot{\delta}/\delta)/(R/R) = 0, \quad (4.16)$$

for absolute stability (no growth of perturbation), and

$$(\dot{\delta}/\delta)/(R/R) < 1, \quad (4.17)$$

for relative stability (perturbation grows no faster than the sphere itself). It is clear that the quantity $(\dot{\delta}/\delta)/(R/R)$ can be easily calculated from the equations (4.15) and (4.8).

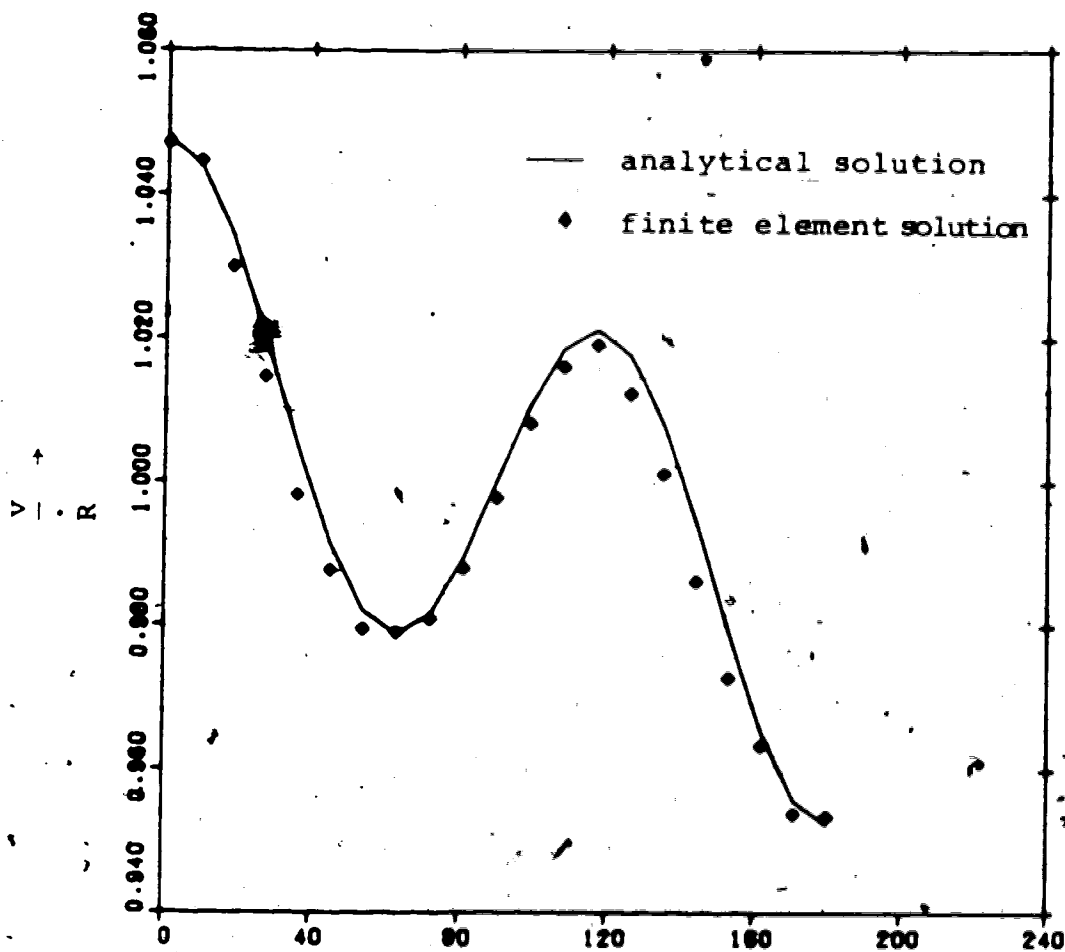
Several computer runs were made to test the applicability of the finite element method to the problem of the stability of a slightly perturbed sphere growing in an originally uniformly supercooled melt. The angular harmonics considered were Y_{20} and Y_{30} . Figures 4.7 through 4.9 and



Angular Position Along the Interface
(Angle in Degrees From the Z Axis)

Figure 4.7

A Comparison of the Analytical Solution and the Finite Element Solution for the Growth Rate of a Sphere Perturbed by the Harmonic Y_{30} ($R = 100 R^*$; $\frac{k_s}{k_l} = 1$)



Angular Position Along the Interface
(Angle in Degrees from the z Axis)

Figure 4.8 A Comparison of the Analytical Solution
With the Finite Element Solution for
the Growth Rate of a Sphere Perturbed
by the Harmonic Y_{30} ($R = 100 R^*$;

$$\left(\frac{k_s}{k_l} = 0\right)$$

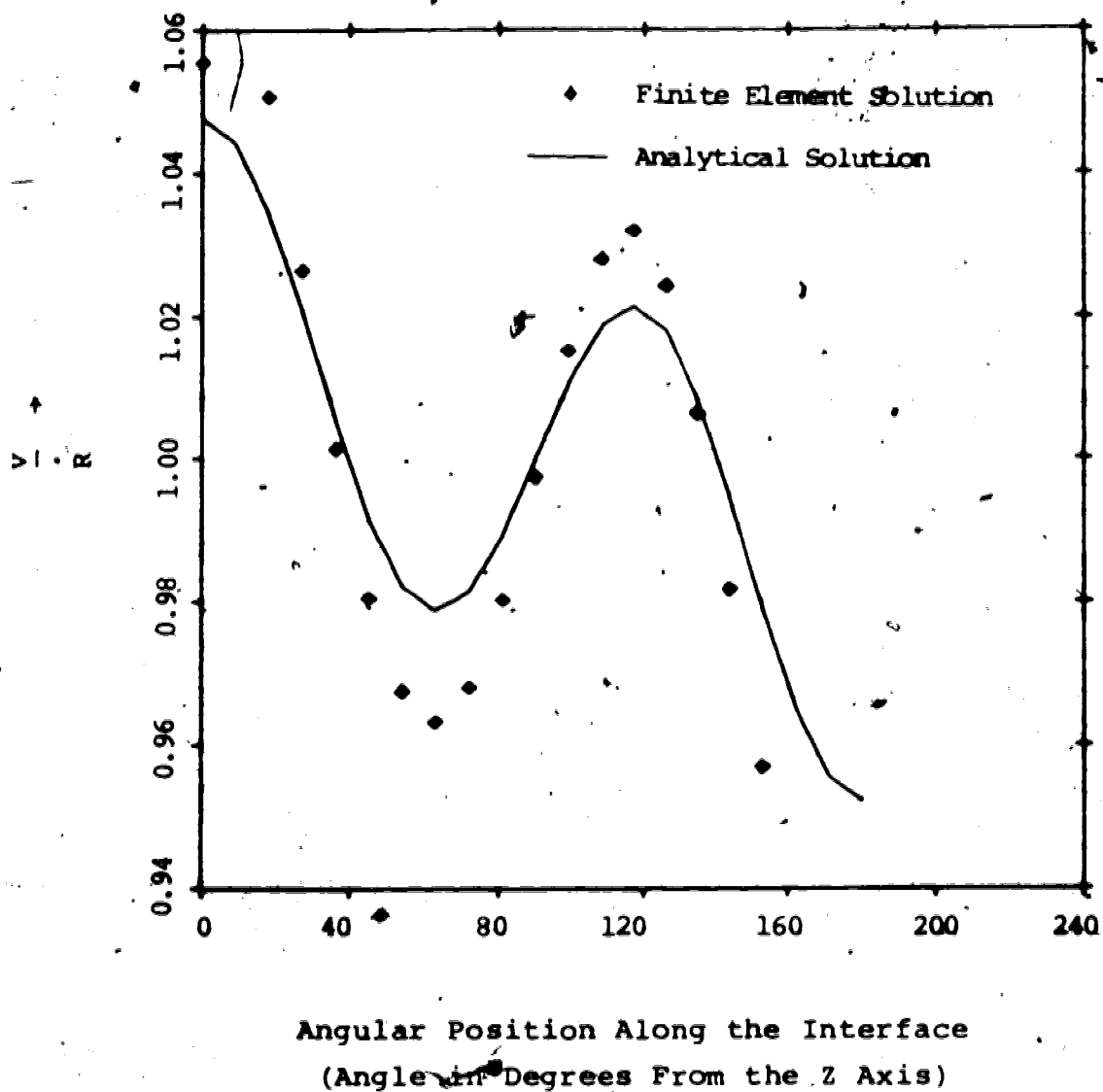


Figure 4.9 A Comparison of the Analytical Solution and the Finite Element Solution for the Growth Rate of a Sphere Perturbed by the Harmonic Y_{30} ($R = 100 R^*$; $\frac{k_s}{k_l} = 4$)

and Table 4.5 and 4.6 summarize the comparison of the finite element calculations and the analytical results. It is evident that generally good agreement exists between the two methods, the maximum error in the quantity $\delta/\delta / R/R$ being about 40 percent for the case $k_s/k_l = 4$, but less than 10 percent when $k_s/k_l = 0$. However, it should be noted that these errors are numerically magnified because the calculations for $\delta/\delta / R/R$ involve subtraction of quantities which are very close to each other. This means that the finite element results are much closer to the analytical results when the heat transfer in the solid side is neglected. This should be expected because it is difficult to model the solid side of the sphere very accurately since the sizes involved are so small. The accuracy of the finite element calculations can be further improved by increasing the number of nodes.

4.4 The Stability of a Solid Cylinder Growing in a Supercooled Liquid

The next geometrical shape considered is a cylinder in an infinite liquid. The length of the cylinder is assumed to be large enough to avoid end corrections.

4.4.1 The Unperturbed Growth of a Cylinder

Using arguments similar to those used for the sphere would result in the Laplace equation

TABLE 4.5

A COMPARISON OF THE ANALYTICAL METHOD AND THE FINITE ELEMENT
METHOD TO STUDY THE STABILITY OF A SLIGHTLY PERTURBED
SPHERE GROWING IN A SUPERCOOLED LIQUID
(THE SPHERE PERTURBED BY THE HARMONIC Y_{20})

R/R^*	k_s/k_l	Analytical $\delta/\delta / R/R$	Finite Element $\delta/\delta / R/R$
25	0	0.750	0.792
25	1	0.583	0.634
25	4	0.083	0.116
50	0	0.878	0.913
50	1	0.796	0.873
50	4	0.551	0.695
100	0	0.939	0.961
100	1	0.899	0.942
100	4	0.777	0.901

TABLE 4.6

A COMPARISON OF THE ANALYTICAL METHOD AND THE FINITE ELEMENT
METHOD TO STUDY THE STABILITY OF A SLIGHTLY PERTURBED
SPHERE GROWING IN A SUPERCOOLED LIQUID
(THE SPHERE PERTURBED BY THE HARMONIC Y_{30})

R/R*	k_s/k_l	Analytical $\delta/\delta / R/R$	Finite Element $\delta/\delta / R/R$
25	0	1.167	1.223
25	1	0.542	0.595
25	4	-1.333	1.220
50	0	1.592	1.766
50	1	1.286	1.53
50	4	0.367	0.624
100	0	1.798	1.914
100	1	1.647	1.843
100	4	1.191	1.434

$$\nabla^2 T_\ell = 0, \quad (4.18)$$

subject to the boundary conditions

$$T_\ell (r = \alpha) = T_\alpha \quad (4.19)$$

$$-T_\ell (r=R) = T_f - \frac{\Gamma T_f}{R} = T_{if} \quad (4.20)$$

and the heat balance condition

$$-k_\ell \left[\frac{\partial T_\ell}{\partial r} \right]_{r=R} + k_s \left[\frac{\partial T_s}{\partial r} \right]_{r=R} = L \frac{dR}{dt} \quad (4.21)$$

The solution of the above equation (4.18) is

$$T_\ell (r) = A \ln(r) + B \quad (4.22)$$

where A and B are to be evaluated using boundary conditions.

However, the boundary condition $T_\ell (r=\alpha) = T_\alpha$, makes T_ℓ at $r = \alpha$ infinite, so there is a difficulty in using the Laplace equation with a boundary at $r = \alpha$. The steady state cylindrical case can therefore, only be solved in a finite domain. If the outer boundary is taken as R_λ , the temperature distribution is

$$T_\ell (r) = T_\alpha + (T_{if} - T_\alpha) \left[1 - \frac{\ln(r/R)}{\ln(R_\lambda/R)} \right] \quad (4.23)$$

when equation (4.23) is used in the boundary condition for the conservation of heat we find

$$\frac{dR}{dt} = \frac{k_l}{LR \ln(R_\lambda/R)} (T_f - T_\alpha - \frac{\Gamma T_f}{R}) \quad (4.24)$$

Figures 4.10 through 4.12 and Tables 4.7 and 4.8 present the comparison of the finite element calculations and analytical results for the growth of a cylinder in a supercooled liquid. The results show a very close agreement. It should be noted that in the case of a sphere the results obtained from a finite but sufficiently large domain were compared with analytical solutions based on an infinite domain while in the case of the cylinder the results from a finite domain are compared with analytical solutions based on a finite domain. Thus, it should be expected that the finite element results for the cylinder agree much more closely with the analytical results.

4.4.2 The Stability of a Perturbed Cylinder

Consider a cylinder of radius R slightly perturbed by a set of spatial harmonics. The position of the perturbed surface is given by

$$r = R + \delta \cos(K\phi) \quad (4.25)$$

where δ is a positive length very small compared to R and K is a positive integer, so that r returns to its original value when ϕ changes by 2π . Hardy and Coriell [35] have shown that to the first order, if normal gradients on the interface

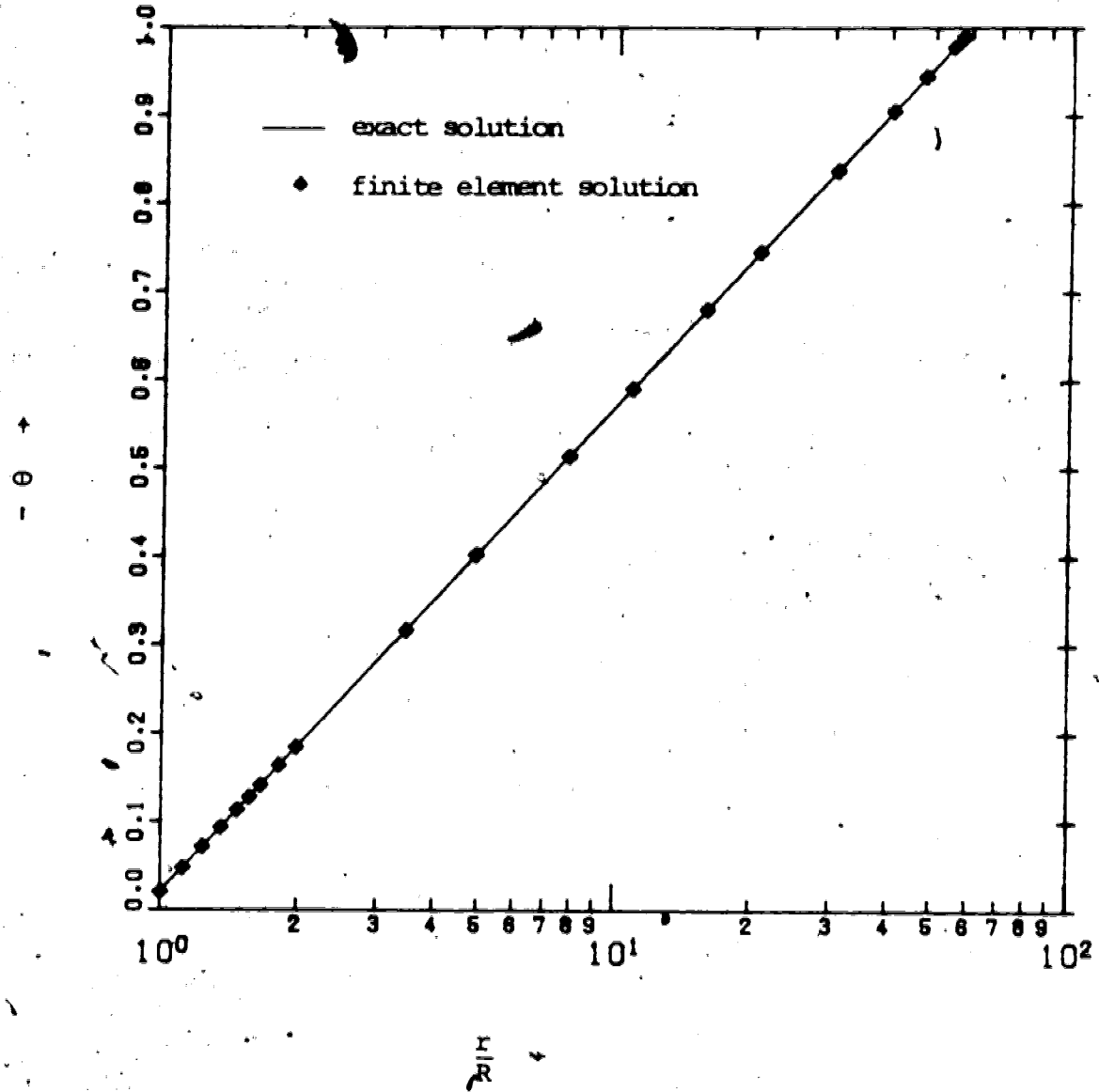


Figure 4.10 A Comparison of the Analytical Solution and the Finite Element Solution for the Temperature Distribution Around a Cylinder Growing in a Supercooled Liquid
($R = 50 R^*$; $R_\lambda/R = 60$)

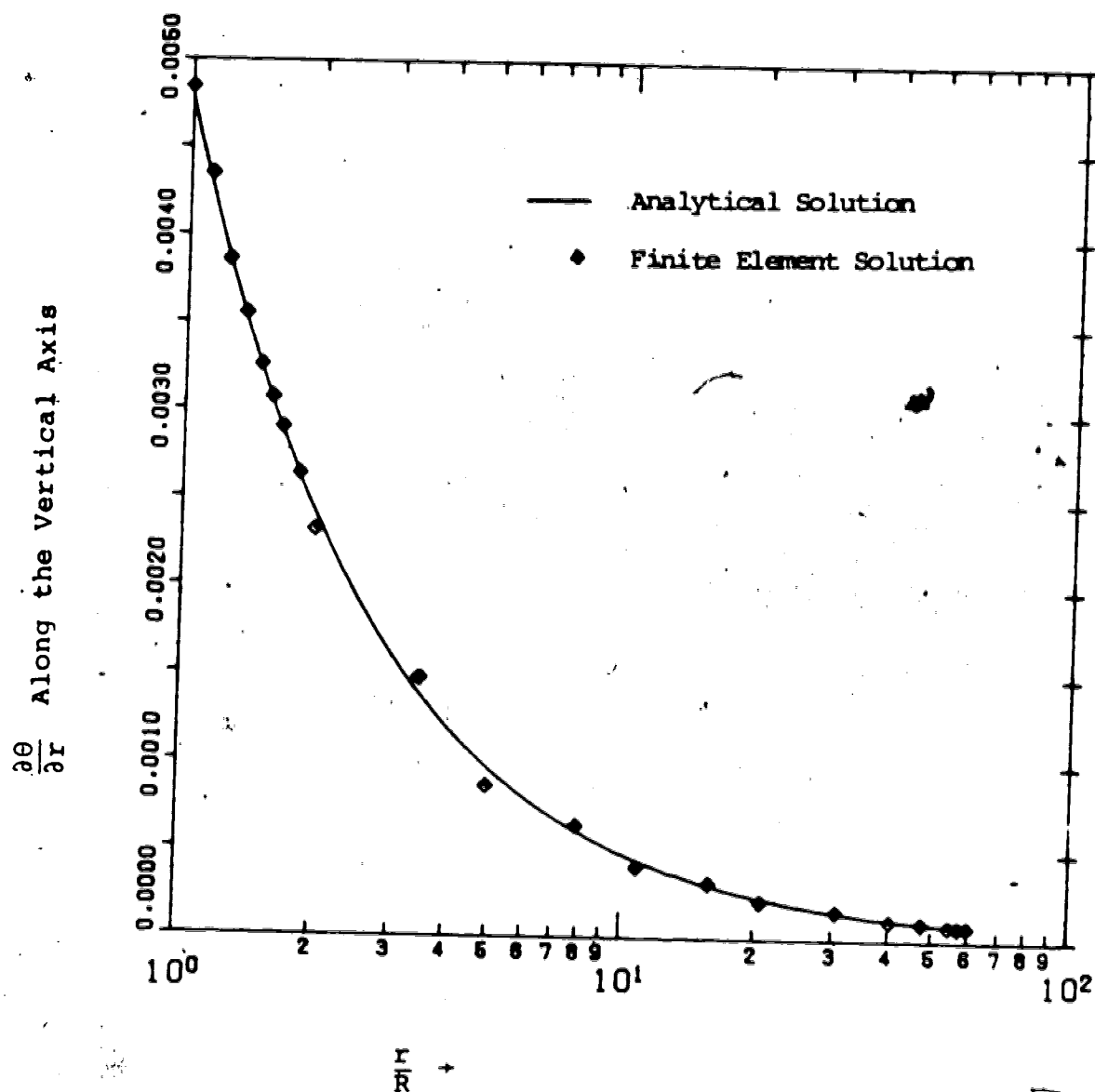


Figure 4.11 A Comparison of the Analytical Solution and the Finite Element Solution for the Temperature Gradient Around a Cylinder Growing in a Supercooled Liquid

$$(R = 50 R^*, \quad R_\lambda/R = 60)$$

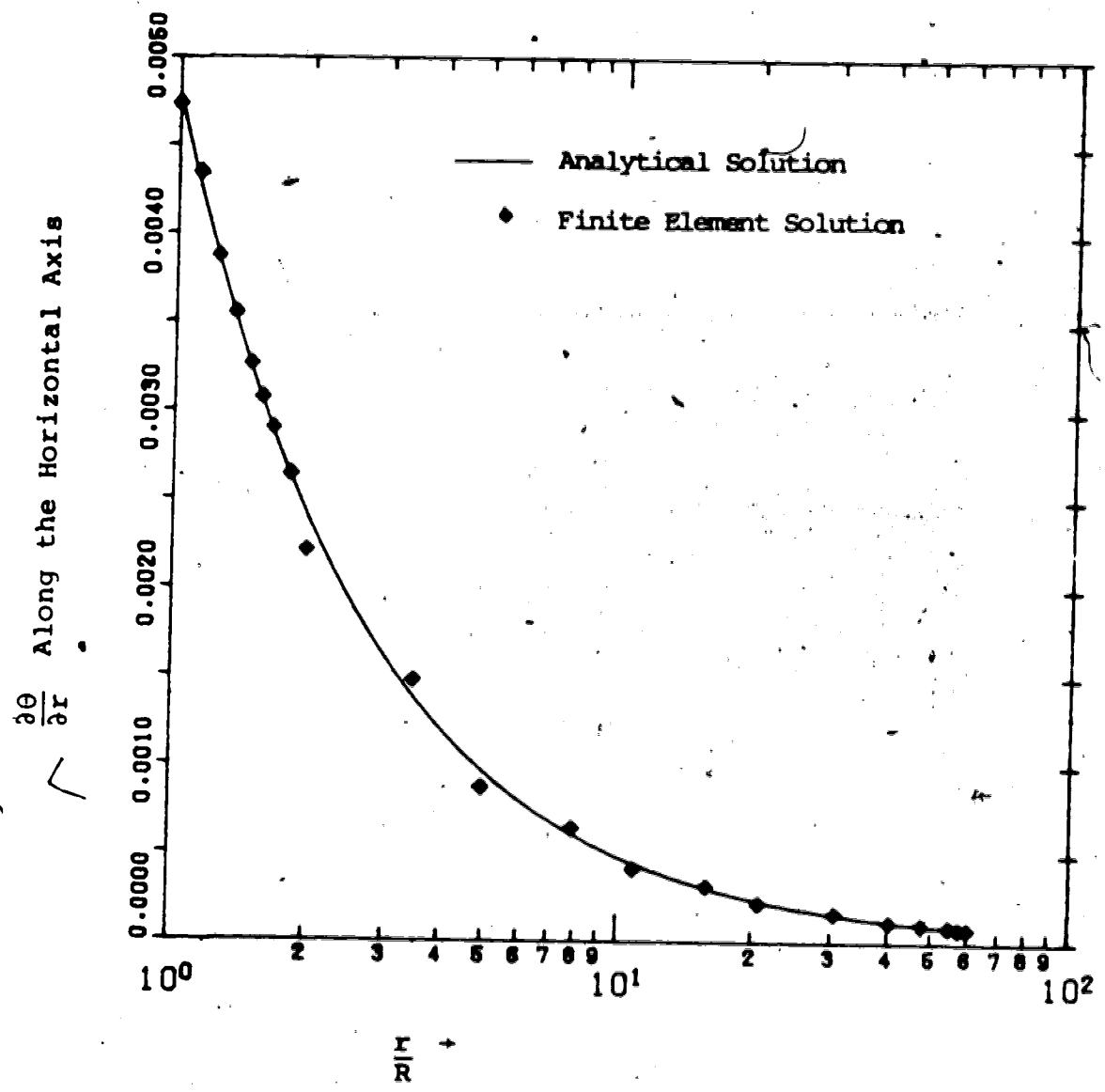


Figure 4.12 A Comparison of the Analytical Solution and the Finite Element Solution for the Temperature Gradient Around a Cylinder Growing in a Supercooled Liquid
($R = 50 R^*$; $R_\lambda/R = 60$)

TABLE 4.7

A COMPARISON OF THE EXACT SOLUTION AND THE FINITE ELEMENT SOLUTION FOR THE GROWTH RATE OF VARIOUS POINTS ALONG THE INTERFACE OF A CYLINDER GROWING IN A SUPERCOOLED LIQUID

$$(R = 1024 R^*, R_\lambda/R = 60, k_s/k_l = 4)$$

Position Along the Interface (Angle in Degrees from the Z Axis)	Finite Element Solution for the Growth Rate (Non-Dimensionalized)	Exact Solution for the Growth Rate (Non-Dimensionalized)
0	0.6000 E -04	0.6010 E -04
12	0.6017 E -04	0.6010 E -04
24	0.6017 E -04	0.6010 E -04
36	0.6018 E -04	0.6010 E -04
48	0.6018 E -04	0.6010 E -04
60	0.6019 E -04	0.6010 E -04
72	0.6019 E -04	0.6010 E -04
90	0.6062 E -04	0.6010 E -04

TABLE 4.8

A COMPARISON OF THE EXACT SOLUTION AND THE FINITE ELEMENT SOLUTION FOR THE GROWTH RATE OF VARIOUS POINTS ALONG THE INTERFACE OF A CYLINDER GROWING IN A SUPERCOOLED LIQUID

$$(R = 512 R^*, R\lambda/R = 60, k_s/k_l = 4)$$

Position Along the Interface (Angle in Degrees from the Z Axis)	Finite Element Solution for the Growth Rate (Non-Dimensionalized)	Exact Solution for the Growth Rate (Non-Dimensionalized)
0	0.1199 E -03	0.1202 E -03
12	0.1204 E -03	0.1202 E -03
24	0.1204 E -03	0.1202 E -03
36	0.1204 E -03	0.1202 E -03
48	0.1204 E -03	0.1202 E -03
60	0.1204 E -03	0.1202 E -03
72	0.1204 E -03	0.1202 E -03
90	0.1212 E -03	0.1202 E -03

are considered the same as radial gradients,

$$\frac{\dot{\delta}}{\delta} = \frac{k_l}{LR^2} \left\{ \frac{(K-1)}{\ln(R_\lambda/R)} [1 - (R^*/R)] - \frac{R^*}{R} K (K^2-1) \left(1 + \frac{k_s}{k_l}\right) \right\} \quad (4.26)$$

where R^* is the classical nucleation radius. Equations (4.26) and (4.24) can be used in combination to obtain the quantity $(\dot{\delta}/\delta)/(R/R)$ which determines the stability criterion.

Several computer runs were made using different values of K , R_λ/R , and k_s/k_l for testing the stability of a perturbed cylinder. Figures 4.13 through 4.15 and Tables 4.9 through 4.10 show the comparison of the finite element results with the analytical results. Again, the results are in good agreement and the accuracy is even better when the solid side heat transfer is neglected.

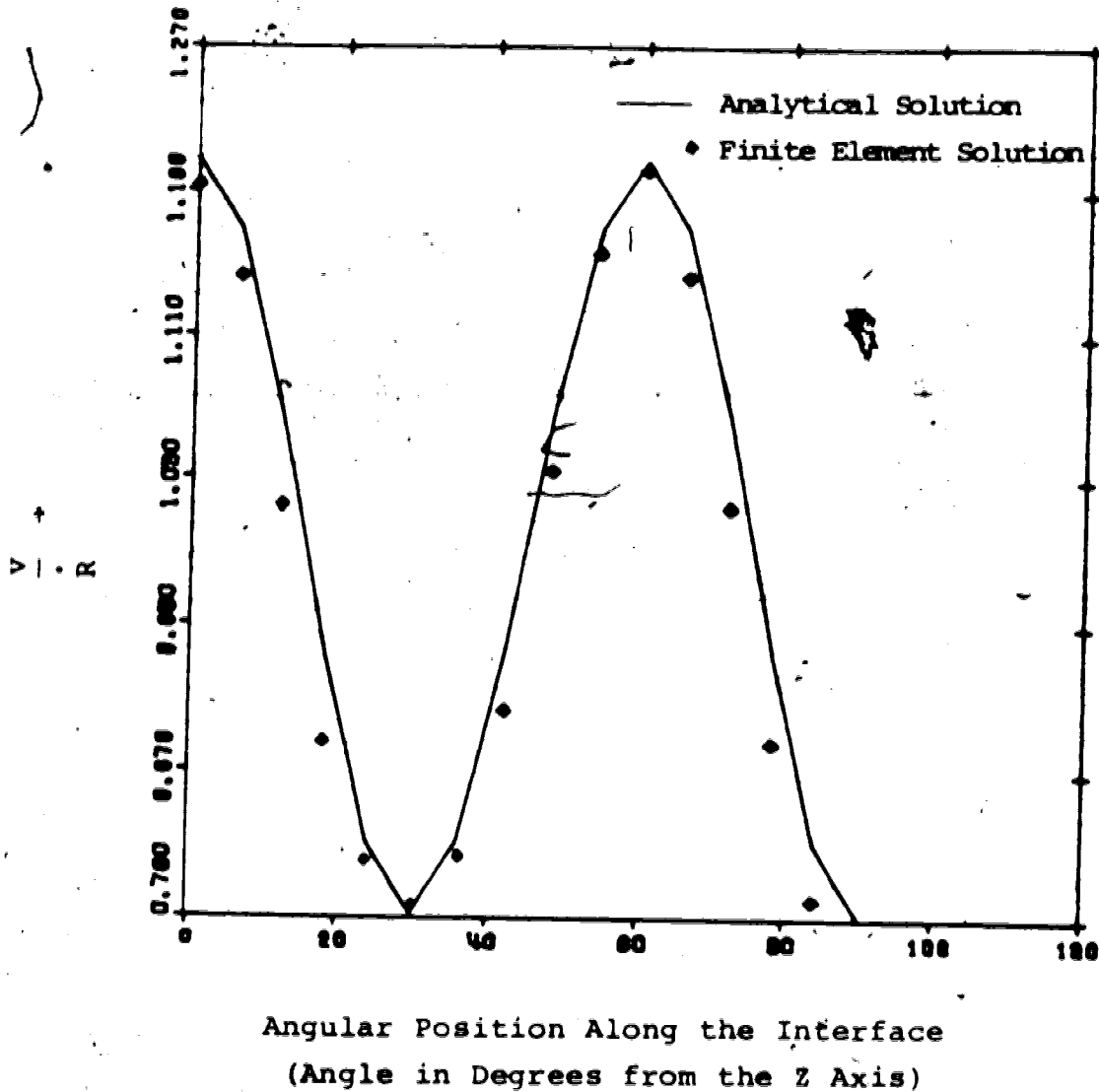
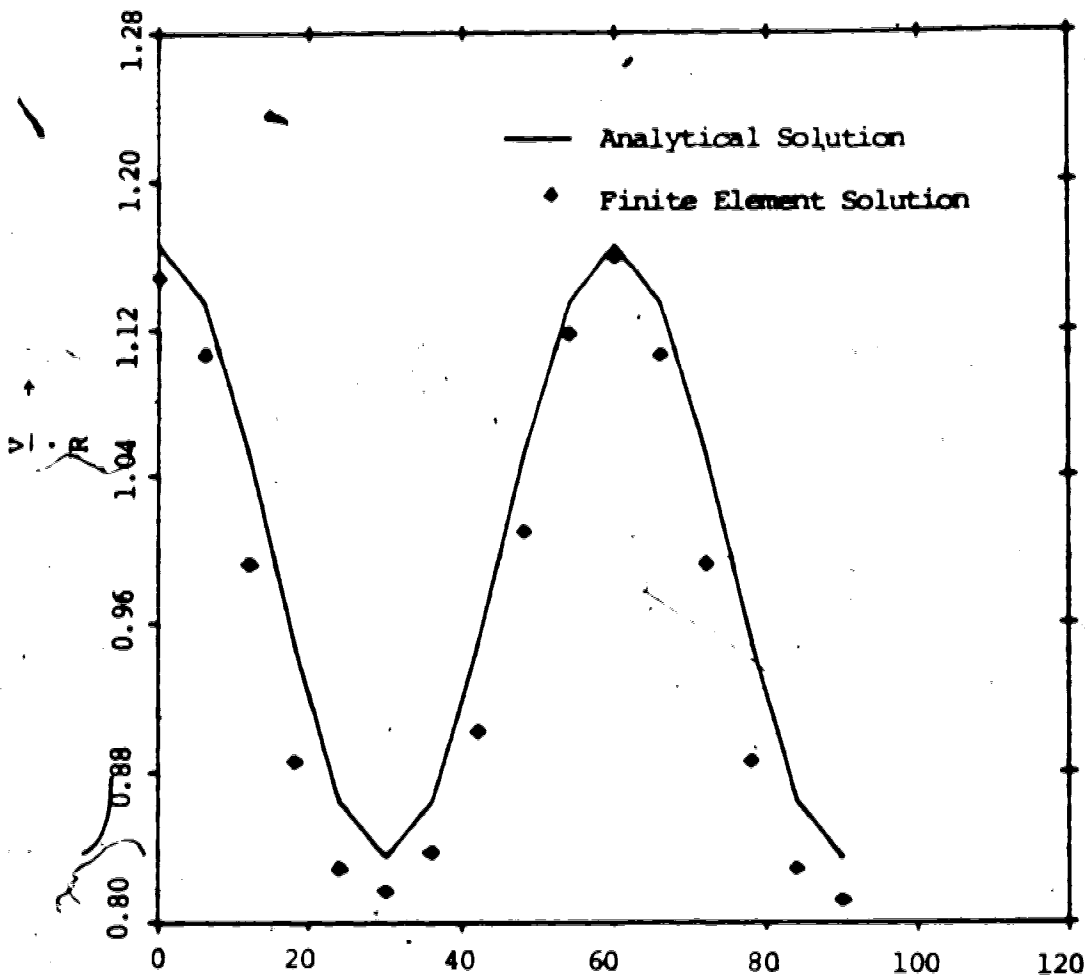


Figure 4.13 A Comparison of the Analytical Solution with the Finite Element Solution for the Growth Rate of a Perturbed Cylinder

$$(R = 1024 R^* ; \frac{k_s}{k_l} = 0 ; K = 6)$$



Angular Position Along the Interface
(Angle in Degrees from the Z Axis)

Figure 4.14 A Comparison of the Analytical Solution with the Finite Element Solution for the Growth Rate of a Perturbed Cylinder

$$(R = 1024 R^* ; \frac{k}{K} = 1, K = 6)$$

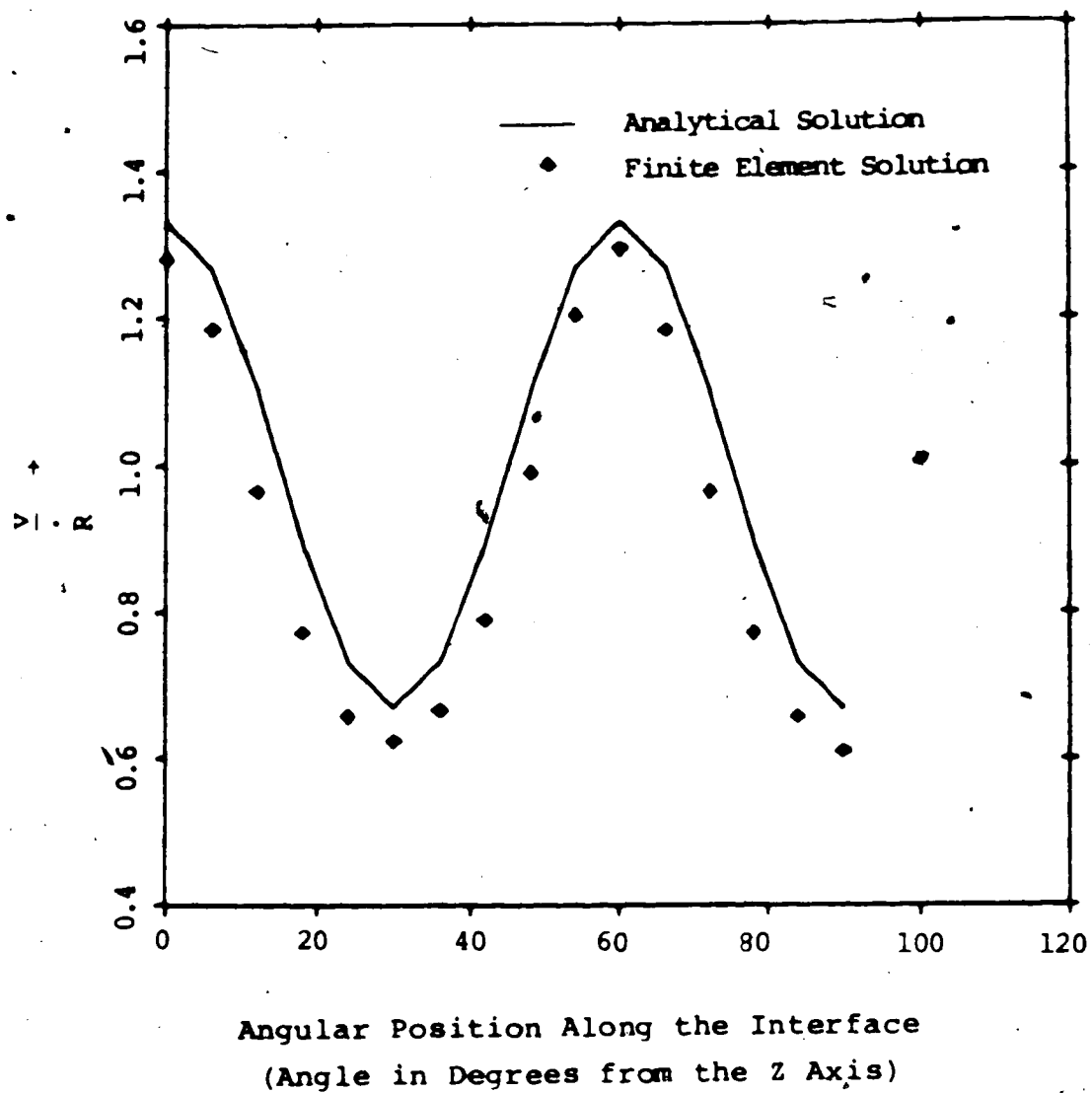


Figure 4.15. A Comparison of the Analytical Solution with the Finite Element Solution for the Growth of a Perturbed Cylinder ($R = 512 R^*$; $\frac{k_s}{k_l} = 1, K = 6$)

TABLE 4.9

A COMPARISON OF THE ANALYTICAL METHOD AND THE FINITE ELEMENT
METHOD TO STUDY THE STABILITY OF A SLIGHTLY PERTURBED
CYLINDER GROWING IN A SUPERCOOLED LIQUID
(THE CYLINDER PERTURBED BY THE HARMONIC $K=6$)

R/R^*	k_s/k_l	Analytical $\delta/\delta / R/R$	Finite Element $\delta/\delta / R/R$
400	0	2.845	3.012
400	1	0.877	1.013
400	4	-5.770	7.234
512	0	3.317	3.498
512	1	1.635	1.785
512	4	-3.413	-4.80
1024	0	4.160	4.390
1024	4	0.798	1.209

TABLE 4.10

A COMPARISON OF THE ANALYTICAL METHOD AND THE FINITE ELEMENT
METHOD TO STUDY THE STABILITY OF A SLIGHTLY PERTURBED
CYLINDER GROWING IN A SUPERCOOLED LIQUID
(THE CYLINDER PERTURBED BY THE HARMONIC $K=2$)

R/R^*	k_s/k_l	Analytical $\delta/\delta / R/R$	Finite Element $\delta/\delta / R/R$
100	1	0.752	0.791
100	1	0.504	0.612
100	4	-0.240	-0.430
200	0	0.876	0.923
200	1	0.753	0.862
200	4	0.383	0.501
400	0	0.938	0.952
400	1	0.876	0.930
400	4	0.692	0.783

CHAPTER 5

DENDRITIC GROWTH

5.1 Introduction

The purpose of this chapter is to demonstrate that the finite element method can be used effectively to calculate the velocity of growth of freely growing dendrites in supercooled liquids. The first portion of this chapter deals with the selection of an appropriate domain for the finite element study, while the latter portion presents the results obtained using this domain for various systems (i.e. dendritic growth in ice, tin, succinonitrile etc.). The results thus obtained are compared with the available analytical and experimental results. The shapes studied are paraboloids of revolution and parabolic cylinders.

5.2 Selection of Domain to be Studied

As described previously in Chapter 2, most of the analytical studies of dendritic growth consider a dendrite growing in a supercooled liquid infinite in extent. However, in practice the domain is always finite. Also, since both the paraboloid of revolution and parabolic cylinder have an axis of symmetry, the domain to be studied can be represented by Figure 5.1. The problem now is to select various dimensions in the Figure 5.1 so that the finite element results become

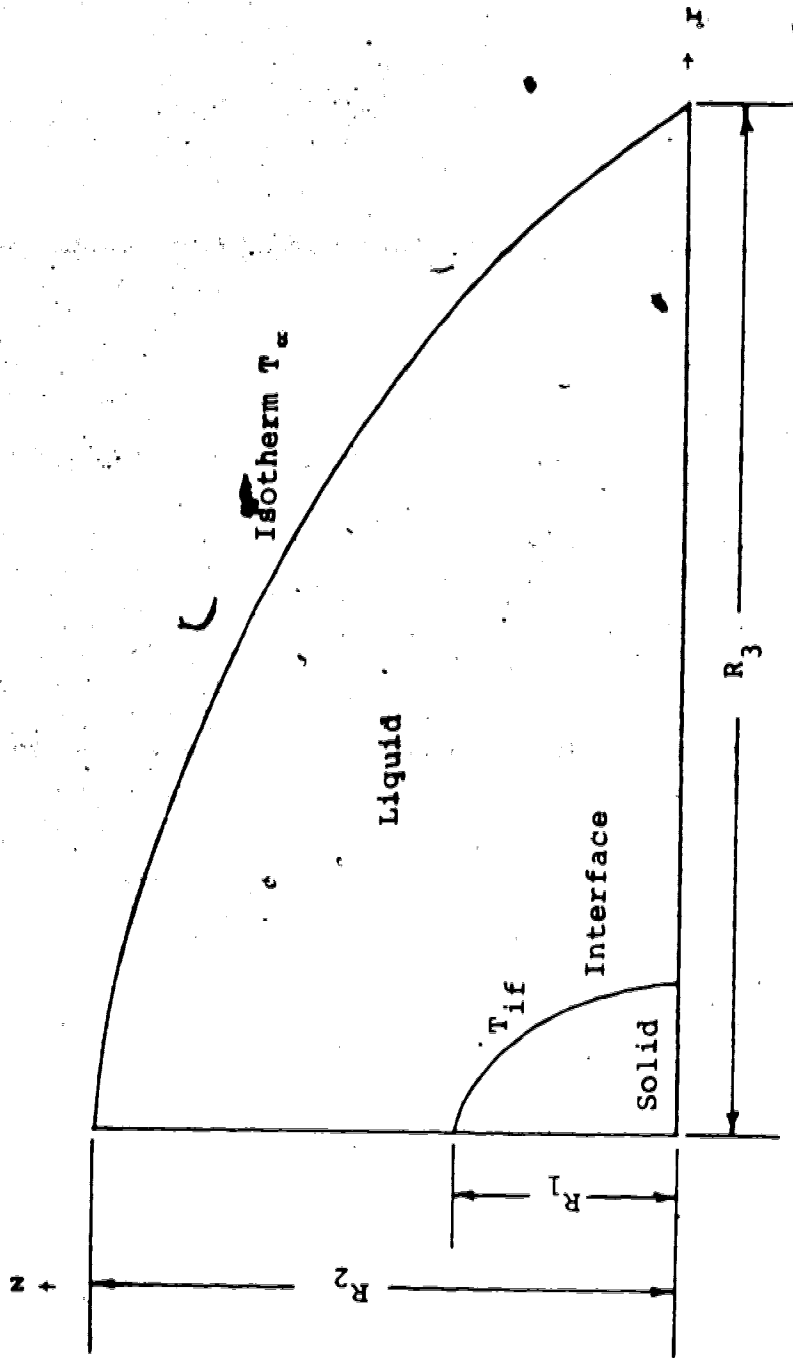


Figure 5.1 The domain to be considered for the finite element study of dendritic growth

as realistic as possible. To achieve this goal the following criteria should be met: (1) the outer boundary should be close to an isotherm with temperature equal to T_α , (2) the domain should be large enough so that the calculated interface velocity changes very little by increasing domain any further, (3) the number of nodes should be optimized in a way that the results are reasonably accurate yet the computer time required is not excessive.

To avoid a costly and long trial and error procedure to obtain an appropriate domain some guidelines were adopted from the available literature. Bolling and Tiller [16] have shown that a melt may be considered infinite with respect to the dendrite when its boundaries are $\sim 10 \alpha_l / v$ away from the body of the growing dendrite and it is sufficiently long for the steady state to be reached. Kotler and Tarshis [39] have noted that a paraboloid of revolution is an excellent approximation for the shape over a distance on the order of $10R$ back from the tip. Holzman [46] has presented a contour map of isotherms in and around a growing dendrite which can be used to define a domain to be studied. An approximate value of the tip curvature of a dendrite for various systems can be easily determined from the available literature.

Keeping the above mentioned guidelines in mind, an initial domain was selected. The finite element method as described in Chapter 3 was used to obtain the temperature field inside and around a growing dendrite. The assumptions

and mathematical formulation were the same as those described in Chapter 3. Sensitivity studies were made to select the most appropriate domain to be studied. The finite element grid was such that the mesh was finer near the dendrite tip (where temperature gradients are large) and coarse away from the tip (where temperature gradients are small). Figure 5.2 presents the effect of the size of the dimension R_2 on the tip velocity of the dendrite. It is clear that when the domain is small (i.e. when the boundary with the temperature T_a is not very far from the tip) the driving force is such that the dendrite will grow with a high velocity. However, as the domain is made larger the tip velocity tends to reach a limiting value. To fix the dimension R_3 it can be argued on physical grounds that R_3 should be larger than R_2 so that the temperature gradients near the outer boundary are nearly the same. After only a few trials it was found that to study the growth of dendrites with the shape of paraboloids of revolution the most appropriate domain was such that $R_1 = 10R$, $R_2 = 20R$, and $R_3 = 40R$. The temperature field obtained from this domain further justified its appropriateness. Figures 5.3 and 5.4 present the temperature field along the vertical and horizontal axes respectively. It is clear that the temperature gradients near the outer boundary in both figures are very small and equal (ideally the temperature gradient at the outer boundary should approach to zero), while the gradients near the interface are such that the tip velocity is greater than the velocity at the

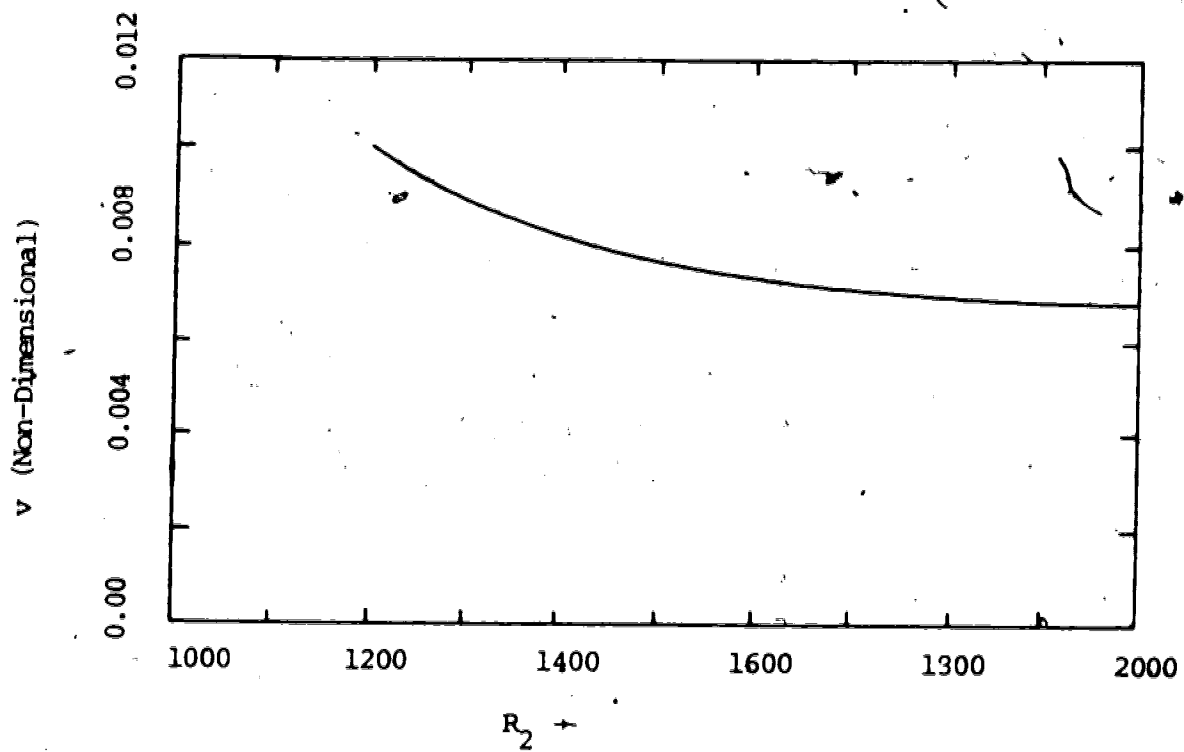


Figure 5.2

Plot to determine the effect of the finite element domain size on the growth rate of dendrites

$$\left(\frac{k_s}{k_l} = 4, Ste = 0.05\right)$$

$$R_1 = .900, R_3 = 2R_2, \bar{K} = -.0022)$$

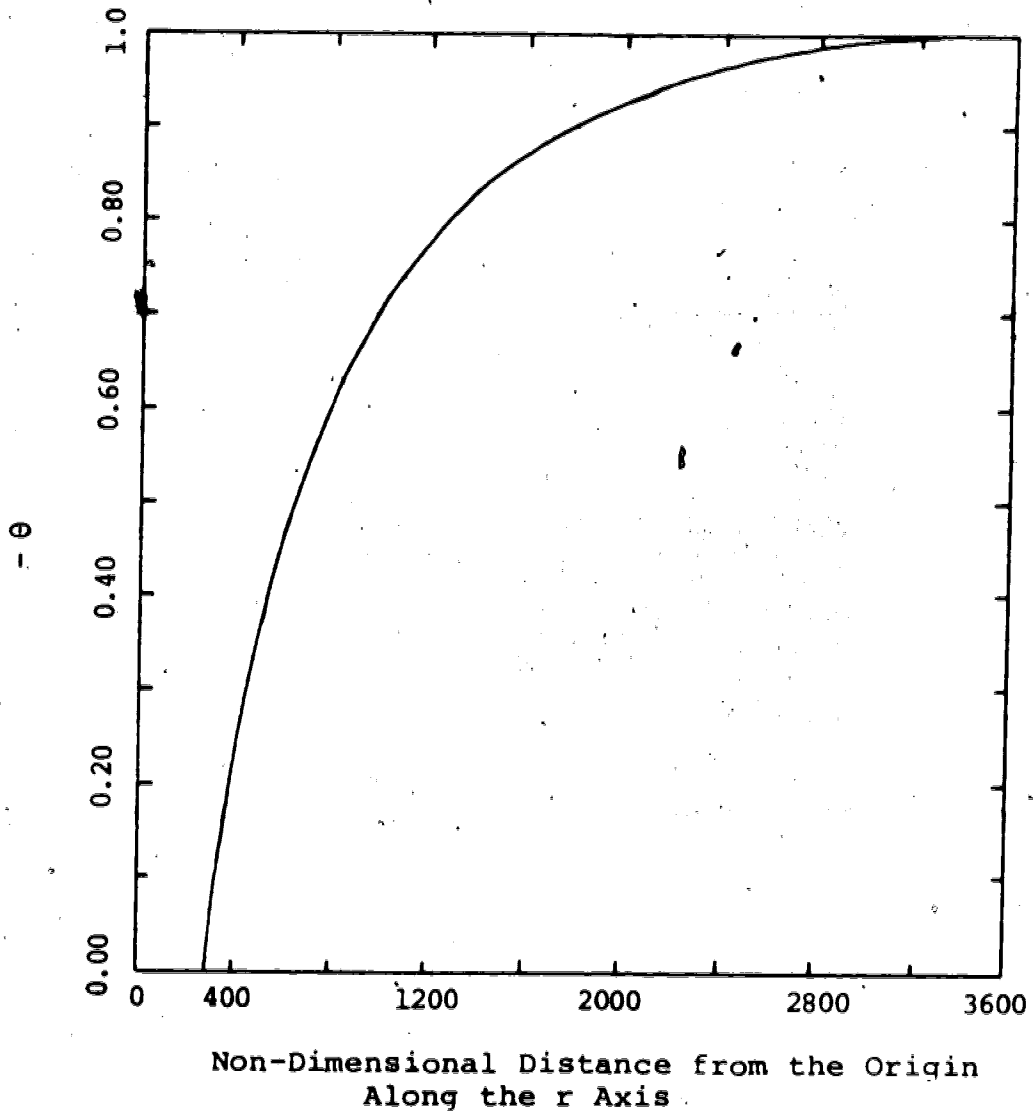


Figure 5.3 Plot of the temperature distribution around a dendrite growing in a supercooled liquid

$$\left(\frac{k}{k_l}\right) = 4, \text{ Ste} = 0.05,$$

$$\bar{K} = -0.022)$$

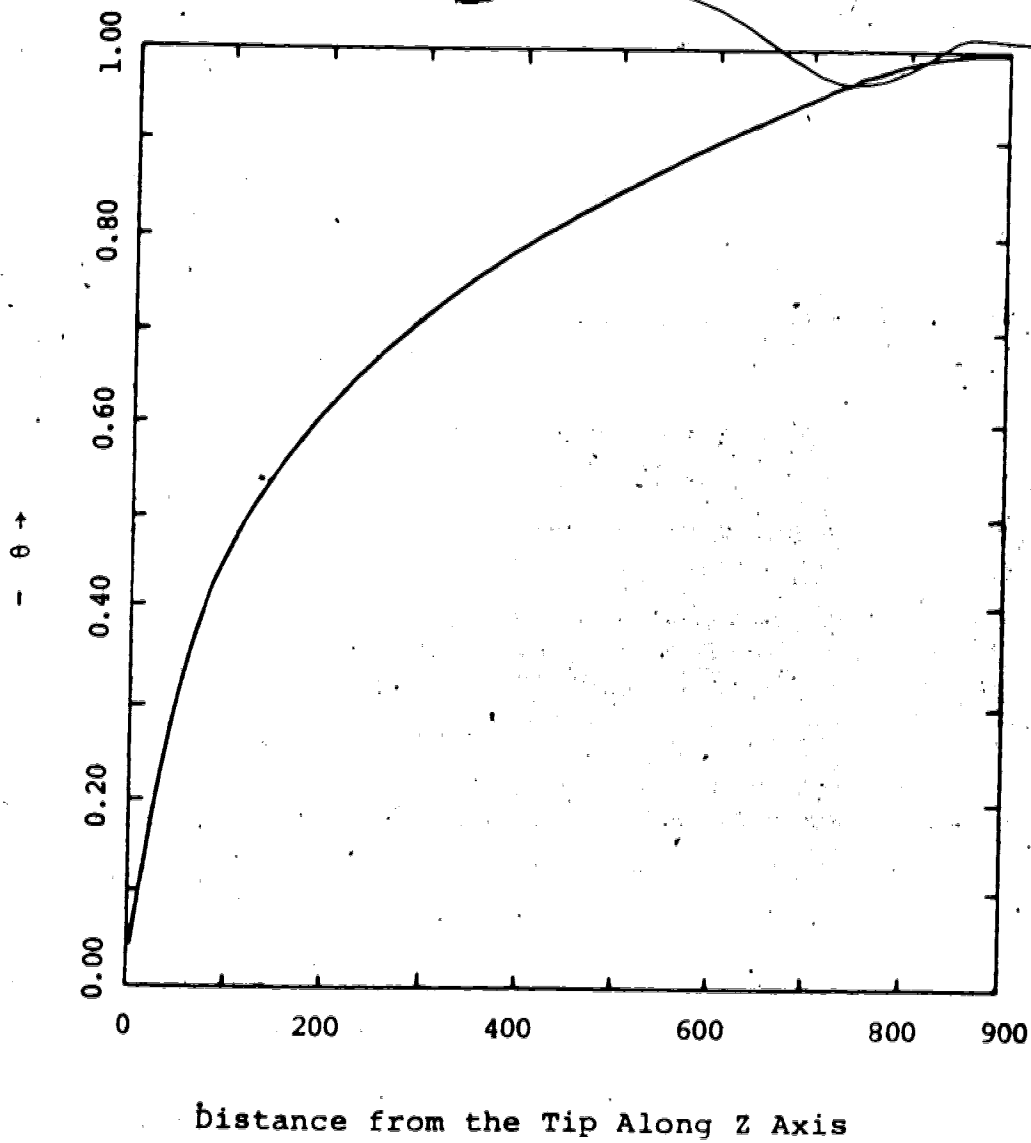


Figure 5.4 Plot of the Temperature Distribution around a Dendrite Growing in a Supercooled Liquid

$$\left(\frac{k_s}{k_l} = 4, \text{Ste} = 0.05, \bar{K} = -0.022 \right)$$

bottom end of the dendrite. This is very true in real situations. Each side of the domain (liquid and solid) was divided into 200 triangular elements. It was found that by increasing the number of nodes any further the accuracy did not change significantly.

5.3 Dendritic Growth Velocity

5.3.1 Isothermal Dendrite

Ivantsov's calculation has already been mentioned in Chapter 2. It was easily possible to simulate his model by the finite element method since the only change needed in the problem formulation was to eliminate the Gibbs-Thompson effect. The main characteristic of the Ivantsov model is that for different tip curvatures chosen the tip velocity is such that the product vR is constant. Also, the axial component of surface growth remains constant since the dendrite retains its shape as it grows according to the Ivantsov model. Figure 5.5 presents the comparison of the tip velocity obtained by the finite element method and the analytical method for an isothermal dendrite. The results are in very close agreement. Also, it is seen that the product vR remains almost constant in the finite element calculations. Table 5.1 lists the axial velocities calculated at the points along the dendrite interface. It can be seen that again all the velocities calculated are within 1% of the theoretical value.

TABLE 5.1

A COMPARISON OF THE IVANTSOV'S METHOD AND THE FINITE ELEMENT METHOD FOR THE AXIAL GROWTH VELOCITIES OF VARIOUS POINTS ON THE INTERFACE OF AN ISOTHERMAL DENDRITE (NON-DIMENSIONAL TIP CURVATURE = -0.022)

Position Along the Interface (Angle in Degrees from the Z Axis)	Growth Rate by the Ivantsov Method (Non-Dimensionalized)	Growth Rate by the Finite Element Method (Non-Dimensionalized)
0	0.0125	0.0124
17	0.0119	0.0118
28	0.0112	0.0110
39	0.00942	0.00964
50	0.00771	0.00797
61	0.00569	0.00601
	0.00335	0.00383

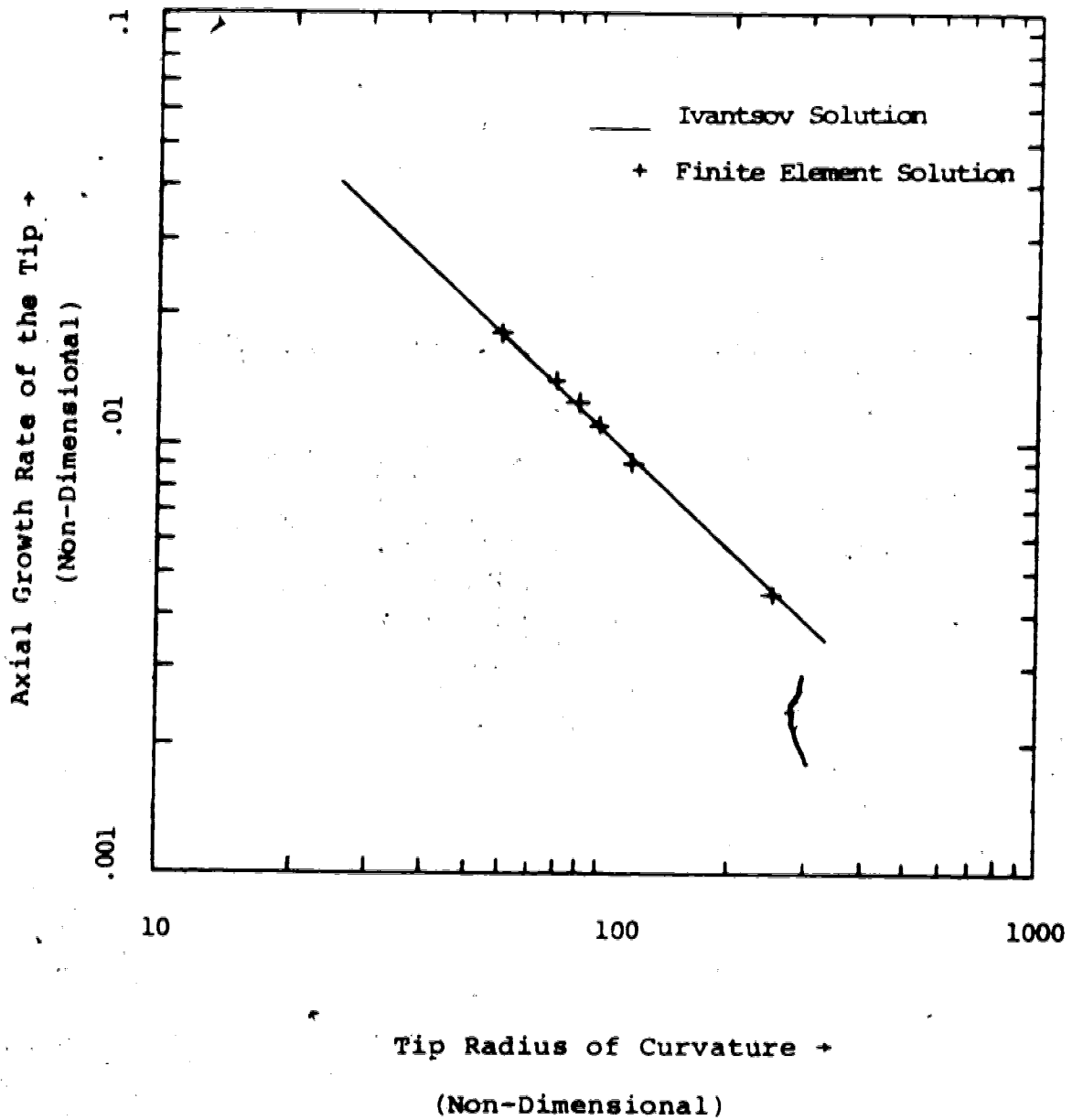


Figure 5.5 A Comparison of the Finite Element Solution and the Ivantsov Solution for the Growth Rate of a Dendrite as a Function of the Tip Radius of Curvature

5.3.2 Non-Isothermal Dendrite

Computations were next performed on a non-isothermal dendrite following the Bolling & Tiller and Temkin models: Calculations were performed for various values of subcoolings (i.e. various Stefan numbers ranging from 0 to 1). Although the computer program is based on non-dimensionalized variables, the physical constants given in Appendix III are used to convert the results to specific systems such as ice, tin, succinonitrile etc. The maximum velocity criterion of Bolling and Tiller was used to determine the actual tip radius of curvature of the dendrite. The stability criterion of Langer and Muller-Kriembhaar was also considered to obtain a comparison with the maximum velocity principle.

Figure 5.6 presents the non-dimensional tip velocity of an ice dendrite as a function of the non-dimensional tip curvature for various values of the stefan number. It is clear that at each Stefan number the v-K curve passes through a maximum which is the actual tip curvature for a dendrite according to the maximum velocity principle. Figure 5.7 presents a comparison of present calculations with those obtained by the Temkin model and the Ivantsov model for a Stefan number of 0.05. The curvature and velocity based on the L-MK stability theory are also shown in the figure.

Figure 5.8 shows the relationship between the actual velocity of growth of ice dendrites as a function of supercooling based on available experimental correlations as well

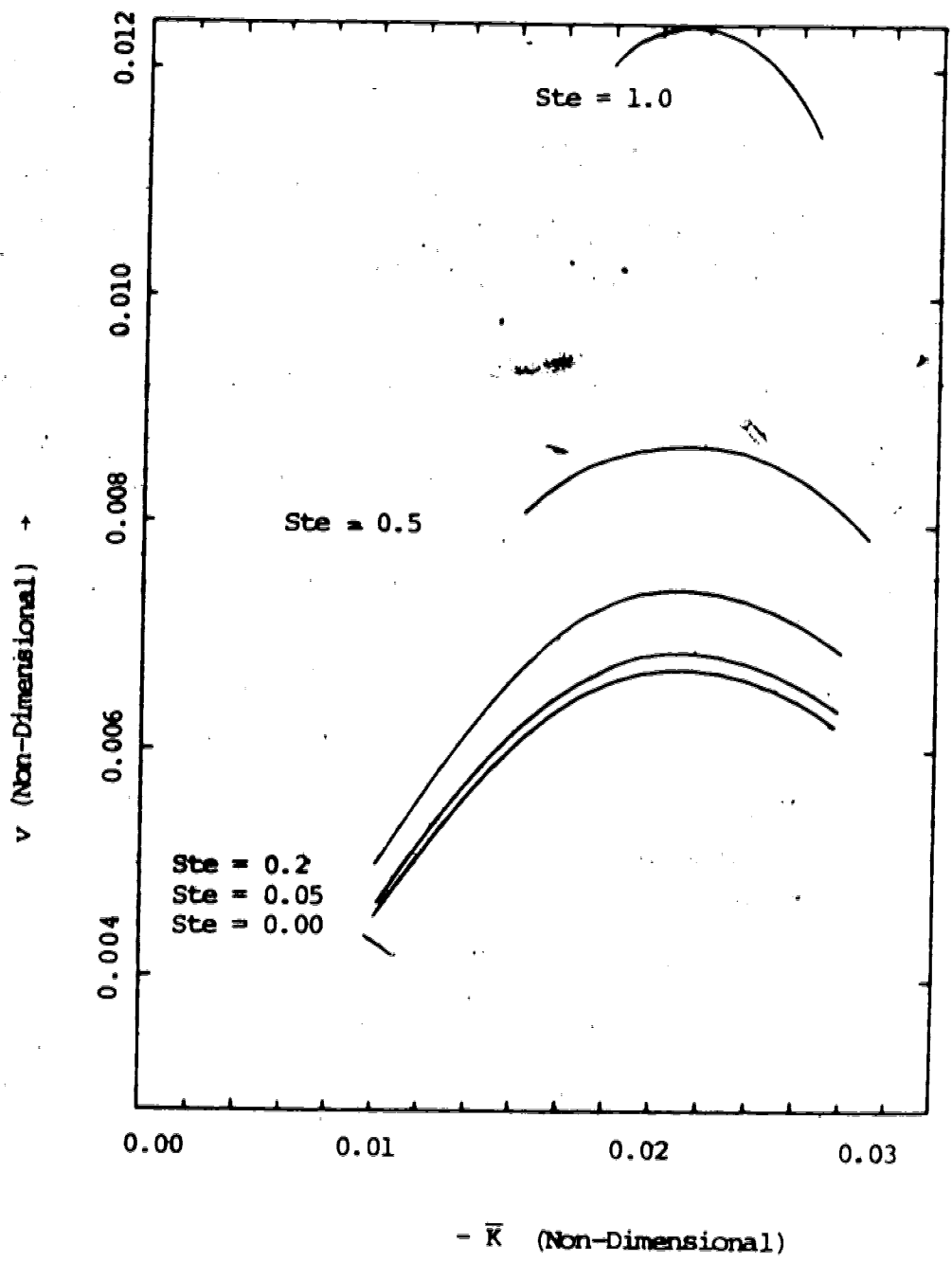


Figure 5.6 Plot of the Growth Velocity of a Dendrite Growing in a Supercooled Water as a Function of the Tip Curvature for Various Stefan Numbers
 $\left(\frac{k_s}{k_l} = 4\right)$

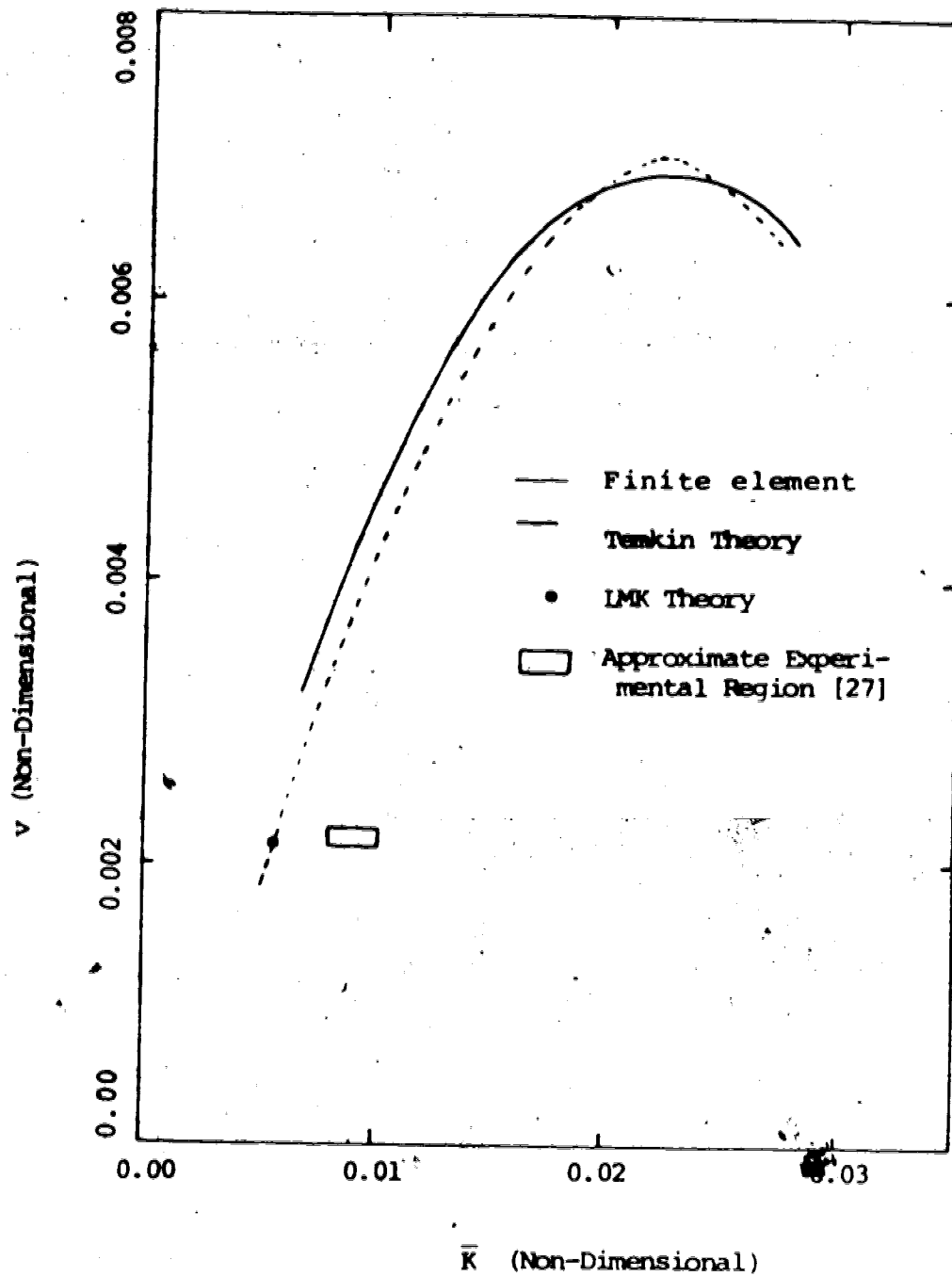


Figure 5.7 Plot of Tip Growth Velocity of a Dendrite as a Function of the Tip Curvature $\left(\frac{k}{k_0} = 4, Ste = 0.05\right)$

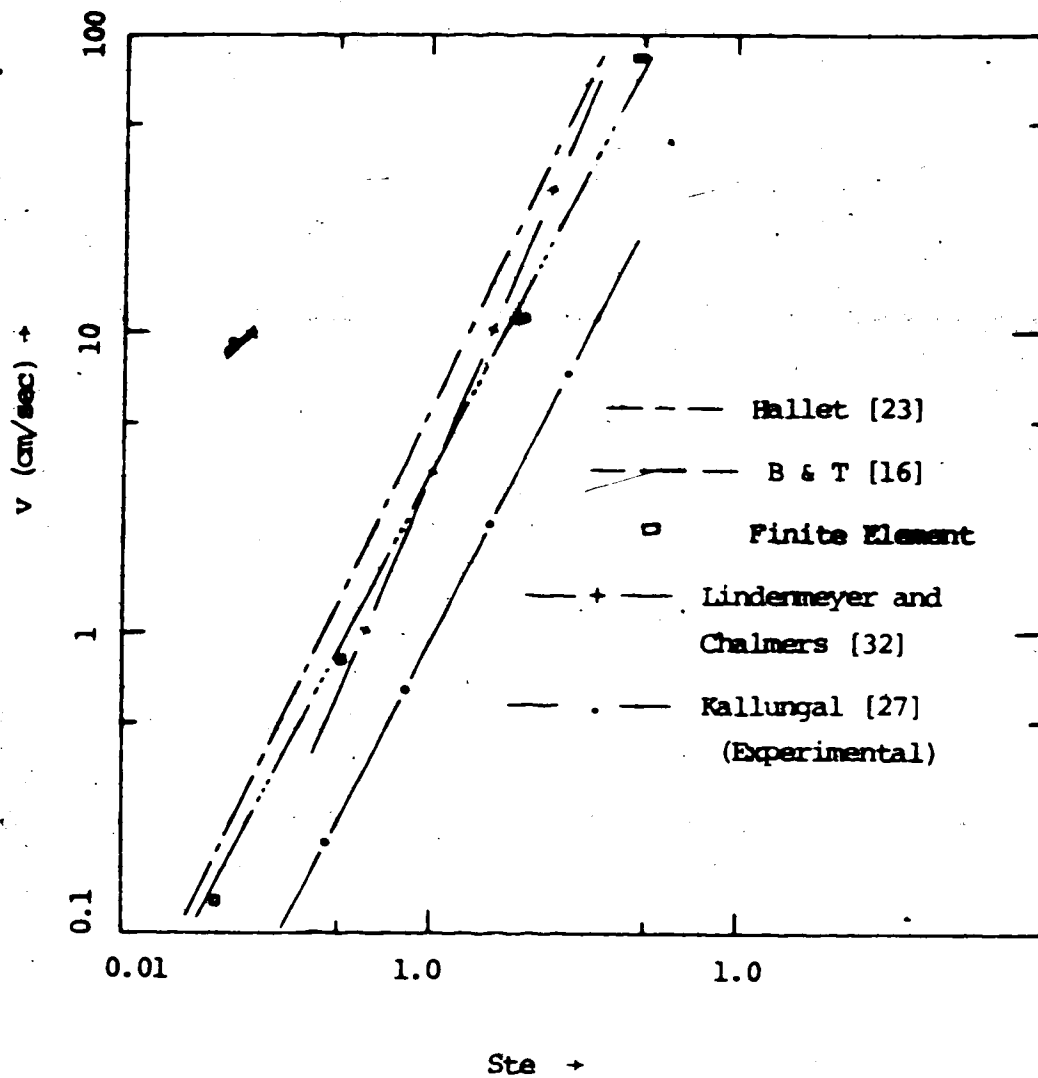


Figure 5.8 Plot of the Growth Velocity of Ice Dendrites as a Function of Supercooling

as the present calculations based on the maximum velocity principle. It is seen that although no two correlations agree completely, the results based on present calculations fall well within the range of values obtained by different correlations. Figure 5.9 compares the values of tip radius of curvature obtained by the present method with those of previous researchers. Again, the values obtained here compare favourably with the available data in the literature.

It is to be noted that all the correlations available in the literature show a simple power law relationship between the velocity of growth and the amount of subcoolings, i.e. all the lines in Figure 5.8 except the one based on the finite element calculations have constant slope. The line based on the present calculations deviates from a constant slope showing the true effect of the varying Stefan number.

Figures 5.10 and 5.11 present the comparisons between the present method and the available experimental data for the velocity of growth of tin and succinonitrile dendrites respectively. The results show that the present method using the maximum velocity criterion gives growth velocities which are consistently a factor of two to three too high, but are consistent with other approximate analytical techniques that use the maximum velocity criterion.

In all of the above calculations it was assumed that the dendrite shape was a paraboloid of revolution. Although, it is agreed by most researchers that most dendrites are closer

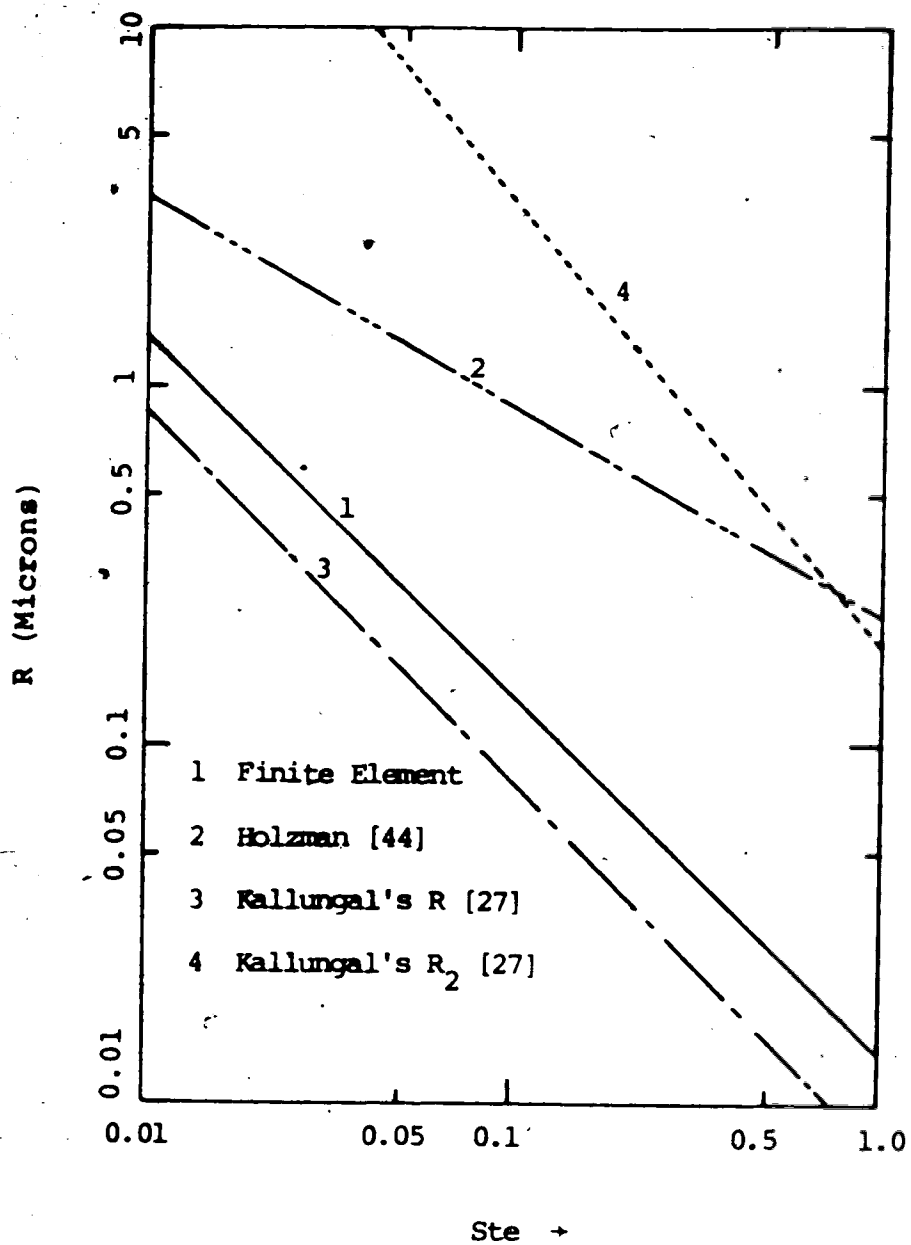


Figure 5.9 Plot of the Tip Radius of Curvature as a Function of Supercooling for Ice Dendrites

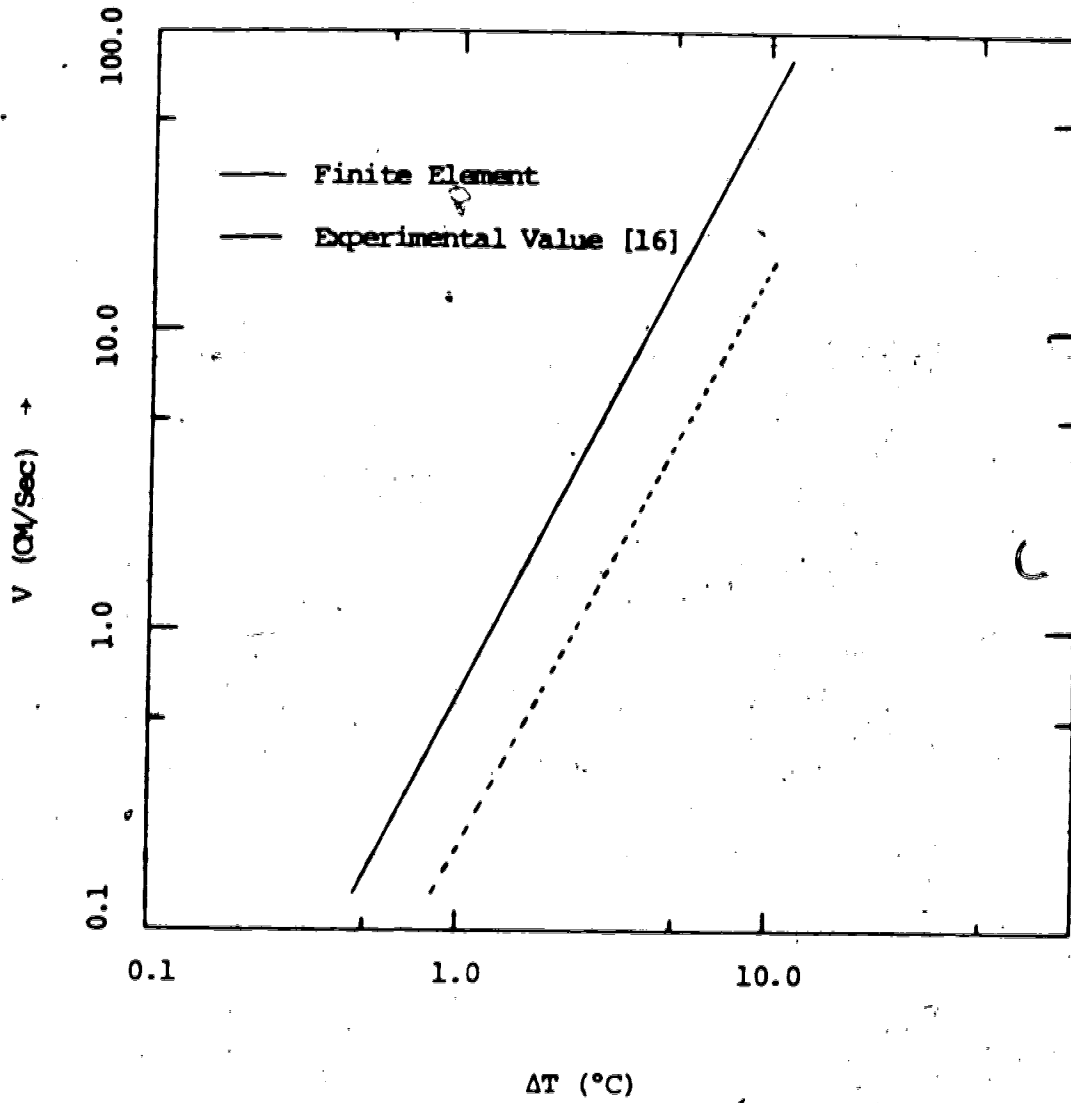


Figure 5.10 Plot of the Growth Velocity of Tin Dendrites as a Function of Supercooling.

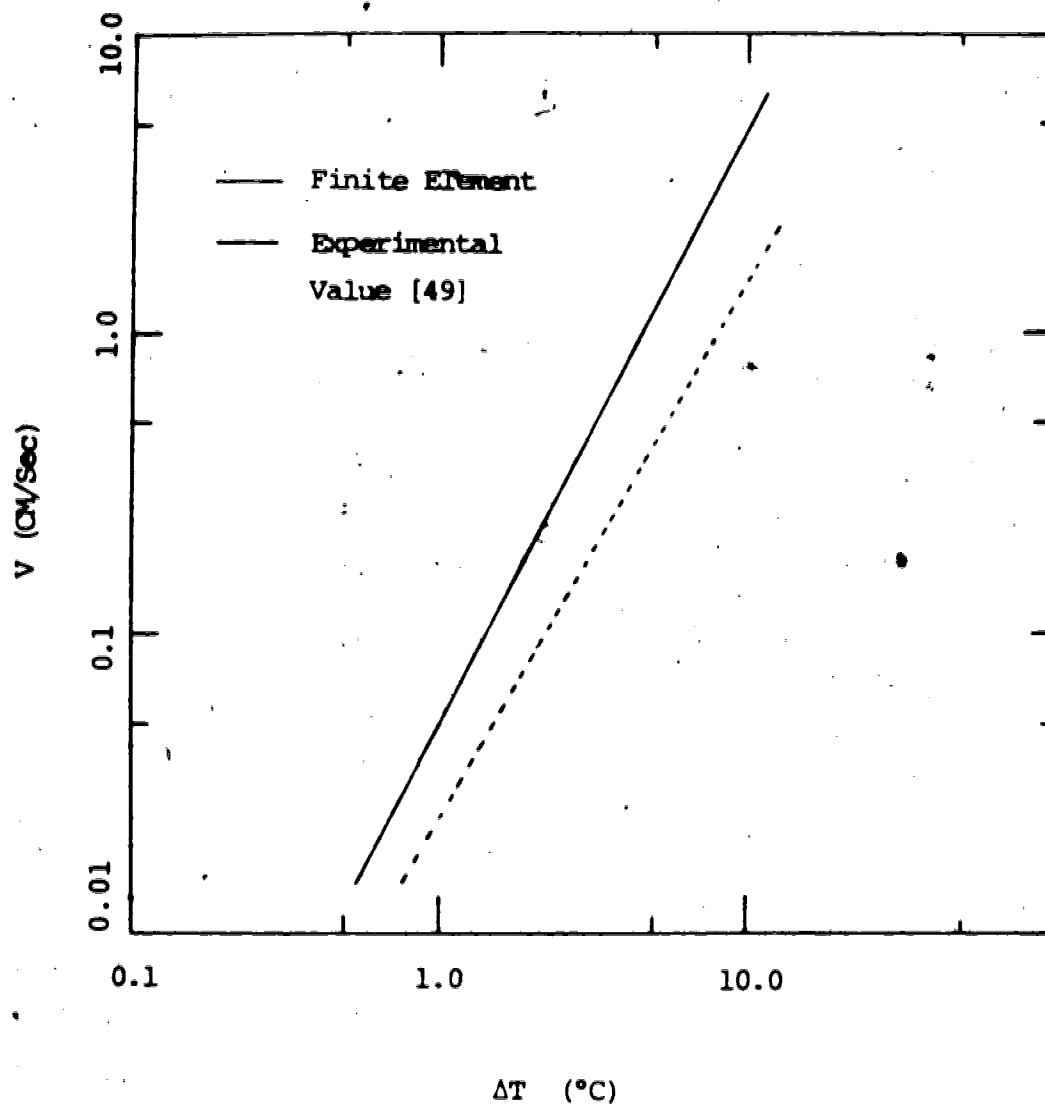


Figure 5.11 Plot of the Growth Velocity of Succinonitrile Dendrites as a Function of Supercooling

to a paraboloid shape, many authors believe that the actual shape varies somewhere between a paraboloid of revolution and a parabolic cylinder. In particular the two principle radii of the ice dendrite appear to be largely different [27]. Figure 5.12 presents the results based on isothermal and non-isothermal parabolic cylinders, isothermal and non-isothermal paraboloids, and various experimental correlations for the growth of ice dendrites. It is clear that the dendritic growth velocity will depend strongly on the three dimensional shape of the dendrite as the results based on various models differ by several orders of magnitude. Although the values of velocities based on the current non-isothermal paraboloidal model using the maximum velocity criterion come close to the experimental data, this result may be somewhat fortuitous.

Examining the results in more detail will show that either the quasi-steady state growth, assumption model is not appropriate for a dendrite or the shape which obeys the quasi-steady state growth is other than a paraboloid of revolution. Holzman [45], [46] showed that both the paraboloid (needle crystal) and the parabolic cylinder (platelet) shapes do not satisfy the heat balance conditions. He calculated a quantity he defined as an excess velocity for both these shapes. He showed that if one calculates the velocity of interface along each point, the condition of steady growth is violated. Similar calculations by the present method confirmed his results. Figures 5.13 and 5.14 show the excess velocity obtained by the

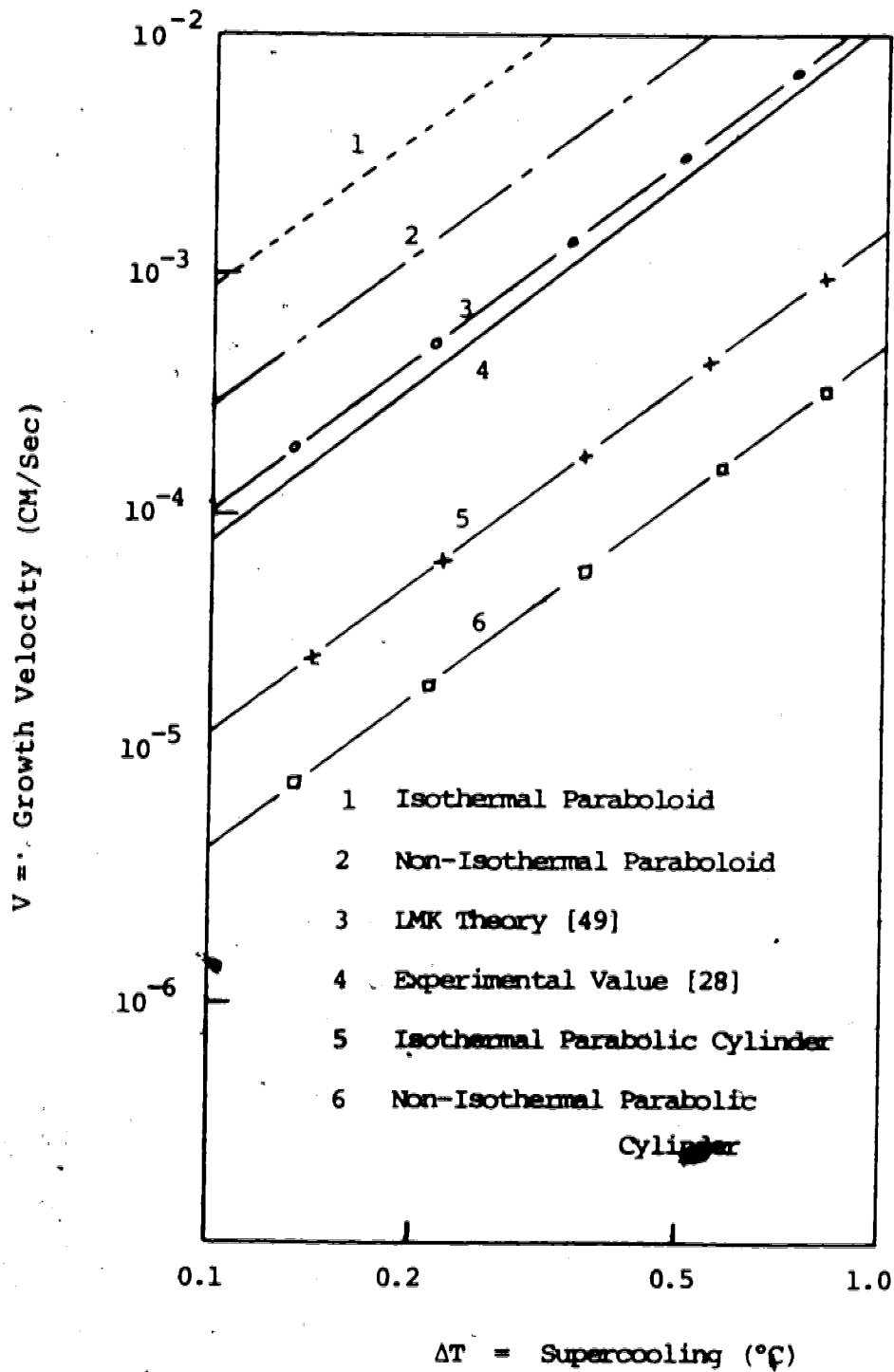


Figure 5.12 Plot of the Growth Velocity of Ice Dendrites as a Function of Supercooling for Various Dendrite Tip Shapes

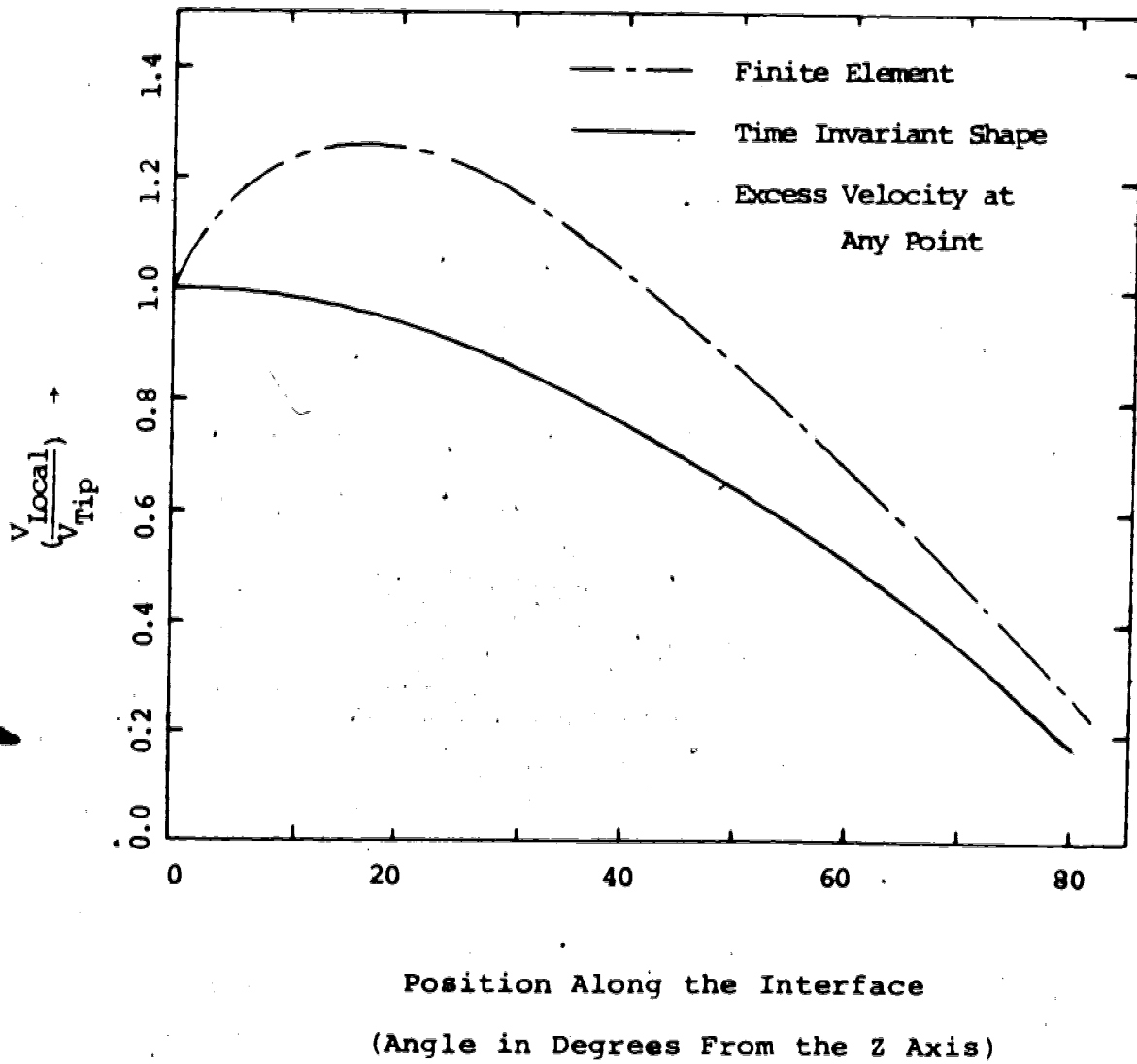


Figure 5.13 Plot of the Growth Velocity of Various Points Along the Interface of a Paraboloidal Dendrite $\frac{k}{k_l} = 4, Ste = 0.05$

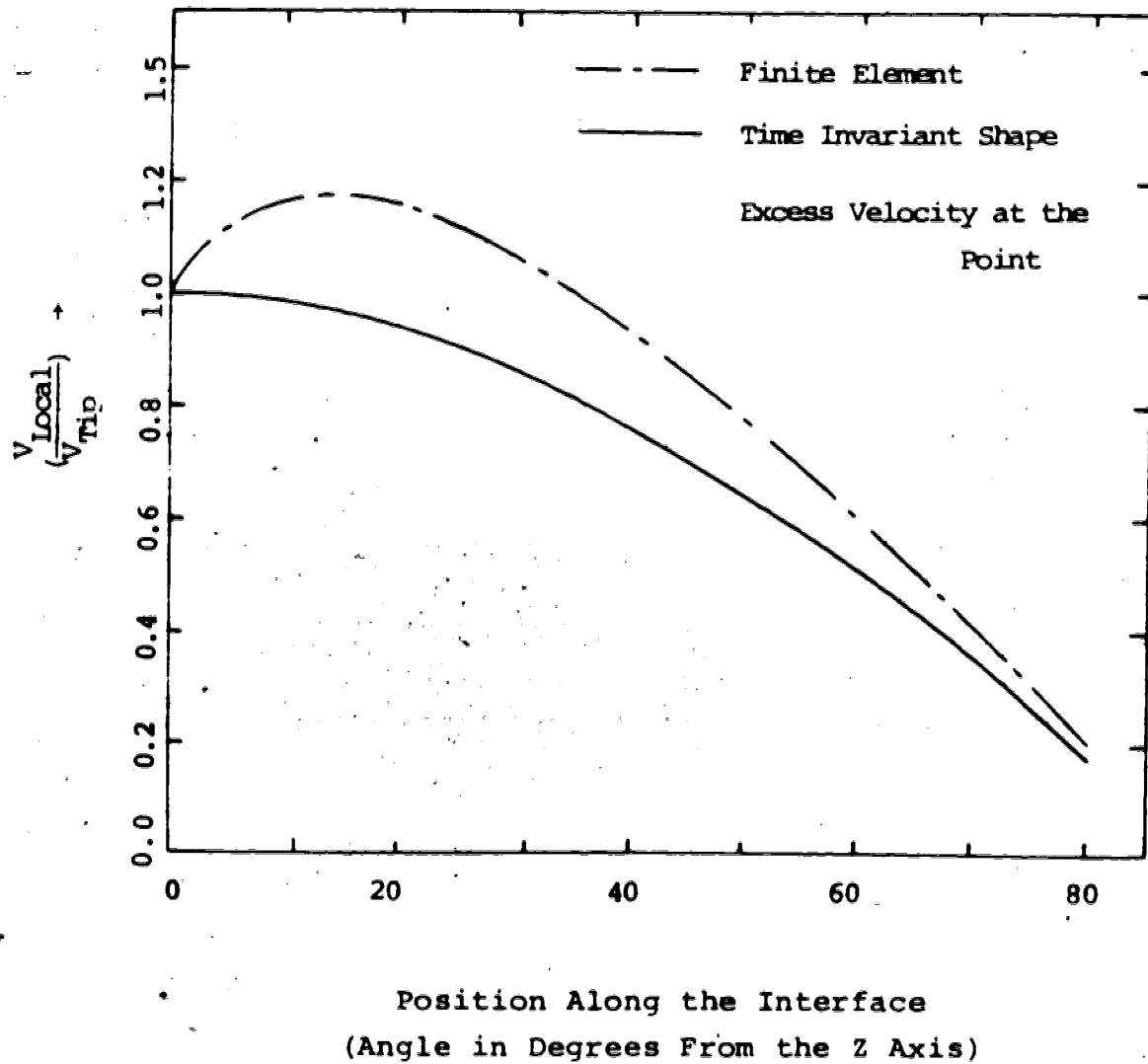


Figure 5.14 Plot of the Growth Velocity of Various Points Along the Interface of a Parabolic Dendrite $\frac{k_s}{k_l} = 4, Ste = 0.05$

finite element method for the two shapes under consideration. It is seen that the hypothetical paraboloid and the parabolic cylinder bulge behind the tip as found by Holzman. The dotted line in both figures represents the velocities required to maintain the time invariant shape, while the solid line shows the actual velocity obtained by calculation.

Summarizing the results of this chapter, it is evidently clear that the finite element method can be used to study the dendritic growth phenomenon. However, to gain a better understanding of dendritic growth, it is important to simulate dendrite growth over a time period. The next chapter is devoted to this study.

CHAPTER 6

SIMULATION OF DENDRITIC GROWTH

The purpose of this chapter is to make an attempt to study the development of the crystal shape with time. As described previously, the experimental evidence shows that dendrites grow with a constant speed for a given supercooling. But the study of dendrite growth by the finite element model gave no hint that the dendrite would grow with a time invariant shape and velocity. The maximum velocity principle presented a convenient tool to obtain a unique value for the velocity of growth, but it is not based on any strict physical reasoning. The stability criterion of Langer and Muller-Krumbhaar has also not been thoroughly tested. The aim here is to make an attempt to obtain a shape which is time invariant and the corresponding velocity of growth of a dendrite.

To simulate dendrite growth, the following steps were required.

1. An initial dendrite shape was chosen.
2. The finite element program was used to calculate heat fluxes at the interface and from these heat fluxes the velocity of advance at each point on the interface was calculated in the same way as it was done in the previous chapter.

3. Each interface node was then advanced by an amount equal to the velocity times a time step. This time step was chosen such that the maximum advance of a node was about 0.1 to 0.2 of the tip radius.

4. The interface nodes were then shifted in the negative Z direction so that the finite element domain remained centered on the node at the dendrite tip. In this shift, the nodes must be moved along radial lines so that their spacing is not severely distorted by changes in dendrite shape.

5. New interface curvatures were then calculated for each nodal point. The technique used in this step will be discussed later.

6. The finite element grid was then constructed again using the new interface position and the velocities at the interface nodes recalculated.

7. Steps (3) through (6) were then repeated a large number of times. The result was a simulation of the dendrite interface evolution as a function of time.

Perhaps the most difficult step in this procedure is step (5)—the calculation of interface curvature. Cubic splines were considered first to represent the moving shape-changing interface. Cubic splines were selected because it is known that splines can fit various shapes easily and continuity of slope and curvature is maintained at each knot. Ability to calculate the curvature at each node is essential since the

curvature is needed to calculate the freezing point depression due to Gibbs-Thompson effect at each point.

The use of cubic splines was however, not very successful. It was found that the cubic spline routine interpolated the moving interface very accurately, but the curvatures calculated near the tip were not very satisfactory. Since the cubic spline is required to pass through every point and the nodal points near the tip are spaced very closely, the curvature values obtained fluctuated wildly from one node to the next. This provided a numerical instability that grew as the calculation proceeded.

To eliminate the above mentioned problem a slightly different curve-fitting strategy was employed. Since the difficulty in the curve fitting was near the tip, the curve fitting routine was split in two parts. Near the tip a parabola was fitted using the least square technique and for the remaining part of the interface, the interface curvature was obtained by using the finite difference method to evaluate the second derivative. In fitting a parabola to the dendrite tip the node right at the tip was not included. As was the case for the sphere in Chapter 4, the calculated velocity at this point is not consistent with that at the adjacent nodes presumably because of the singular nature of this point in the finite element grid. Using this technique a smoothly varying curvature that appeared reasonable was obtained. However, the calculation of curvatures from a set position coordinates for

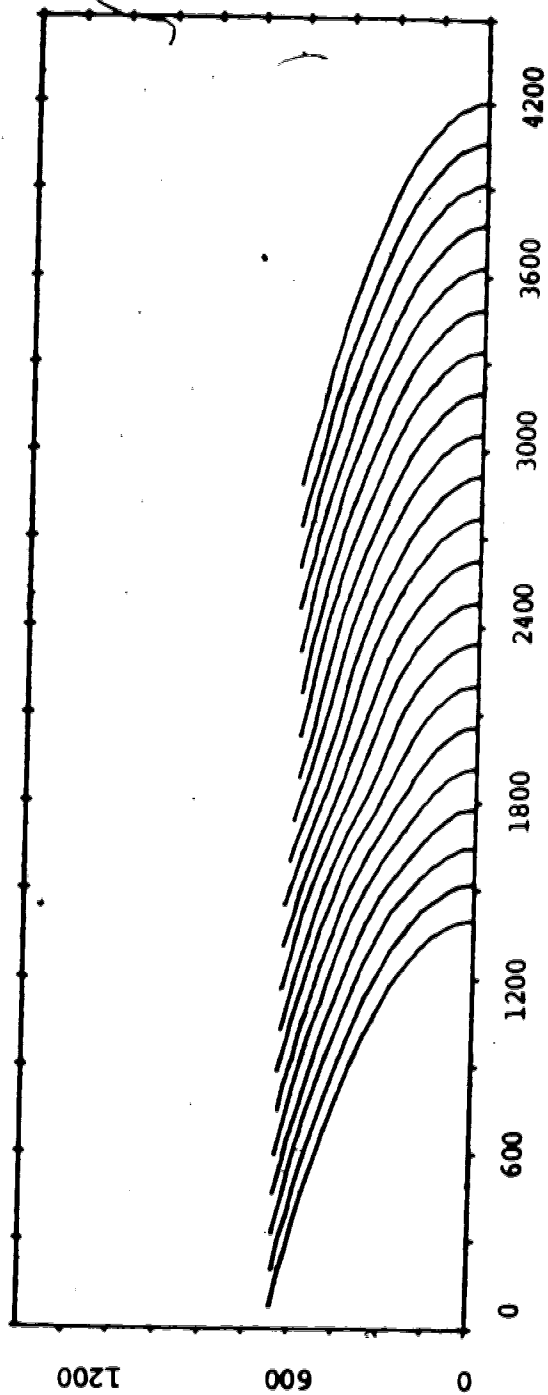
the interface remains as one of the major sources of potential numerical errors.

Initially, to make the long-term growth calculations simpler, the flux on the solid side of the dendrite was neglected. In all calculations presented in this section the Stefan number was set equal to zero. The results will, therefore, apply only to cases where the supercooling is relatively small. Figures 6.1 through 6.4 present the results obtained for the long-term growth of dendrites with $k_s = 0$. Figure 6.1 shows the evolution in shape of a dendrite interface. It is seen that starting with a paraboloidal shape, as the dendrite grows, instabilities develop near the dendrite tip. The tip becomes broader and slows down before ultimately reaching a time invariant shape with constant velocity of growth.

To determine if the results obtained for the long-term growth by the finite element method are dependent on the initial conditions, the program was run with two different initial paraboloids. Figure 6.2 presents the velocity and curvature obtained by using an initial paraboloid with broad tip while Figure 6.3 shows similar results for an initial paraboloid with a sharp tip. The final velocity and tip curvature for the two initial shapes are within 0.5 percent of each other.

Figures 6.2 and 6.3 do show an oscillatory behaviour as would be suggested by the Langer-Krumbhaar stability analysis; however, they also suggest that the oscillations are highly damped so that the dendrite quickly approaches a time invariant

Non-Dimensional Distance Along X-Axis



Non-Dimensional Distance Along Z Axis

Figure 6.1 Computer Plot of the Long Term Growth of a Dendrite Interface ($k_s = 0$; initial shape - Perfect Paraboloid)

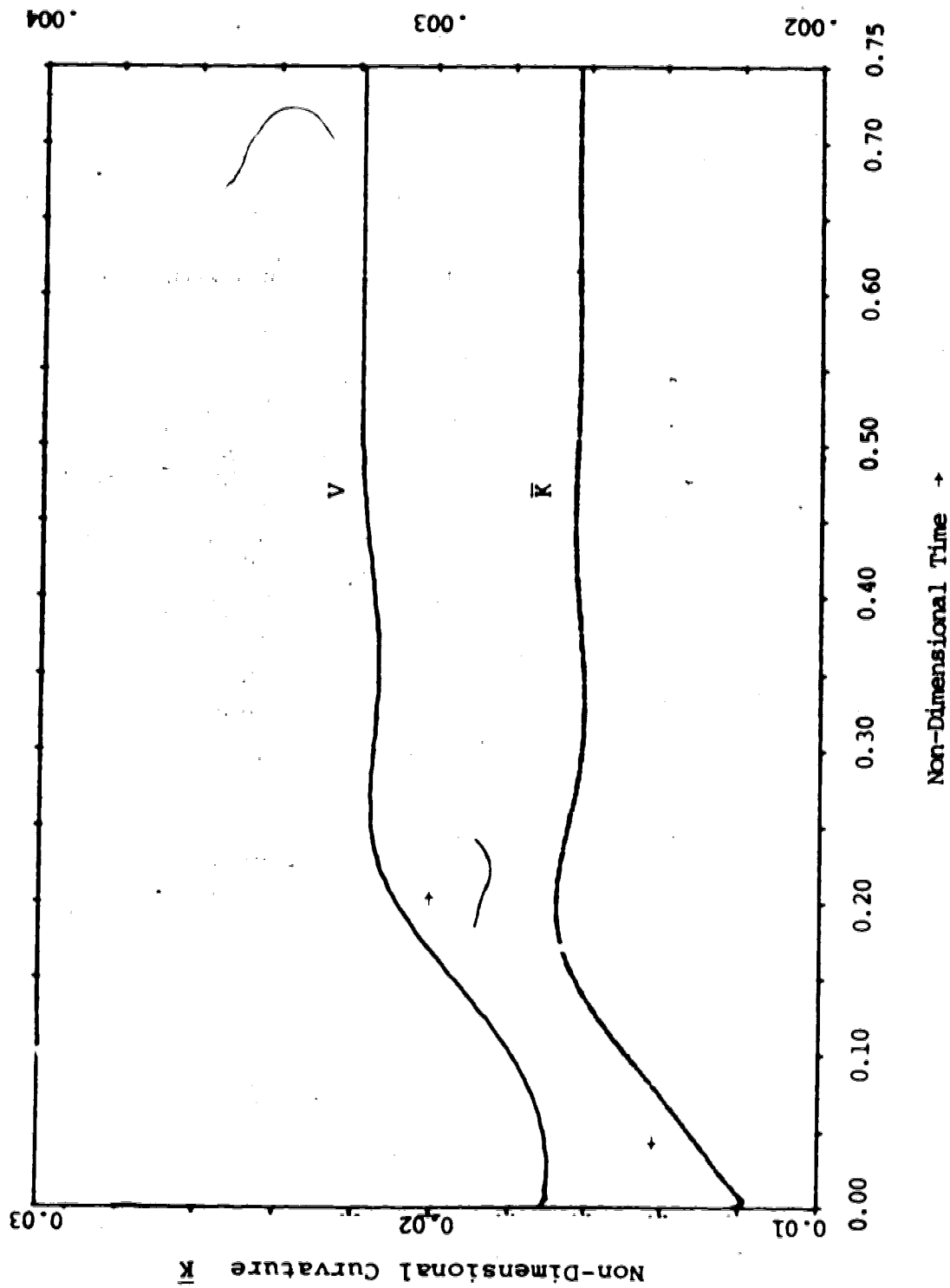


Figure 6.2 Plot of Growth Rate and Tip Curvature Versus Time to Determine the Time Invariant Shape of a Dendrite ($k_B = 0$)

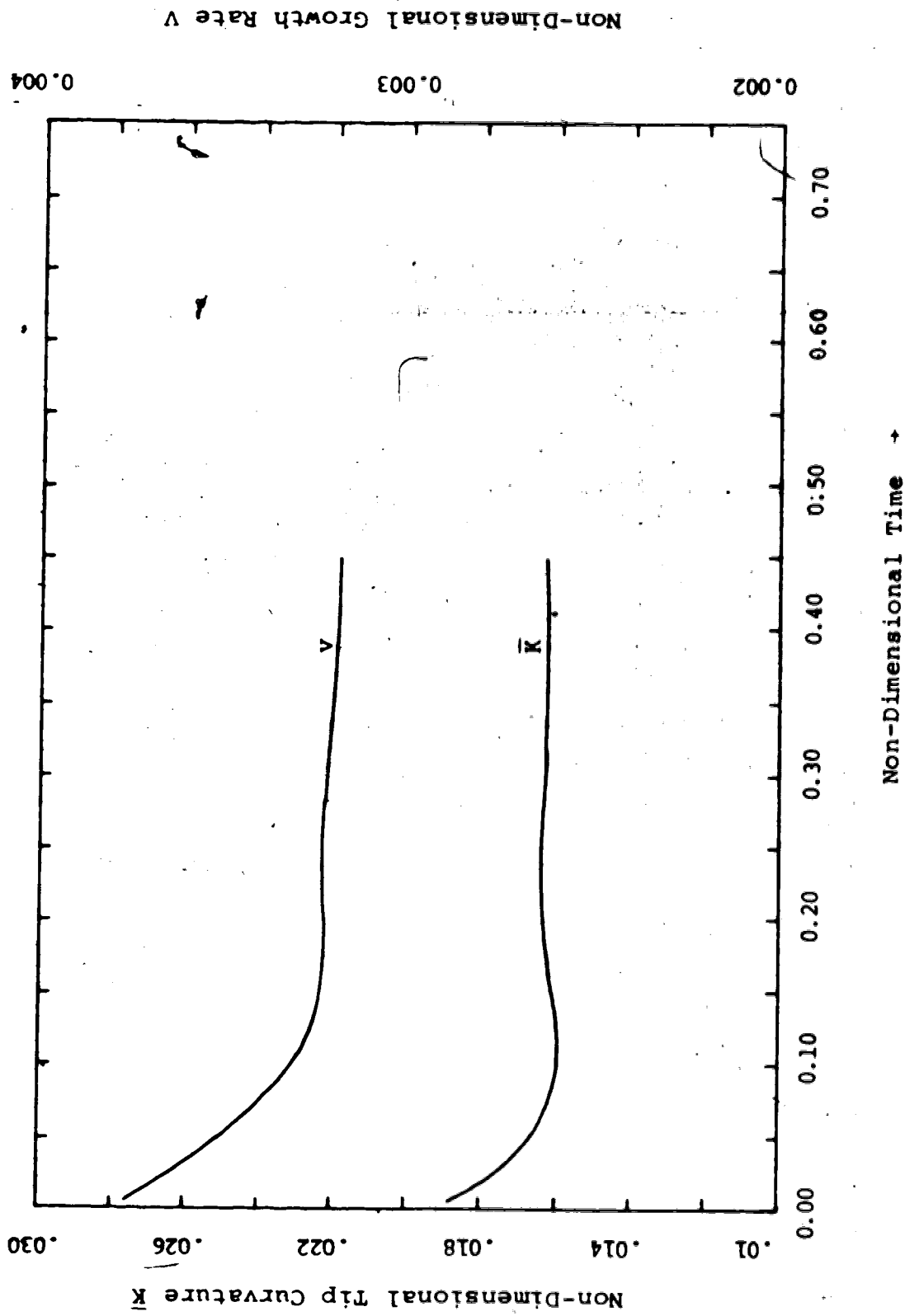
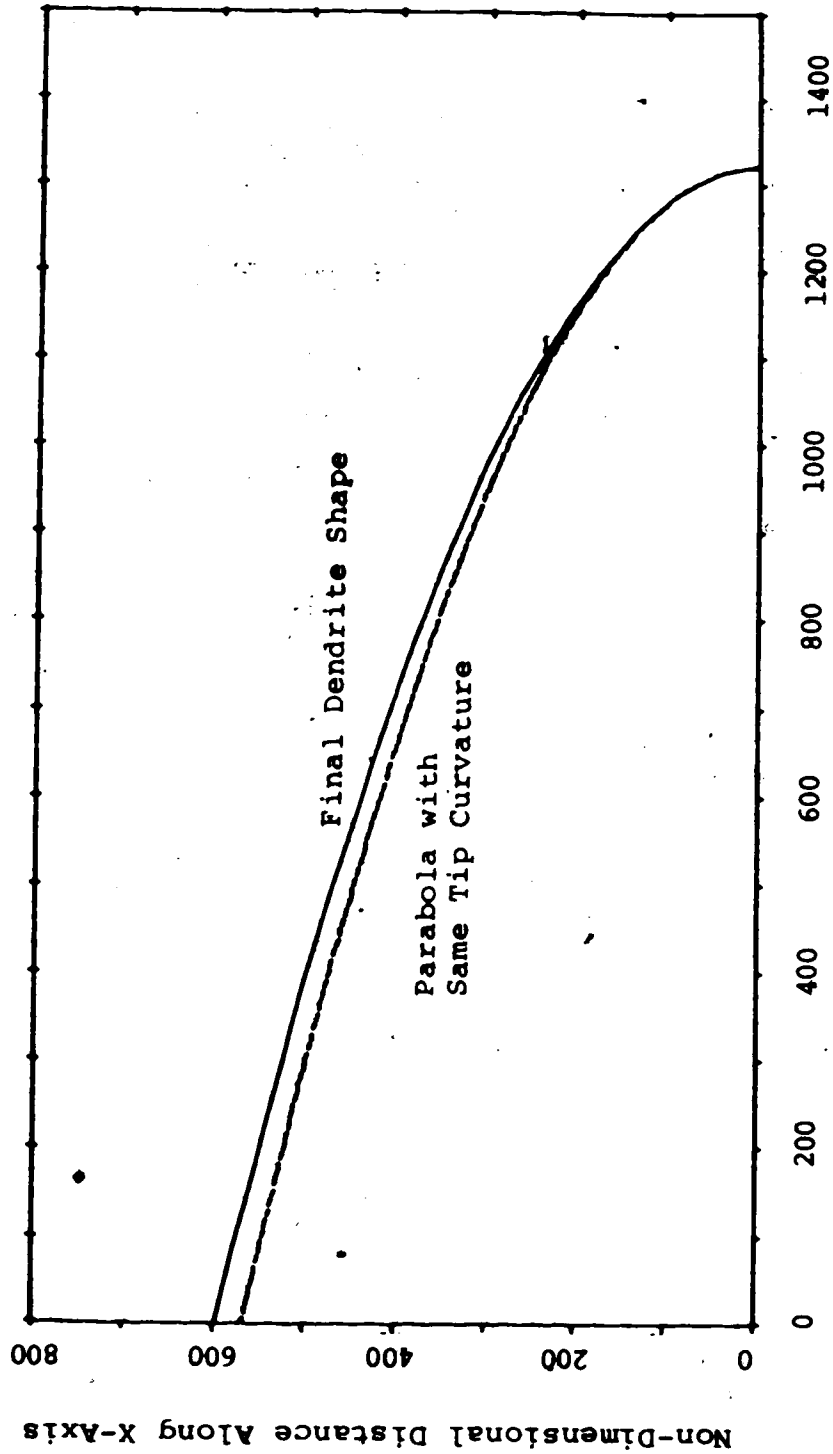


Figure 6.3 Plot of Growth Rate and Tip Curvature Versus Time to Determine the Time Invariant Shape of a Dendrite ($k_s = 0$)



Non-Dimensional Distance Along the Z Axis

Figure 6.4 The Final Shape of a Time Invariant Dendrite Interface and a Paraboloid with Same Tip Curvature

shape. The ultimate time-invariant shape is shown in Figure 6.4 and compared with a paraboloidal shape with the same tip curvature. These results would suggest that the dendrite obeys the quasi-steady state assumption, but the shape is slightly different than the paraboloid of revolution as assumed previously.

Next, calculations were attempted including the flux on the solid side. With $k_s = 4k_l$ (i.e. ice-water system) similar calculations were performed as described before. Figure 6.5 presents the results of these calculations. Starting with two different paraboloids, the dendrites reach a steady velocity and tip curvature.

The above described results suggest that the dendrites grow with a time-invariant shape which is slightly different from a paraboloid of revolution. Also, it is found that the velocity of growth of the dendrites is considerably lower than that predicted by the maximum velocity principle. In fact, the velocity obtained by the current method is closer to that predicted by the Langer-Krumbhaar stability criterion. Figure 6.6 presents the comparison of velocity of growth for ice dendrites as a function of supercooling obtained by different methods. It is evident that the velocities obtained by the long-term growth model and the Langer-Krumbhaar stability criterion are very similar and also in agreement with some measurements for growth of ice dendrites made by Kallungal and Barduhn [28] recently.

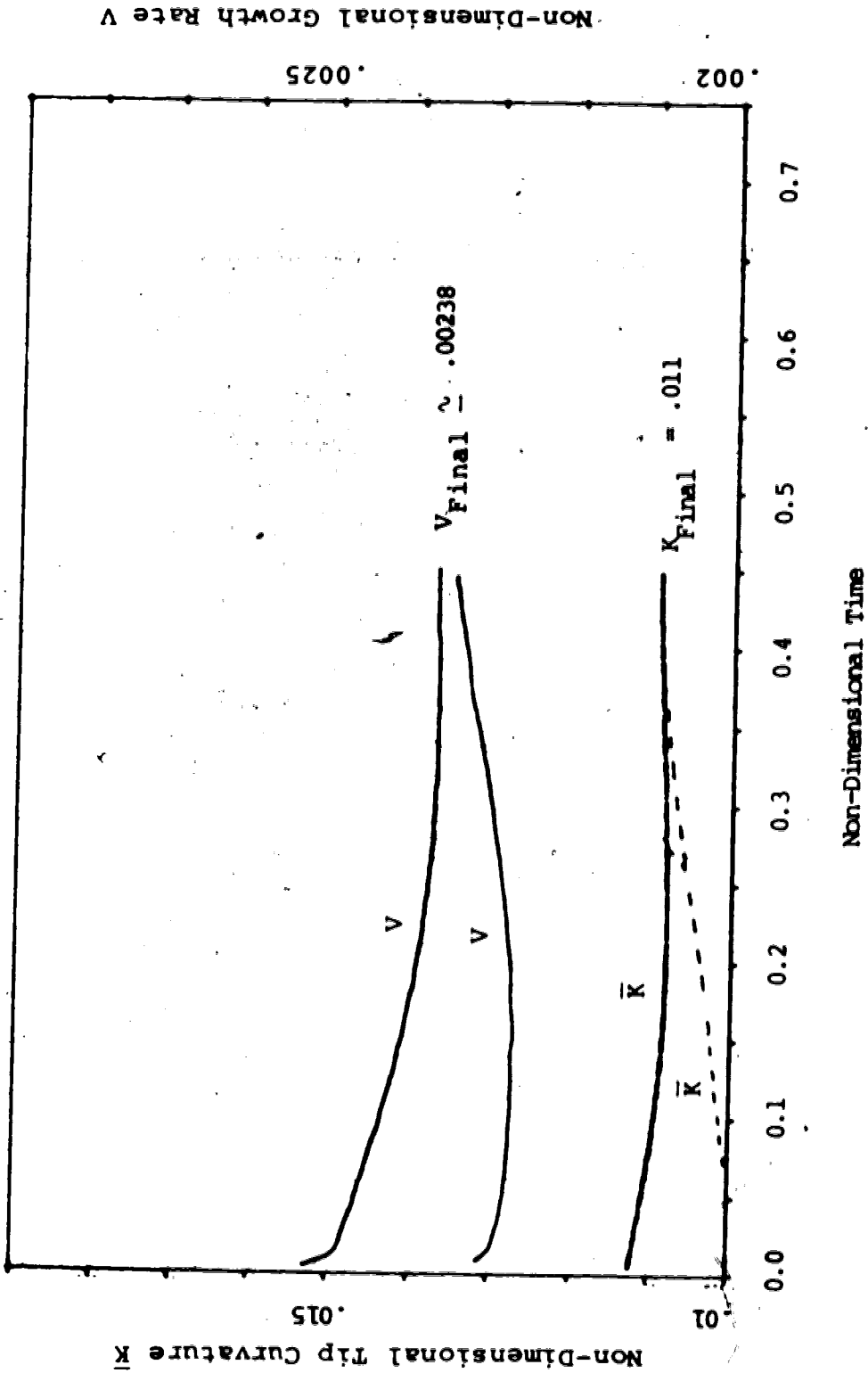


Figure 6.5 Plot of Growth Rate and Tip Curvature Versus Time to Determine the Time Invariant Shape of a Dendrite Starting From Two Different Parabolic Tip Curvature $k \frac{a}{k_1} = 4$

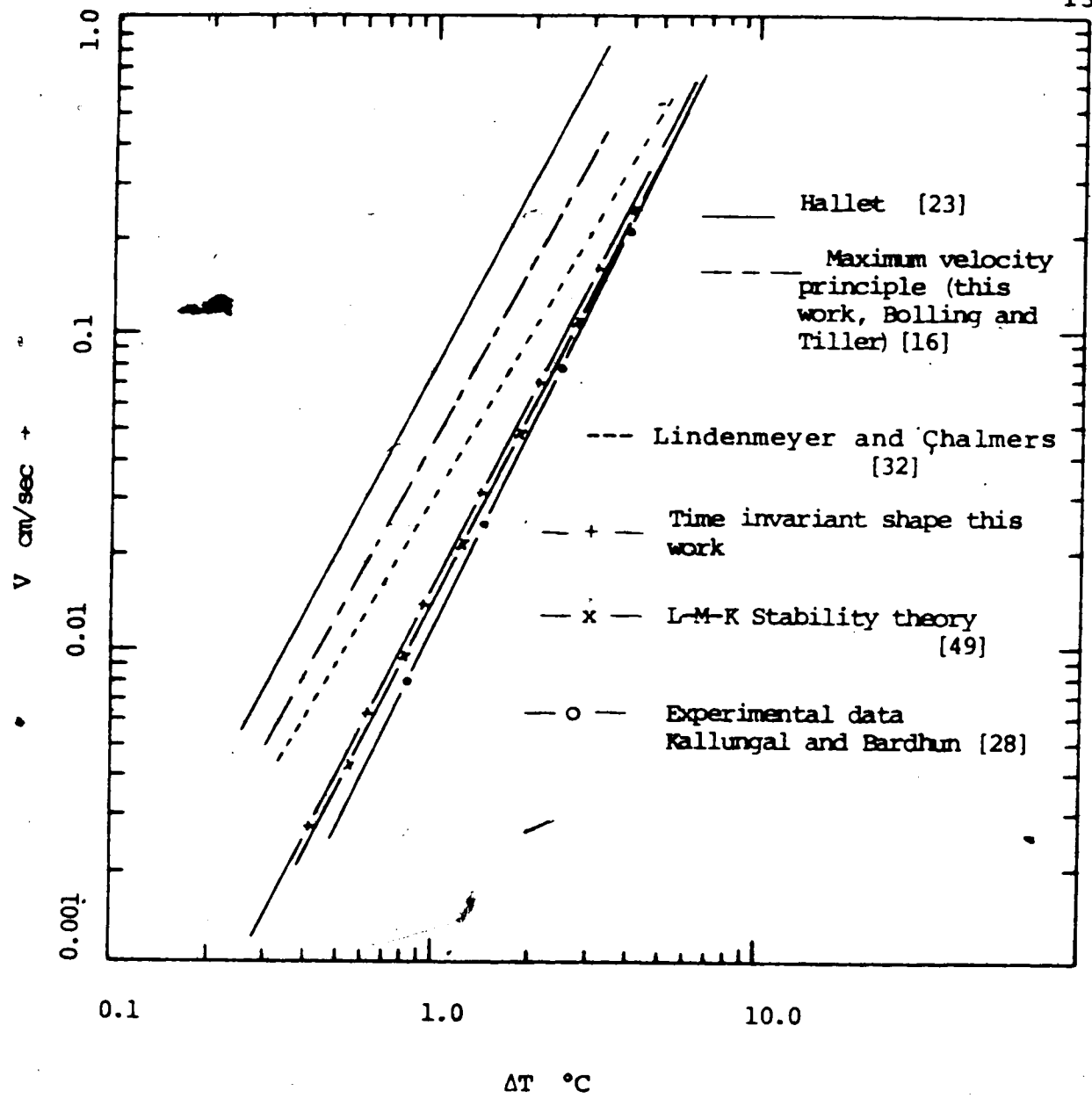


Figure 6.6 Plot of Dendrite Growth Rate as a Function of Supercooling ΔT for ice.

Although simulations were not done for the conductivity ratio k_s/k_ℓ , appropriate for tin or succinonitrile, it is probable that the calculation of the time-invariant dendrites for these materials would give velocities closer to what is measured than the use of the maximum velocity criterion would. For $k_s = 0$ and $k_s/k_\ell = 4$, the non-dimensional velocities were respectively a factor of 2 and 2.7 less for the time-invariant solution than the maximum velocity one. This is very close to the differences observed in Figures 5.10 and 5.11 between the measured values and the predictions based on the maximum velocity assumption.

CHAPTER 7

SUMMARY AND CONCLUSIONS

This work has been an investigation of the applicability of the finite element method to the study of crystal growth transport processes. The objective was to see if the finite method can be applied to gain a better understanding of dendritic growth phenomenon.

To attain the objective set out for this work, the approach was developed in three stages,

1. The first stage was designed to demonstrate that the finite element method can be successfully applied to study the problems of stability of spherical and cylindrical particles growing in supercooled liquids. This was done by comparing the solution of simple heat flow problems by the analytical method with solution by the finite element method. Both approaches were shown to give identical results (Chapter 4). It was found that the finite element method could give accurate results for stability problems involving irregular boundaries (perturbed cylinders and spheres).

2. In the second stage, a finite element model was used to study the dendritic growth problem. This problem was chosen because of the great difficulty experienced in the analytical treatments in the solution of the diffusion

equations which govern the process of dendritic growth. The choice was reinforced by the widespread occurrence of this phenomenon, which has great technological importance.

The dendritic growth problem was formulated such that the essential features of the growth process were included in this model. A paraboloid of revolution or a parabolic cylinder of isotropic, pure material was considered to grow into a pure, supercooled melt. The heat flow in the solid side was also accounted for. The results obtained from this model were compared with the available data based on experimental as well as analytical research. The results obtained by the present method agree very well with the corresponding available correlations. However, the calculations from the model at this stage, as well as the available analytical data, did not fully explain the observed dendritic growth phenomenon.

3. In the third stage, an attempt was made to study the long-term growth of a dendrite. The moving interface was described in a manner that could adequately represent the dendritic growth process. It was determined that the steady state shape for a growing dendrite was close to a paraboloid but not exactly a paraboloid of revolution. It was also found that the growth velocity thus obtained was smaller than that predicted by the often used maximum velocity principle. The growth velocities were closer to those predicted by the Langer-Krumbhaar stability criterion.

The most interesting future application of the finite element method is to the simulation of crystal growth, such as the studies done in the last chapter. Although the preliminary results presented in that chapter are encouraging, there remain some major concerns about its success in other applications.

1. The calculation of surface curvatures are necessary for the application of the Gibbs-Thompson effect on interface temperatures. This can be done with relative ease for a surface described by an analytical function; however, for a surface defined only by a finite set of coordinate points this calculation, which involves second differences of the coordinates, can introduce large numerical errors. Improvements in the method by which this calculation was done may be required to improve the accuracy with which the method simulates the long-time behaviour of crystal growth. A method based on coordinate transformation may reduce some of the difficulties faced here.

2. A second concern is that numerical instabilities may be mistaken for or confused with real instabilities when one is using a numerical technique to study a problem like this. Generally one would expect the numerical instabilities would be very sensitive to changes in nodal spacing whereas the real instabilities would not; therefore, repeatability of the results for different nodal spacing is an essential computational test of the reliability of the predictions.

3. In simulation of crystal growth it is the 'velocity excess' that determines the changes in crystal shape with time. This means that it is not sufficient to calculate the mean velocity of, for example, a dendrite to an acceptable degree of accuracy, say one percent, but one must be concerned about calculating differences in velocities between nodal points to this accuracy. In such things as determining the required domain size or nodal spacing one should, therefore, do the selection on the basis of calculated 'velocity excess' rather than just the mean growth rate.

4. A final concern is the computer time required to carry out these simulations. In the calculations that were shown in Chapter 6, 871 nodes were normally used. This produced 21 discrete coordinate points along the dendrite surface to define its shape which was considered to be bare minimum needed. Carrying out a simulation of a dendrite growth over a distance of the order of 30 times the tip radius required 900 seconds of CPU time on an Amdahl 460/V7. One would ideally like to double the number of nodes on the dendrite surface, which would increase the total number of nodes by a factor of two and the computational time by about a factor of eight. Some runs were made using this increased number of nodes; however, the availability of computer time became a limiting factor on the amount of work that could be done. Obviously if extensive crystal growth simulation work was to be done an effort would

have to be made to reduce the computational time required and as well it could only be done on the faster of the new computer machines.

If these concerns and problems with the use of the finite element method of crystal growth simulation can be overcome, a number of interesting applications can be envisioned.

1. With a small modification of the present program the time evolution of a crystal from a spherical nucleus could be simulated. Small perturbation analysis suggests that the Y_{30} mode is the lowest unstable mode of perturbation for a sphere. The large amplitude growth of this perturbation is, however, unknown.

2. Also with small modification the effects of interface kinetics on the growth shapes can easily be studied. For this one just has to introduce an additional term into the equation for the interface temperature that depends on the local interface velocity.

3. With some more extensive modification it should be possible to simulate the effect of solutes on crystal growth. This would require the solution of the mass diffusion as well as heat diffusion equations at each time step.

4. Theoretically it should be possible to do three-dimensional simulations; however, at present such work would probably not be feasible because of the computation time required.

REFERENCES

1. Mott, N.F., "Theory of Crystal Growth," Discussions Faraday Society, Vol. 5, 1949, pp. 11-12.
2. Parker, R.L., "Crystal Growth Mechanisms: Energetics, Kinetics, and Transport," Solid State Physics Advances in Research and Applications, Vol. 25, 1970, pp. 151-299.
3. Chalmers, B., Principles of Solidification, John Wiley & Sons Inc., New York, 1964.
4. Zienkiewicz, O.C., and Cheung, Y.K., The Finite Element Method in Structural and Continuum Mechanics, McGraw Hill Publishing Co., London, 1967.
5. Newman, S.P., and Witherspoon, P.A., "Finite Element Method of Analyzing Steady Seepage With a Free Surface," Water Resources Research, Vol. 6, No. 3, 1970, pp. 889-897.
6. Chan, S., Finite Element Analysis of Irrotational Flows of an Ideal Fluid, Ph.D. Thesis, University of California, Davis, 1971.
7. Zienkiewicz, O.C., and Cheung, Y.K., "Finite Elements in the Solution of Field Problems," The Engineer, Vol. 24, Sept. 1965, pp. 507-510.
8. Wilson, E.L., and Nickell, R.E., "Application of the Finite Element Method to Heat Conduction Analysis," Nuclear Engineering and Design, Vol. 4, 1966, p. 276.
9. Jackson, K.A., "Current Concepts in Crystal Growth from the Melt," Progress in Solid State Chemistry, Vol. 4, 1967, pp. 53-80.
10. Smith, C.S., A History of Metallography," The University of Chicago Press, 1965.
11. Wineburg, F., and Chalmers, E., "Dendritic Growth of Lead Crystals," Can. Journal of Physics, Vol. 29, 1951, p. 382.
12. Wineburg, F., and Chalmers, B., "Further Observations on Dendritic Growth in Metals," Can. Journal of Physics, Vol. 30, 1952, pp. 488-502.

13. Lindenmeyer, C.S., and Chalmers, B., "Growth Rate of Ice Dendrites in Aqueous Solutions," *Journal of Chemical Physics*, Vol. 45, 1966, pp. 2807-2808.
14. Orrok, T., *Dendritic Solidification of Metals*, Ph.D. Thesis, Harvard University, 1958.
15. Lindenmeyer, C.S., Orrok, G.T., and Jackson, K.A., and Chalmers, B., "Rate of Growth of Ice Crystals in Supercooled Water," *Journal of Chemical Physics*, Vol. 27, 1957, p. 822.
16. Bolling, G.F., and Tiller, W.A., "Growth from Melt," *Journal of Applied Physics*, Vol. 32, 1961, pp. 2587-2605.
17. Hillig, W.B., and Turnbull, D., "Theory of Crystal Growth in Undercooled Pure Liquids," *Journal of Chemical Physics*, Vol. 24, 1956, p. 914.
18. Rosenberg, A., and Winegard, W.C., "The Rate of Growth of Dendrites in Supercooled Tin," *Acta Metallurgica*, Vol. 2, 1954, pp. 342-343.
19. Walker, J., Unpublished Research. Quoted by B. Chalmers in *Principles of Solidification*, John Wiley & Sons, New York, 1964.
20. Glicksman, M.E., Schaeffer, R.J., and Aiyers, J.D., "Dendritic Growth - A Test of Theory," *Met. Trans.*, Vol. 7, Nov. 1976, pp. 1747-59.
21. Ryan, B.F., "The Structure of Ice Growth in Supercooled Water," *Journal of Crystal Growth*, Vol. 5, 1969, pp. 284-289.
22. Mason, B.J., "The Growth of Ice Crystals in Supercooled Water," *Journal of Adv. Physics*, Vol. 7, 1958, pp. 235-253.
23. Hallet, J., "Experimental Studies of the Crystallization of Supercooled Water," *Journal of Atmos. Sci.*, Vol. 21, 1964, pp. 671-682.
24. Macklin, W.C., and Ryan, B.F., "Habits of Ice Grown in Supercooled Water," *Phil. Mag.*, Vol. 14, 1966, pp. 847-860.
25. Pruppacher, H.R., "Growth Models of Ice Crystals in Supercooled Water and Aqueous Solutions," *Journal of Glaciology*, Vol. 6, 1967, pp. 651-62.

26. Glicksman, M.E., and Schaefer, R.J., "In Situ Measurements of Dendritic Profiles in Pure Tin," *Acta Metallurgica*, Vol. 14, 1966, pp. 1126-29.
27. Kallungal, J.P., The Growth of Single Ice Crystals Parallel to the A-Axis in Subcooled Quiescent and Flowing Water, Ph.D. Thesis, Syracuse University, 1975.
28. Kallungal, J.P., and Barduhn, A.J., "Growth Rate of an Ice Crystal in Subcooled Pure Water," *AICHE Journal*, Vol. 23, No. 3, 1977, pp. 294-303.
29. Arakawa, K., "The Growth of Ice Crystals in Water," *Journal of Glaciology*, Vol. 2, 1955, pp. 463-464.
30. Arakawa, K., and Higuchi, "Studies on the Freezing of Water," *Journal of the Faculty of Sciences, Hokkaido University, Series 2(Physics)*, Vol. 4, No. 3, 1952, pp. 201-208.
31. Williamson, R.B., and Chalmers, B., "Growth of Ice Disks in Slightly Supercooled Water," *Proceedings International Conference on Crystal Growth, Boston, June 1966, Pergamon Press, London, 1967*, pp. 739-743.
32. Lindenmeyer, C.S., and Chalmers, B., "Morphology of Ice Dendrites," *Journal of Chemical Physics*, Vol. 45, 1966, pp. 2804-2806.
33. Morris, L.R., and Winegard, W.C., "Growth of Dendrites in Supercooled Water," *Journal of Crystal Growth*, Vol. 1, 1967, pp. 245-246.
34. Hardy, S.C., and Coriell, S.R., "Morphological Stability of a Growing Cylindrical Crystal of Ice," *Journal of Applied Physics*, Vol. 39, 1968, p. 3505.
35. Hardy, S.C., and Coriell, S.R., "Morphological Stability and the Ice-Water Interfacial Free Energy," *Journal of Crystal Growth*, Vol. 3, No. 4, 1968, pp. 569-576.
36. Papapetrou, A., "Untersuchungen uber dendritisches wachstum von kristallen," *Z Kristi*, Vol. 92, 1935, pp. 89-130.
37. Ivantsov, G.P., "Thermal and Diffusion Processes in Crystal Growth," in *Growth of Crystals*, Vol. 1, 1958, pp. 76-85.

38. Temkin, D.E., "Growth Rate of the Needle Crystal Formed in a Supercooled Melt," Dokl. Akad. Nauk SSSR, Vol. 132, 1960, pp. 1307-1310.
39. Kotler, G.R., and Tashish, L.A., "On the Dendritic Growth of Pure Materials," Journal of Crystal Growth, Vol. 3, No. 4, 1968, pp. 603-610.
40. Horvay, G., and Cahn, J.W., "Dendritic and Spheroidal Growth," Acta Met., Vol. 9, 1961, pp. 695-705.
41. Hillig, W.B., "The Solution of the Dendritic Problem for the Edgewise Growth of a Platelet," Journal of Crystal Growth, Vol. 3, No. 4, 1968, pp. 611-620.
42. Trivedi, R., "Growth of Dendritic Needles from a Supercooled Melt," Acta Met., Vol. 18, 1970, pp. 287-296.
43. Trivedi, R., "Growth of Dendrites from a Supercooled Melt," Scripta Met., Vol. 3, 1969, pp. 613-618.
44. Holzman, E.G., On Dendritic Growth, Ph.D. Thesis, Stanford University, 1969.
45. Holzman, E.G., "Excess Velocity Potential of the Needle Crystal," Journal of Applied Physics, Vol. 41, No. 4, 1970, pp. 1460-1469.
46. Holzman, E.G., "Excess Velocity Potential of the Platelet Crystal in a Supercooled Melt," Journal of Applied Physics, Vol. 4, No. 12, 1970, pp. 4769-4773.
47. Oldfield, W., Geering, G.T., and Tiller, W.A., Joint Conference on Solidification, Brighton, England, December, 1967 (Iron and Steel Institute).
48. Oldfield, W., Computer Model Studies in Materials Science, Ph.D. Thesis, Stanford University, 1969.
49. Langer, J.S., and Muller-Krumbhaar, H., "Theory of Dendritic Growth - I. Elements of a Stability Analysis," Acta. Met., Vol. 26, 1978, pp. 1681-1687.
50. Langer, J.S., and Muller-Krumbhaar, H., "Theory of Dendritic Growth - II. Instabilities in the Limit of Vanishing Surface Tension," Acta Met., Vol. 26, 1978, pp. 1689-1695.

51. Langer, J.S., and Muller-Krumbhaar, H., "Theory of Dendritic Growth - III. Effects of Surface Tension," *Acta Met.*, Vol. 26, 1978, pp. 1697-1708.
52. Langer, J.S., Sekerka, R.F., and Fujioka, T., "Evidence for a Universal Law of Dendritic Growth Rates," *Journal of Crystal Growth*, Vol. 44, 1978, pp. 414-418.
53. Mullins, W.W., and Sekerka, R.F., "Morphological Stability of a Particle Growing by Diffusion or Heat Flow," *Journal of Applied Physics*, Vol. 34, 1963, pp. 323-329.
54. Ham, F.S., "Growth of Ellipsoids in Supercooled Melt," *Journal of Applied Physics*, Vol. 30, 1959, p. 1518.
55. Coriell, S.R., and Parker, R.L., "Stability of the Shape of a Solid Cylinder Growing in a Diffusion Field," *Journal of Applied Physics*, Vol. 36, 1965, pp. 632-637.
56. Tarshis, L.A., "Interface Morphology Considerations During Solidification," Ph.D. Thesis, Stanford University, 1968.
57. Kotler, G.R., "Theoretical Investigations of Dendritic Growth," Ph.D. Thesis, Stanford University, 1968.
58. Knight, C.A., "The Freezing of Supercooled Liquids," D. Van Nostrand Co., 1967.
59. Chambre, P.L., "On the Dynamics of Phase Change," *Journal of Mech. and Appl. Math*, Vol. 9, No. 2, 1956, p. 24.
60. Gilpin, R.R., "The Influence of Natural Convection on Dendritic Ice Growth," *Journal of Crystal Growth*, Vol. 36, 1976, pp. 101-108.
61. Sokolnikoff, I.S., "Variational Methods", Chapter 7, *Mathematical Theory of Elasticity*, McGraw-Hill, 1956.
62. Forray, M.J., *Variational Calculus in Science and Engineering*, McGraw-Hill, 1968.
63. Kantorovich, L.V. and Krylov, V.I., *Approximate Methods of Higher Analysis*, Translated from 3rd Russian Ed., by C.D. Benster, P. Noordhoff, The Netherlands, 1964.

64. Zienkiewicz, O.C., *The Finite Element Method in Engineering Science*, 2nd Ed., McGraw-Hill, 1971.
65. Hubner, K.H., *The Finite Element Method for Engineers*, John Wiley & Sons, 1975.
66. Desai, C.S., and Abel, J.F., *Introduction to the Finite Element Method*, Van Nostrand, 1972.
67. Tong, P. and Rosettas, J.N., *Finite-Element Method, Basic Technique & Implementation*, M.I.T. Press, 1977, pp. 256-264.
68. Strang, G. and Fix, G., *An analysis of the Finite Element Method*, Prentice-Hall, 1973, Chapter 8.
69. Tong, P. and Pian, T.H.H., "On the Convergence of the Finite Element Method for Problems with Singularity," *International Journal of Solids and Structures*, Vol. 9, 1973, pp. 313-321.
70. Guggenheim, E.A., *Thermodynamics*, North Holland, Amsterdam, 1959.
71. Landau, L.D., and Lifshitz, E.M., *Statistical Physics*, Pergamon Press, London, 1959.

APPENDICES.

APPENDIX 1

THERMODYNAMIC EQUILIBRIUM ACROSS A CURVED INTERFACE

APPENDIX 1

THERMODYNAMIC EQUILIBRIUM ACROSS A CURVED INTERFACE

In the physical model described in Chapter III it was stated that the equilibrium fusion temperature of the tip (interface) of a dendrite is depressed an amount ΔT_r owing to the radius of curvature of the non-flat interface. The derivation for this phenomenon, known as capillarity (or Gibbs-Thompson effect) will be discussed briefly in this appendix. For a detailed study on this subject the reader is referred to textbooks on thermodynamics such as Guggenheim [70] and Landau and Lifshitz [71].

Consider a very small section of the interface, over which the curvature is nearly uniform, and with small adjacent regions of the solid and liquid phases which are nearly uniform in composition and temperature. A pressure difference exists across the interface, which can be determined by minimizing the free energy with respect to an infinitesimal change of volume of one phase, the total volume being constant. This leads to the condition

$$P_s - P_l = \gamma_{sl} \frac{d \text{ surface area}}{d V_s} = \gamma_{sl} \left(\frac{1}{r_1} + \frac{1}{r_2} \right) \quad (\text{A-1})$$

P_s and P_l are the pressures at the curved interface, r_1 and r_2 are the principal radii of curvature and are positive if the

interface is concave toward the solid.

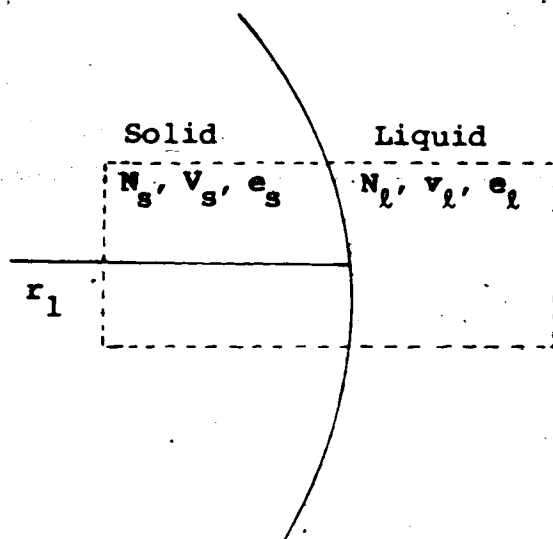


Figure A1-1 Equilibrium Across a Curved Interface

If the pressures P_s and P_l are nearly the same as the pressures at a flat interface,

$$\Delta P_s = P_s - P_s(\text{flat}); \quad |\Delta P_s| \ll P_s, \quad (\text{A-2})$$

it may be appropriate to use the Gibbs-Duhem relations,

$$\Delta \mu_s N_s = V_s \Delta P_s - S_s \Delta T_r, \quad (\text{A-3})$$

$$\Delta \mu_l N_l = V_l \Delta P_l - S_l \Delta T_r. \quad (\text{A-4})$$

At a flat interface $P_s(\text{flat}) = P_l(\text{flat})$, so from equation (A-1)

$$\Delta P_s - \Delta P_l = \gamma_{sl} \left(\frac{1}{r_1} + \frac{1}{r_2} \right) \quad (\text{A-5})$$

and $\Delta \mu_s = \Delta \mu_l$ because the phases are always in equilibrium.

If the liquid is assumed to be under constant pressure, then $\Delta P_l = 0$, and from equations (A-2), (A-3), and (A-4) it is found that

$$- \Delta T_r \left(\frac{S_l}{N_l} - \frac{S_s}{N_s} \right) = \frac{V_s \gamma_{sl}}{N_s} \left(\frac{1}{r_1} + \frac{1}{r_2} \right). \quad (\text{A-6})$$

Now, $T_f (S_l/N_l - S_s/N_s)$ is the latent heat of fusion per atom, so

$$\Delta T_r = - T_f \frac{\gamma_{sl}}{L} K, \quad (\text{A-7})$$

where $K = \left(\frac{1}{r_1} + \frac{1}{r_2} \right)$ is the mean curvature of the interface.

APPENDIX 2

DERIVATION OF ELEMENT MATRICES

APPENDIX 2

DERIVATION OF ELEMENT MATRICES

In the finite element formulation for the dendritic growth phenomenon described in section 3.5.1 the functional minimization problem was reduced to a simple matrix equation. The matrix equation (3.56) can be simplified considerably if all quantities independent of triangle size and shape are evaluated once and for all. In this appendix the derivation of the element matrices for a six-node triangular element as shown below is briefly discussed.

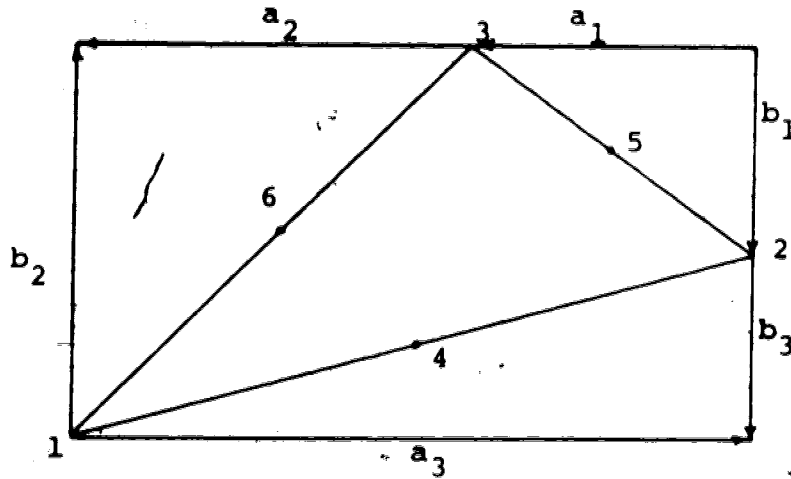


Figure A2-1 Six Node Triangular Element

1. Matrices for Axisymmetric Formulation

From Chapter III the element matrices are:

$$SA_{ij}^m = \sum_{k=1}^3 \eta_K \iint \psi_K (P_i P_J + \hat{P}_i \hat{P}_J) \, dn d\xi$$

and

$$(i, J = 1 \text{ to } 6) \quad (A2-1)$$

$$QA_{iJ}^m = \sum_{k=1}^3 \eta_K \iint_D \psi_K \chi_i \chi_j \, dn \, d\xi \quad (A2-2)$$

with

$$\langle P_1, P_2, \dots, P_6 \rangle = (4\psi_1 - 1) b_1 / 2A^m, (4\psi_2 - 1) b_s / 2A^m,$$

$$(4\psi_3 - 1) b_3 / 2A^m, 2(\psi_2 b_1 + \psi_1 b_2) / A^m,$$

$$2(\psi_3 b_2 + \psi_2 b_3) / A^m, 2(\psi_1 b_3 + \psi_3 b_1) / A^m \rangle \quad (A2-3)$$

$$\langle \chi_1, \dots, \chi_6 \rangle = \langle \psi_1 (2\psi_1 - 1), \psi_2 (2\psi_2 - 1), \psi_3 (2\psi_3 - 1),$$

$$4\psi_1 \psi_2, 4\psi_2 \psi_3, 4\psi_3 \psi_1 \rangle \quad (A2-4)$$

$$b_k = \eta_i - \eta_j \quad i, J, K \text{ cyclic} \quad (A2-5)$$

$$a_k = \xi_j - \xi_i \quad i, J, K \text{ cyclic} \quad (A2-6)$$

and

$$A^m = (a_1 b_3 - a_3 b_1) / 2 \quad (\text{A2-7})$$

The array \hat{P}_i is found by replacing the b's with a's in the expression for P_i .

To assist in simplifying the derivation of the element matrices, define

$$R_{ij}^k = \iint \psi_K (P_i P_J + \hat{P}_i \hat{P}_J) \, d\eta d\xi \quad (\text{A2-8})$$

and

$$T_{iJ}^k = 2 \iint \psi_K \chi_i \chi_J \, d\eta d\xi \quad (\text{A2-9})$$

Then in terms of these quantities

$$SA_{iJ} = \sum_{k=1}^3 n_K R_{iJ}^k \quad (\text{A2-10})$$

and

$$QA_{iJ} = \sum_{k=1}^3 n_K T_{iJ}^k \quad (\text{A2-11})$$

An explicit evaluation of equations (A2-8) and (A2-9) is obtained by a straight forward substitution of the appropriate quantities into the equations and making use of Table A.1. For example, to evaluate T_{11}^1 , the following expression is to be evaluated:

$$T_{11}^1 = 2 \iint \psi_1 \chi_1 \chi_1 \, d\eta d\xi \quad (\text{A2-12})$$

On substituting appropriate value of χ_1 in terms of ψ_1 , the equation (A2-12) becomes

$$T_{11}^1 = 2 \iint \psi_1^3 (2\phi_1 - 1)^2 \, d\eta d\xi \quad (\text{A2-13})$$

and using the Table A.1 for integration, results in

$$T_{11}^1 = 60 \frac{A^m}{1260} \quad (\text{A2-14})$$

Similarly, all the elements of the matrices R and T can be evaluated and thus the coefficient matrices SA and QA can be obtained. The various matrices are listed below for convenience. Also, since all these matrices are symmetric, only the lower triangular elements are listed. The quantity α_{iJ} is used to represent the sum $(a_i a_J + b_i b_J)/60A^m$.

$$R_{ij}^1 = 9 \alpha_{11}$$

$$-2 \alpha_{12} - 2 \alpha_{22}$$

$$-2 \alpha_{13} - \alpha_{23} \quad 3 \alpha_{33}$$

$$3 \alpha_{11} + 14 \alpha_{12} \quad 3 \alpha_{12} - 2 \alpha_{22} \quad - \alpha_{13} - 2 \alpha_{23} \quad 8 (\alpha_{11} + 2 \alpha_{12} + 3 \alpha_{22})$$

$$3 (\alpha_{12} + \alpha_{13}) \quad - \alpha_{22} + 3 \alpha_{23} \quad 3 \alpha_{23} - \alpha_{33} \quad 8 \alpha_{13} - 4 \alpha_{12} \quad 8 (\alpha_{22} + \alpha_{23} + \alpha_{33})$$

$$3 \alpha_{11} + 14 \alpha_{13} - \alpha_{12} - 2 \alpha_{23} \quad 3 \alpha_{13} - 2 \alpha_{33} \quad 8 \alpha_{23} - 4 \alpha_{11} \quad 8 \alpha_{12} - 4 \alpha_{13} \quad 8 (\alpha_{11} + 2 \alpha_{13} + 3 \alpha_{33})$$

 $B_{IJ}^2 =$ $3\alpha_{11}$ $-2\alpha_{12} \quad 9\alpha_{22}$ $-\alpha_{13} \quad -2\alpha_{23} \quad 3\alpha_{23}$ $-2\alpha_{11} + 3\alpha_{12} \quad 14\alpha_{12} + 3\alpha_{22} \quad -2\alpha_{13} - \alpha_{23} \quad 8(3\alpha_{11} + 2\alpha_{12} + \alpha_{22})$ $-\alpha_{13} - 2\alpha_{13} \quad 3\alpha_{22} + 14\alpha_{23} \quad 3\alpha_{23} - 2\alpha_{33} \quad 24\alpha_{13} - 4\alpha_{22} \quad 8(\alpha_{22} + 2\alpha_{23} + 3\alpha_{33})$ $-\alpha_{11} + 3\alpha_{13} \quad 3\alpha_{12} + 3\alpha_{23} \quad 3\alpha_{13} - \alpha_{33} \quad 8\alpha_{23} - 4\alpha_{12} \quad 8\alpha_{12} - 4\alpha_{23} \quad 8(\alpha_{11} + \alpha_{13} + \alpha_{33})$

and

$$\begin{aligned} R_{IJ}^3 = & 3\alpha_{11} \\ & -\alpha_{12} \quad 3\alpha_{22} \\ & -2\alpha_{13} \quad -2\alpha_{23} \quad 9\alpha_{33} \\ & \alpha_{11} + 3\alpha_{12} \quad 3\alpha_{12} - \alpha_{22} \quad 3\alpha_{13} + 3\alpha_{23} \quad 8(\alpha_{11} + \alpha_{12} + \alpha_{22}) \\ & -2\alpha_{12} - \alpha_{13} \quad -2\alpha_{22} + 3\alpha_{23} \quad 14\alpha_{23} + 3\alpha_{33} \quad 8\alpha_{13} - 4\alpha_{23} \quad 8(3\alpha_{22} + 2\alpha_{23} + \alpha_{33}) \\ & -2\alpha_{11} + 3\alpha_{13} \quad -2\alpha_{12} - \alpha_{23} \quad 14\alpha_{13} + 3\alpha_{33} \quad 8\alpha_{23} - 4\alpha_{13} \quad 24\alpha_{12} - 4\alpha_{33} \quad 8(3\alpha_{11} + 2\alpha_{13} + \alpha_{33}) \end{aligned}$$

$$T_{iJ}^1 = \frac{60A^m}{1260}$$

	30					
	-4	6				
	-4	1	6			
	12	-8	-12	96		
	-4	-4	-4	32	32	
	12	-12	-8	48	32	96

$$T_{iJ}^2 = \frac{60A^m}{1260}$$

	6					
	-4	30				
	1	-4	6			
	-8	12	-12	96		
	-12	12	-8	48	96	
	-4	-4	-4	32	32	32

$T_{1J}^3 = \frac{60A^m}{1260}$	6					
	1	6				
	-4	-4	30			
	-4	-4	-4	32		
	-12	-8	12	32	96	
	-8	-12	12	32	48	96

TABLE A.1

COEFFICIENTS (C) FOR AREA INTEGRALS IN AREA-
 COORDINATE SYSTEM (FROM REFERENCE [6])

Order $n = \beta_i + \beta_j + \beta_k$	β_i	β_j	β_k	C
1	1	0	0	1/3
2	2	0	0	2/12
	1	1	0	1/12
3	3	0	0	1/10
	2	1	0	2/60
	1	1	1	1/60

Remark:

$$\iint_{A^m} \psi_i^{\beta_i} \psi_j^{\beta_j} \psi_k^{\beta_k} dA = C A^m$$

and i, j, k represent any permutation of
 1, 2, 3.

2. Matrices for Two-Dimensional Formulation

The element matrices for two-dimensional formulation are:

$$S_{iJ}^m = \iint_{A^m} (P_i P_J + \hat{P}_i \hat{P}_J) dA \quad (i, J=1 \text{ to } 6) \quad (\text{A2-15})$$

and

$$Q_{iJ}^m = 2 \iint_{A^m} X_i X_J dA \quad (\text{A2-16})$$

with arrays P_i , P_J , X_i , X_J and A^m defined exactly the same as those in previous section, except that the coordinates η , ξ , now represent two-dimensional system. The integrals can be evaluated by following the same procedures described previously for axisymmetric case, and one can obtain the corresponding matrices for two-dimensional formulation, which are listed below. Here α_{iJ} is used to represent the sum $(a_i a_J + b_i b_J)/12A^m$.

$$B_{IJ} = 3 \alpha_{11}$$

$$- \alpha_{12} \quad 3 \alpha_{22}$$

$$- \alpha_{13} \quad - \alpha_{23} \quad 3 \alpha_{33}$$

$$4 \alpha_{13} \quad 4 \alpha_{12} \quad 0 \quad 8(\alpha_{33} - \alpha_{12})$$

$$0 \quad 4 \alpha_{23} \quad 4 \alpha_{23} \quad 8 \alpha_{13} \quad 8(\alpha_{11} - \alpha_{23})$$

$$4 \alpha_{23} \quad 0 \quad 4 \alpha_{13} \quad 8 \alpha_{23} \quad 8 \alpha_{12} \quad 8(\alpha_{22} - \alpha_{13})$$

and

$$Q_{iJ} = \frac{A^m}{1260}$$

6

1

6

1

1

6

0

0

-4

32

-4

0

0

16

32

0

-4

0

16

16

16

APPENDIX 3

AUTOMATIC MESH GENERATION

APPENDIX 3

AUTOMATIC MESH GENERATION

As mentioned in chapter 3, the element mesh is generated automatically by the computer on supplying a minimum amount of data. For a domain which is divided into twenty blocks similar to one shown in Figure 3.9, the following input data is required:

1. The z coordinate of nodes 1 and 21.
2. The angle between the line drawn from the origin to the node and the z axis, for nodes 43, 63, 85, 105, 127, 147,, 799, 819.
3. The desired spacing between the nodes 1, 3, 5, 7,, 21 as fraction of the total distance between the nodes 1 and 21.

With the above information, the r and z coordinates of nodes 43, 63, 85, 105, 127, 147,, 799, 819, 841, and 861 can be obtained provided the shape of the interface and the outer boundary is known (i.e. spherical, parabolic etc.). The coordinates for remaining nodes can be determined by using the fractional ratios of distances between the nodes 1 and 21, 43 and 63, 85 and 125,, 841 and 861. The node numbering on the solid side is similar to the numbering on the liquid side. The interface node members are common between

the solid and liquid sides. Such a mesh generation scheme facilitates quick and easy change in spacing of nodes as required by the problem under investigation.

APPENDIX 4

PHYSICAL CONSTANTS FOR WATER, TIN, AND SUCCINONITRILE
USED IN THIS WORK

APPENDIX 4

PHYSICAL CONSTANTS FOR WATER, TIN, AND SUCCINONITRILE

USED IN THIS WORK

(1) WATER

Equilibrium melting temperature	273 K
Latent heat of fusion	80 cal/cm ³
Density of solid	0.91 gm/cm ³
Density of liquid	1 gm/cm ³
Thermal conductivity of liquid	0.00133 cal/cm.deg.sec
Thermal conductivity of solid	0.00532 cal/cm.deg.sec
Specific heat of liquid	1 cal/gm °C
Thermal diffusivity of liquid	0.00144 cm ² /sec
Interfacial surface energy	7.17 cal/cm ²

(2) TIN

Equilibrium melting temperature	505 K
Latent heat of fusion	102 cal/cm ³
Density of solid	7.3 gm/cm ³
Density of liquid	6.98 gm/cm ³
Thermal conductivity of solid	0.144 cal/gm.deg.sec
Thermal conductivity of liquid	0.064 cal/cm.deg.sec
Specific heat of liquid	0.060 cal/gm °C
Thermal diffusivity of liquid	0.2 cm ² /sec.
Interfacial surface energy	13.01 x 10 ⁻⁷ cal/cm ²

(3) SUCCINONITRILE

Equilibrium melting temperature	331.24° K
Latent heat of fusion	10.72 cal/cm ³
Density of solid	1.016 gm/cm ³
Density of liquid	0.970 gm/cm ³
Thermal conductivity of solid	5.36 x 10 ⁻⁴ cal/cm.deg.sec
Thermal conductivity of liquid	5.32 x 10 ⁻⁴ cal/cm.deg.sec
Specific heat of liquid	0.478 cal/gm °C
Thermal diffusivity of liquid	0.00116 cm ² /sec.
Interfacial surface energy	2.14x10 ⁻⁷ cal/cm ²